A Study on the Effects of Sequential Turbocharged Diesel Engines

Michael Alexander Loonstijn

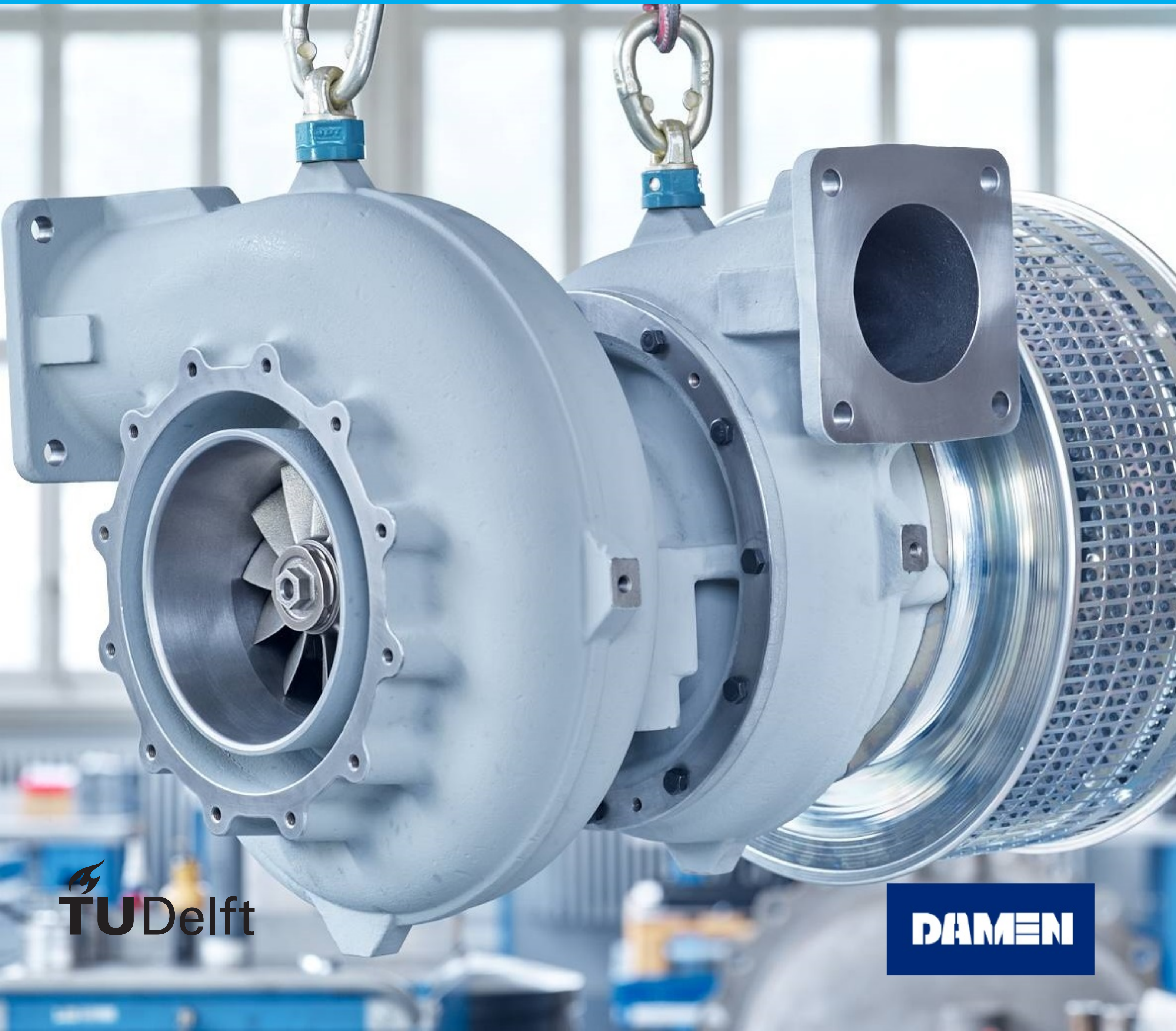

A Study on the Effects of Sequential Turbocharged Diesel Engines

by

Michael Alexander Loonstijn

to obtain the degree of Master of Science - Mechanical Engineering
at the Delft University of Technology,
to be defended publicly on Tuesday July 12, 2016 at 14:00.

Student number:	1334298	
Project duration:	December 1, 2015 – July 12, 2016	
Thesis committee:	Prof. Ir. J.J. Hopman,	TU Delft, committee chair
	Rear-Admiral(ME)ret. Ir. K. Visser,	TU Delft, supervisor
	Ir. M. de Boer,	DSNS, supervisor
	Prof. Dr. Ir. S. Klein,	TU Delft

This thesis is confidential and cannot be made public until 12-July-2021.

TU Delft

Abstract

Sequential turbocharging is a technique where multiple turbochargers are connected to an engine. These turbochargers are switched in sequentially. The manufacturers of engines with this system claim that the part-load and transient performance is better in comparison to engines with a single turbocharger. These claims and other effects in these engines are not well documented in scientific literature.

The motivation for this research assignment is the application of the Pielstick PA6B V20 STC on board of the Indonesian navy SIGMA corvettes. The sequentially turbocharged engines have been selected for this design, based on the operating envelope of the engine. At low speed, the sequentially turbocharged engines are able to deliver more torque than a normal turbocharged Diesel engine. Based on the operating envelope, the sequentially turbocharged Diesel engine is able to deliver similar benefits that are normally present in gas turbine and electric motor propulsion systems; high torque at low speed. However, DSNS prefers the use of Diesel engines for their robustness and available maintenance support. The design decision for a sequentially turbocharged Diesel engine during transient and low load operation is evaluated in this report.

The TU Delft Diesel B model has been adapted to model the sequential turbocharging strategy. This has resulted in two different models, each with their own benefits and drawbacks. The first model is the Simple STC model; this model gets its name from the simple implementation in Simulink. It is able to reproduce the trends of a sequentially turbocharged engine. The Simple STC model is of the same complexity as the TU Delft Diesel B model, both in application and in computational load. The drawback of this model is that it does not correctly model the transition when the sequential switching occurs, but this error is only present for a few seconds. The Full STC model also gets its name from the implementation in Simulink; in this model the full gas exchange of the sequential turbochargers is modeled. This model is a significantly more complex model than the Simple STC model, both in application as well as in computational load. However, it does provide the possibility to model each turbocharger separately and as a result the transient switching effect is modeled more accurately. Both models have been thoroughly tested in a test-bench environment, both for steady state and transient analysis. The results have proven that the characteristics of a sequentially turbocharged engine are modeled correctly.

It was proven that for the sequentially turbocharged engine, there are significant benefits for having two different turbocharger modes. Under steady state conditions, the mass supplied to the engine is of better quality in terms of mass flow and pressure for each of the different turbocharging modes in their respective working regions. This increased quality of air supply leads to lower temperatures, lower fuel consumption and higher available power for the same power rating.

The Simple STC model has been applied in a model of the complete SIGMA corvette to simulate acceleration tests and to test new control strategies. This has provided insight into the limits of the engine-propeller-hull interaction during acceleration. The propeller and ships ability to absorb power are limiting the engine's available power when the results are analyzed in the operational envelope. It has been proven that the engine needs to ramp-up in speed almost instantaneously to utilize the full available power. The engine is not able to ramp-up that fast due to the dynamic interaction of the engine and turbocharger. When accelerating the engine it was found that at higher acceleration rates the turbocharger does not spin up fast enough and as a result the air excess ratio decreases during acceleration; this phenomenon is also known as turbo-lag. The maximum acceleration limit is determined to be 12.8 [rpm/s] which results in a minimum air excess ratio of 1.5.

An alternative control strategy based on a minimum air excess ratio has been analyzed but this method did not result in a good control alternative. It did however give some insight into the maximum possible acceleration limits and provides a basis for future research into alternative control strategies.

Nomenclature

Table 1: A list of all the abbreviations used in this report.

Abbreviation	Full name
AC	Air Cover
AF	Air Filter
BDC	Bottom Dead Center
BMEP	Brake Mean Effective Pressure
CAC	Charge Air Cooler
COM	Compressor
CYL	Cylinder
DE	Diesel Engine
DSNS	Damen Schelde Naval Shipbuilding
EC	Exhaust Close
ENG	Engine
EO	Exhaust Open
GB	Gearbox
HE	Heat Exchanger
HTHE	High Temperature Heat Exchanger
IC	Inlet Close
IO	Inlet Open
IR	Inlet Receiver
IV	Inlet Volume
LMTD	Log Mean Temperature Difference
LTHE	Low Temperature Heat Exchanger
NRMSE	Normalized Root Mean Square Error
NTU	Number of Transfer Units
OR	Outlet Receiver
PROP	Propeller
RMSE	Root Mean Square Error
SFC	Specific Fuel Consumption
SIGMA	Ship Integrated Geometrical Modularity Approach
SIL	Silencer
STC	Sequential Turbocharging
SV	Silencer Volume
TC	Turbocharger
TDC	Top Dead Center
TUR	Turbine

Table 2: A list of all the symbols used in this report.

Symbol	Unit	Description
A	$[m^2]$	Area
c_p	$[J/kg/K]$	Specific heat, at constant pressure
c_v	$[J/kg/K]$	Specific heat, at constant volume
D	$[m]$	Diameter
h	$[W/m^2/K]$	Convective heat transfer coefficient
I	$[kg/m^2]$	Inertia
k	$[W/m/K]$	Thermal conductivity
L	$[m]$	Length
M	$[Nm]$	Torque
m	$[kg]$	Mass
$\dot{m}$	$[kg/s]$	Mass flow
N	$[rpm]$	Rotational speed
n	$[hz]$	Rotational speed
P	$[W]$	Power
Q	$[W]$	Heat
R	$[J/kg/K]$	Gas constant
r	$[m]$	Radius
T	$[K]$	Temperature
V	$[m^3]$	Volume
W	$[W]$	Work
X	$[0-1]$	Fuel rack
x	$[0-1]$	Air fraction
κ	$[-]$	Specific heat ratio: c_p/c_v
μ	$[kg/s/m]$	Dynamic viscosity
ω	$[rad/s]$	Rotational speed
$\dot{\omega}$	$[rad/s^2]$	Rotational acceleration
ρ	$[kg/m^3]$	Density

List of Figures

Preface

When I was very young, I was always taking my toys apart because I was very curious as to how they worked. Sometimes I was able to put them back together but most of the time I had broken something so my parents decided to get me Lego instead. This curiosity about how things worked stayed with me until this day and it has driven my passion for science and engineering in my young adult life. I grew up in a time when fax machines were the most advanced form of communication and I have witnessed the transition in technology to the present day where almost everyone carries around a mobile phone that is able to connect to practically anyone on the planet through the internet. I have been fascinated by how science and technology have progressed our society and I wanted to contribute to the collective scientific knowledge of this endeavor.

After high school I found my home at the Technical University of Delft where I began my studies for the Bachelor of Science in Mechanical Engineering. During my bachelor I took part in many extracurricular activities that widened my perspective on engineering problems and solutions. One of these was the participation in the university team for the Formula Student competition where I was part of the powertrain division. Along with other students we were able to use the theory from the university classes and put them to practical use by improving the performance of the combustion engine of the race-car. The experiences from these extracurricular activities confirmed my passion for science, technology, engineering and combustion engines.

In the second year of my Bachelor studies I met Hugo Grimmelius, who I started to work for as a student assistant. He invited me to join Vulcanus, the student society for marine Diesel engines and propulsion systems. At the end of the year we went on a study tour to Switzerland and the south of Germany. Here we visited Wartsila-Sulzer, MTU and MAN. Seeing the production and engineering that goes into these large Diesel engines was an amazing experience and I have ever since aspired to work in the marine Diesel engine industry. Hugo Grimmelius was the one who motivated me to do the Master of Science in Mechanical Systems Integration and he has been a great source of inspiration throughout my studies. Regrettably he passed away at a young age in 2012, I am very grateful to have known him and I thank him for his part in my journey.

My time at the University of Delft has almost come to an end. Over the past six months I have been working at Damen Schelde Naval Shipbuilding on a research assignment to conclude my Masters education. The topic of this assignment is on the application of sequential turbocharging on Diesel engines and the findings are presented in this report.

I would like to thank Klaas Visser for his support and guidance on the academic aspects of the thesis. I have really enjoyed the open discussions we have had on turbocharging and appreciated how he was able to provide thorough feedback on the delivered work. I would also like to thank Maarten de Boer, he was my supervisor at Damen Schelde and he was able to support me with the practical background and the application of sequentially turbocharged engines on board of warships. I appreciate his time and we have had interesting and fruitful discussions about the thesis. Although he was not an active part of my thesis, I would also like to thank professor Stapersma. For me he has been a very interesting teacher and his sincere passion for Diesel engines and marine engineering is something that I have admired. I have thoroughly enjoyed the courses on Diesel engines and the many discussions during study tours. From my family and friends, I would like to thank Annet Blankensteijn, my mother, and Eline ter Hofstede, my girlfriend. Both have been great sources of support during my studies and Eline, who is a turbocharger CFD engineer, has been a great sparring partner to talk about the engineering problems that I faced.

I hope you enjoy reading this report as I have enjoyed working on the contents. The subject is one that is close to my heart and I have really enjoyed working on this thesis. I hope that after the conclusion of my studies I can continue to work on Diesel engines and contribute to the development of this technology in the future.

Michael Alexander Loonstijn
Delft, June 2016

Contents

1 Introduction

1.1. History of turbocharging

The birth of the turbo charger is credited to a Swiss engineer by the name of Alfred Buechi, depicted in figure 1.1. His patent application for a compound engine in 1905 started the development of the turbo charger. This patent did not look much like the turbochargers of today, rather it was an axial flow turbine and compressor that shared a common shaft with the engine it was connected to. His design was not a commercial success but it did spark the interest of the engineering world. Buechi's simple design gave rise to the further development of integrating gas compressors and turbines with internal combustion engines to improve their performance [11].

Figure 1.1: Alfred Buechi, inventor of the turbocharger (source: ABB Turbo Systems LTD. Baden, Switzerland).

After Buechi, several years passed until a French professor by the name of Auguste C.E. Rateau applied for a patent in 1916. Rateau was famous for being the inventor of the impulse steam turbine and was well respected during his lifetime. His patent for a turbocharger was not published until 1921. Meanwhile across the ocean, during late 1917, the US National Advisory Committee for Aeronautics was interested in improving the power output of airplane engines to support the war effort in the First World War. They approached Sanford A. Moss of General Electric with the task to improve the power of a piston engine at high altitudes. He carried out his research at Pikes Peak Colorado, approximately 4250 meters above sea level. This research led to a functioning turbocharger that was able to attain sea level power at high altitude. This meant military airplanes were able to reach higher cruising speeds and altitudes than ever before, securing the role of the turbocharger for military purposes.

The end of the First World War had slowed down the development of the turbocharger but it also provided much needed time for design considerations. General Electric continued its research in turbochargers and by the time the Second World War broke out, many of the US air plane engine where equipped with Moss's turbochargers, including for instance the famous B-17 Flying Fortress.

In the beginning of the postwar era there was little interest in developing turbochargers, there were more pressing matters, like rebuilding Europe for instance. Gradually the popularity of the turbocharger increased as it found its use in many different commercial applications ranging from farm equipment to power generation and marine transport. The turbocharger allowed engine manufacturers to increase their engine power output without having to constantly increase the sizing of the engine itself.

The 50's and 60's saw the birth of modern turbocharger development, primarily through the commercial use of Diesel engines. This peaking interest coupled with the postwar economic expansion spawned the rapid growth of companies that would specialize in the development of turbocharging technology worldwide. More uses for turbochargers brought about the need for increased efforts in research and development of turbochargers. Modern engineering knowledge and toolsets have helped to increase the performance of turbochargers, figure 1.2 shows a comparison of a modern turbocharger next to a turbocharger from the 60's.

Figure 1.2: The current Schwitzer-BorgWarner model S3 on the left has a slightly higher airflow range than the older Schwitzer model made in the 60's for Cummins Engine Company. While the intended applications are different, it's easy to see the dramatic design differences that have come about from computer-aided designs, improved materials and manufacturing processes (source: Diesel Injection Service Company, Inc.)

As is often the case in history, necessity is the mother of invention. The turbocharger is no exception. If engines are to be applied to a variety of uses, breathing is fundamental to their success. The internal combustion engine has reshaped our world and the turbocharger has helped the engine accomplish this task [11].

1.2. Sequential turbocharging

Since its conception, the turbocharger has been mostly applied in a configuration where a single compressor and turbine are coupled to a single combustion engine. However, in the last twenty years the world of turbocharging has been shaken up with new and advanced turbocharging concepts. One of these concepts is sequential turbocharging, first introduced by Brown Boveri in 1946 [1].

In a sequential turbocharged engine, there are more than one turbochargers fitted to the engine. These turbochargers are connected in parallel and are sequentially switched in and out. A diagram of the gas exchange between the engine and turbochargers is shown in figure 1.3:

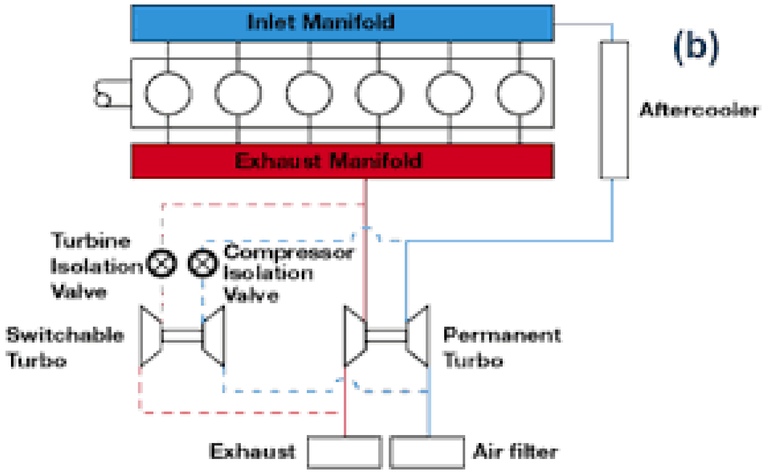

Figure 1.3: A diagram of the gas exchange in an STC engine (source: dieselnet.com).

In figure 1.3 it can be seen how, in this case, two turbochargers are connected to a single engine. One of the turbochargers is always connected (permanent turbocharger) and one is sequentially switched in and out (switchable turbocharger). The switchable turbocharger is connected to the engine via two large valves that are located on the engine side of the turbocharger's compressor and turbine. The switchable turbocharger is only switched in at high load operation, typical values for switching in are at 40% to 60% of the nominal engine load. In the last decades the marine industry has seen several different sequentially turbocharged engines from the major engine manufacturers. Some notable engines with sequential turbocharging are listed in 1.1

Table 1.1: a list of notable STC engine from the major marine Diesel engine manufacturers.

	MAN V28/33D STC	**MTU series 1163 M04**	**Pielstick PA6B**
Bore / Stroke [mm]	280 / 330	230 / 280	280 / 330
Speed range [rpm]	300 - 1035	350 - 1325	300 - 1080
Specific power [kW/cyl]	455	300	405
Cylinder configurations	12V / 18V / 20V	12V / 16V / 20V	12V / 16V / 18V / 20V

Sequential turbocharging is the main subject of this thesis. The reason for its implementation and the governing physical principals are treated in more detail in chapter 2.

1.3. Motivation for research

Damen Schelde Naval Shipbuilding has produced several warships that are outfitted with sequentially turbocharged engines, this thesis will focus on the Sigma-class corvette/frigate. The Sigma-class is a modular design concept created by Damen Schelde where the customer has a high level of customization options, including the number of hull segments and the order in which they are placed. The classification of a corvette or frigate depends on the length of the vessel and the classification standards of the customer. Figure 1.4 shows the KRI Diponegoro, a Sigma 9113-class corvette operated by the Indonesian Navy.

Figure 1.4: Sigma 9113-class corvette, KRI Diponegoro (source: DSNS).

All of the Sigma corvettes and frigate are equipped with two sequentially turbocharged engines, namely the Pielstick PA6B V20 STC. A complete detailed specification of this engine is available in appendix A. These engines have been chosen to improve the vessel performance when sailing at low speed and when rapidly accelerating to full speed. This decision is based on the claims made by the manufacturer, details in 1.4.

DSNS wants to gain more understanding on the limits of a sequentially turbocharged engine and whether it fits the design goal of the vessel. For acceleration purposes, it is best to have a main propulsor that can deliver a large amount of torque at low speeds so that the maximum amount of torque is available right from the start of the acceleration. New means of propulsion are coming into the marine market such as electric motors and gas turbines. These machines have the ability to deliver a large amount of torque at low speeds and thus give very good acceleration performance. However, these machines are more costly to purchase and operate. Even worse is the fact that they often require specialized maintenance when they break down. For this reason, DSNS prefers to use Diesel engines; they are reliable and are able to be repaired at many different locations. But Diesel engines have a torque curve that gradually builds up and is relatively small at low speeds. Sequentially turbocharged engines do have a lot of torque available at low speeds and based on the operating envelope, appendix A, it is expected to provide more torque at low speeds. However it is not known if all of this torque is available during acceleration. This study will provide detailed answers as to whether a sequentially turbocharged engine can combat the shortcomings of a traditional Diesel engine and will help in the selection of propulsors in future designs.

1.4. Research objective

Sequential turbochargers are not commonly applied to simple Diesel engines due to the increased complexity of the system. However for high-performance application, such as warships, the application of sequential turbocharging can provide certain benefits that would offset the increased cost and effort of operation. The engine manufacturers make similar claims when it comes to sequential turbocharged engines [6][2]. These claims are typically:

- Better performance at part load
- Better acceleration performance, less turbo-lag.
- Higher boost pressures when coupled with emission control strategies such as EGR and miller timing.

These claims are made by the engine manufacturers but there is little academic work to support these claims. Not because the claims are false but rather because literature surrounding sequential turbocharging is very sparse. This thesis will try to shed some light on these claims and see whether they stand up against an investigation into the physical processes involved in a sequential turbocharged engine. This will be done by finding an answer to the main research question and its supporting questions. The main research question is explicitly formulated as follows:

What are the effects on part-load and transient performance when sequential turbocharging is applied to marine Diesel engines?

The answer to this question will be investigated by using numerical simulation models of Diesel engines. Several models for a "classic" turbocharged Diesel engine are available for this research; these models have been developed by the TU Delft and were used for different PhD dissertations and M.Sc. thesis research assignments in the past. A suitable model has to be chosen and adapted to be able to simulate the processes in a sequentially turbocharged engine. When this model has been constructed it will be placed in a complete ship simulation that simulates the ship-propeller-engine interaction of the entire propulsion system on board of the KRI Diponegoro. This allows for a detailed investigation into the engine performance and limitations under a dynamic load that is representative of the real world physical process. Finally the ship model will be tested with the application of a new control strategy to improve the vessel performance with the existing propulsion hardware. These research goals form the supporting questions to the main research question; they are explicitly stated as follows:

- Can one of the TU Delft Diesel engine models be adapted to simulate sequentially turbocharged engines?
- Can a simulation model be used to better predict/understand the transient behavior of a sequentially turbocharged engine on board of a naval vessel?
- Can vessel performance be improved by changing the control strategy with the same hardware?

These questions will be answered in the appropriate chapters and repeated in the final conclusions of the thesis.

1.5. structure of the thesis

The structure of the thesis follows a logical path through all of the work that has been performed for this research assignment.

Chapters two and three provide an overview of the theoretical principles that are of importance to the research assignment. These chapters are based on the literature study that was performed prior to the research assignment. Chapter two gives an in-depth explanation on the theory behind turbocharging, here the inherit problems with combining a turbocharger and an engine are discussed. The explanation of these problems leads to the reasoning behind applying sequential turbochargers. The physical principles of sequential turbocharging are discussed and a few alternatives that attempt to solve the same problem are presented. The next chapter deals with the existing TU Delft Diesel B model, this model is superficially explained and only the most important working concepts are treated in more detail. This chapter is finished with a brief discussion on the problems surrounding calibration of the model and the proposed solutions by the author.

Chapters 4 up until 7 treat the models that where created by the author for this research assignment, respectively: An alternative air cooler model, the Simple STC model, the Full STC model and the TNI Corvette model. All of these models are evaluated in the same order: the model hypothesis is explained followed by the implementation as a mathematical model. Each model is tested in both steady state and transient operation, this is followed up with the results and validation of each analysis. For the engine models, a large selection of important engine parameters are discussed and compared to the measurements of the real-world engine. At the end of each chapter, a short sub-conclusion is given to answer some of the questions surrounding the models treated in those chapters

The thesis is concluded with 3 chapters: Discussion, Conclusion and Recommendations. In the discussion, the suspicions of the author and inconclusive findings of the research assignments are discussed. This is where the "soft" conclusions are given, these conclusions have a logical reasoning behind them but they cannot be sufficiently backed up with the results from the research. The next chapter, Conclusion, provides the answers to the questions posed in 1.4. In this chapter, the "hard" conclusions are drawn. These conclusions can be justified with the results of the research assignment. The final chapter presents some recommendations for follow-up research based on the findings of the report.

2

Theoretical principals of sequential turbocharging

As was mentioned in the introduction, Diesel engines have re-shaped the world with the help of turbochargers. The modern era has seen the rise of ever increasing demands on Diesel engines in terms of power density and emission regulation. The concept of the Diesel engine itself has changed very little from its original inception by Rudolf Diesel, much has been done in terms of combustion and injection but the rudimentary engine has seen little change. Most of the development has been focused on the turbocharger(s) supplying air to the Diesel engine. This has led to a wide range of advanced turbocharging concepts. Apart from sequential turbocharging, there are several other turbocharging concepts that have been introduced in recent years:

- Multi stage turbocharging in series (turbo compounding)
- Hybrid turbocharging, where a motor/generator device is connected to the turbocharger shaft.
- Variable geometry turbochargers

A detailed analysis of these concepts is outside of the scope of this thesis but a short explanation of their theory and application will be presented in section 2.3. A superficial understanding of these concepts will help the reader to realize that the development in turbocharging combustion engines is in no way an old and obsolete field of research.

2.1. The problem with turbocharging a Diesel engine

At first the combination of a Diesel engine and a turbocharger seems to be a match made in heaven. The engine requires high pressure air to be supplied by the turbocharger and in term the turbocharger requires hot exhaust gasses supplied by the engine's combustion process. This symbiotic relation allows the engine to run at a higher rated performance while at the same time having the potential to improve the engine efficiency by recovering the waste heat from the exhaust gasses.

Problems start to arise when the combined system, engine and turbocharger, has to be able to operate over a large range of speed and load settings. The application of turbocharging creates a strong coupling effect between the two components. The engine and turbocharger each have their own characteristics that need to be matched to ensure satisfactory operation of the combined system. Normally this coupled system is optimized for, or close to, maximum continuous rating. However this creates problems for operation at part load due to the increased mismatching of the coupled system [9]. The effect of the mismatch is best explained by looking at a compressor map with an overlay of an engine operating line, figure 2.1:

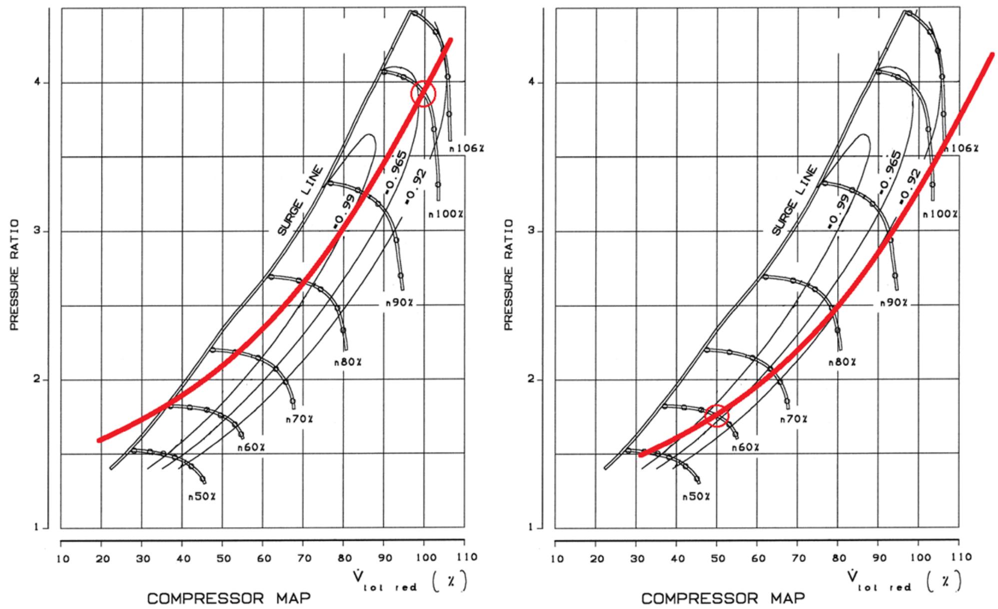

(a) matched to 100% flow

(b) matched to 50% flow

Figure 2.1: a) compressor matched to high engine load. b) compressor matched to low engine load (source of map image: MAN TC NA34 project guide)

Figure 2.1a shows the compressor map of a turbocharger that is matched to the engine operating line at 100% of its nominal mass flow. The engine air demand is within the stable operating envelope of the compressor between 35% and 100% of its nominal mass flow. Below 35%, the engine demands air to be supplied at a pressure that is beyond the surge limit of the compressor. This operating condition is potentially harmful to the equipment and must be avoided at all cost. In practice, the maximum load of the engine is limited in these low flow regions. For a marine application, this is usually achieved by reducing the pitch of the controllable pitch propeller.

Figure 2.1b shows the compressor map of a turbocharger that is matched to the engine operating line at 50% of its nominal mass flow. This is the same type of compressor, hence the same map, but it is smaller in size then the compressor in figure2.1a. The engine air demand is within the stable operating envelope of the compressor between 20% and 85% of its nominal mass flow. At higher mass flow rates, the engine air demand is too large for the smaller compressor and the operating line moves beyond the choking point of the compressor.

The narrow band of the compressor map limits the operation of the engine either at full load or at part load depending on the choice of turbocharger size. This problem is one of the main issues that sequential turbocharging tries to combat and it does so quite effectively. The following section will go into more detail on how this is achieved.

2.2. Theoretical benefits of sequential turbocharging

The engine that is selected for this thesis is the Pielstick PA6B V20 STC engine; it is fitted with two equally sized turbochargers. These turbochargers have the same characteristics and thus they can be plotted in the same compressor map. Figure 2.2 shows the engine operating line in the compressor map of the permanent turbocharger. This is a representation of the general characteristics of a sequentially turbocharged engine and not the specific operating conditions for the Pielstick PA6B V20 STC.

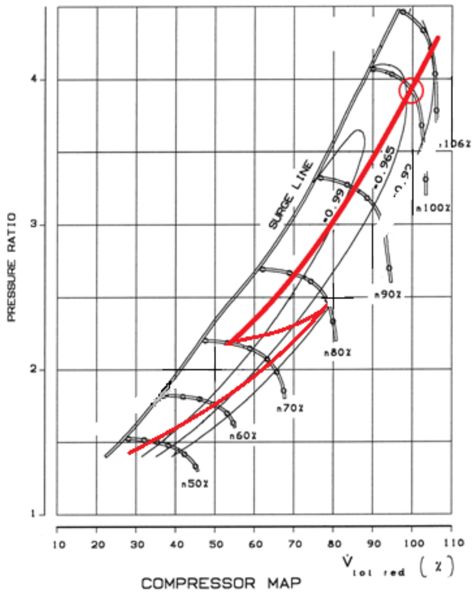

Figure 2.2: compressor map of the permanent turbocharger in a sequential turbocharged engine with 2 equal turbochargers (source of map image: MAN TC NA34 project guide).

The compressor map of figure 2.2 can be compared to the previous maps shown in figure 2.1. At part load, a single small turbocharger is in operation and the system behaves like the small compressor from figure 2.1b. if the engine load increases, the air mass demand also increases. With a single small turbocharger, the compressor starts to choke at a higher mass flow. In the sequential turbocharged configuration, the second turbocharger is switched in at higher loads and the two turbochargers now act like one big turbocharger that resembles the operating line in figure 2.1a.

From figure 2.2 it becomes apparant that applying sequential turbocharging allows the engine to stay within the narrow band of the stable compressor map. This improves the operating ability of the engine over a larger load and speed range. The effect that is shown in the compressor map gives a first indication that the manufacturer's claim of part load improvement has some truth to it. However this still needs to be fully investigated with the use of simulation models.

Another theoretical benefit is improved response times of the turbocharger. Because the air demand is delivered by two smaller turbochargers instead of one large one, the rotational inertia per turbocharger can be smaller. This should result in faster spin-up times of the turbocharger and thus faster response times. This effect is studied with the help of scaling laws in appendix B. This appendix also holds a detailed calculation of the turbocharger inertia of the turbocharger mounted on the Pielstick PA6B.

However, the transition of going from one to two turbochargers is a dynamic effect that is not well-studied in academics or advertised by the manufacturers. This transient effect of switching in and out turbocharger groups can be seen in figure 2.2 as the line that connects the two operating lines from figure 2.1. The transient effects are the main areas of interest for this M.Sc. research assingment on the effects of sequential turbocharging.

2.3. Alternatives for sequential turbocharging

There are several other solutions that can be applied to turbocharged engines to combat the inherit problems of mismatching the turbocharger and engine. These alternatives are briefly presented in this chapter and serve only to give the reader a superficial background on modern turbocharging developments.

2.3.1. Variable geometry turbine

For automotive applications the problems associated with low load are usually resolved with the use of a variable geometry turbine. The stator vanes of the turbine can be changed in position to adjust the effective turbine nozzle area; this is shown in figure 2.3.

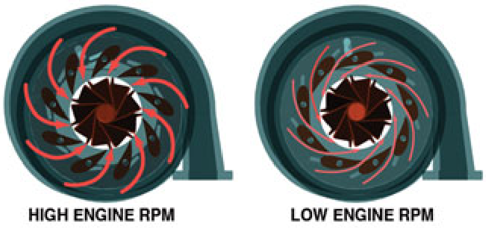

Figure 2.3: A variable geometry turbine at high and low engine RPM. (source: Source: www.import-car.com)

In Serrano et al. [17] it is explained that the efficiency of the turbine at part load does suffer from this implementation due to the change of reaction degree between the stator and rotor. However for automotive application this is justified due to the relative low amount of time that the system operates at part load. The presence of a gear shift allows for the system to operate at or near the desired engine operating point for a variety of different vehicle speeds. This means that low engine speed operation mostly occurs during acceleration and not during continuous operation. Advantages of a variable geometry turbine in automotive applications are: relatively low cost, simplicity, reliability and the possibility for performance optimization with electronic control.

In marine applications a fixed gear ratio between the engine and propeller is a common solution. This means that continuous low vessel speed is accompanied by continues low engine speed operation. The decreased turbocharger efficiency in low load conditions is not acceptable for this type of operation. Another point of contention is that the fuels that are commonly used in marine applications also tend to cause significant more fouling on exhaust components than the fuels used in automotive applications. The increased fouling on the variable stator vanes increases maintenance significantly. For these reasons a variable geometry turbine is not applicable for marine diesel engines.

2.3.2. Waste gate

A waste gate is a valve that allows for gas to bypass the turbine of the turbocharger, in this way the turbine receives less energy and some of the exhaust energy is wasted; a very aptly named device. However it allows for a regulated method of controlling the flow through the turbine which directly affects the net effective turbocharger shaft power which in term affects the pressure ratio of the compressor (the objective parameter). A practical implementation of a waste gate is shown in figure 2.4.

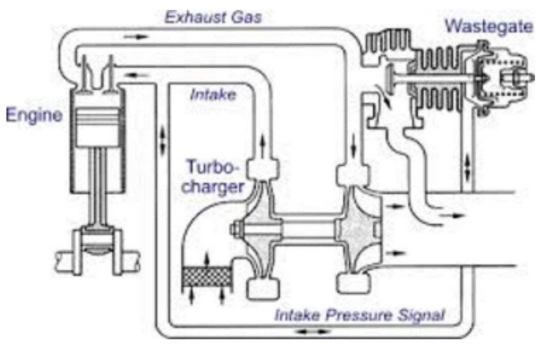

Figure 2.4: Schematic of the location of a waste gate in an internal combustion engine(source: www.dieselnet.com).

Ghazikhani et al. [8] confirms the statements by Jensen et al. [9] on the topic of engine-turbocharger mismatching: If the turbine flow area is matched for full speed and load conditions (large turbocharger), then exhaust flow velocities at low engine speed are very low and turbocharger response is very slow. On the other hand, if the turbine area is matched to get a good response (small turbocharger), then either turbocharger overspeed, peak cylinder pressure or surge limits are reached. This trade-off between the need for transient operation and maximum limits can be addressed with the help of a waste gate.

Carter et al. [5] explains that in the case of a waste gate implementation, the turbine area is smaller than it would be when matched to full load conditions; the whole turbocharger is smaller. This ensures that boost pressure at lower load is maintained. At higher load, the waste gate is progressively opened up to control the boost pressure and prevent the turbocharger from going into overspeed and subsequent surging of the compressor.

Because the implementation of a waste gate is simple and cost effective, this system is widely used in marine applications to give better performance in transient and low load operation. The addition of a bypass valve on the turbine is a relatively simple and cheap part to add to the engine and reduction in size of turbocharger means a cheaper turbocharger can be installed. If the waste gate is controlled via a pneumatic valve (as shown in figure 2.4.), the control strategy is very simple and robust.

2.3.3. Mechanical turbo compounding

In mechanical turbo compounding, an extra power turbine is placed after the turbocharger turbine to extract more energy from the exhaust gas flow out of the engine. This power is fed back to the main drive shaft via a mechanical connection; a schematic representation of this system is given in figure 2.5. In this schematic, a variable transmission (Toroidal variator) is used to transfer the power from the power turbine to the main shaft, a variable transmission is used to have the power turbine operating at or near the ideal speed.

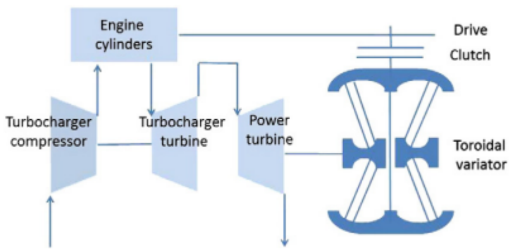

Figure 2.5: A mechanical turbo compounding system (source: Boretti [3]).

Boretti [3] analyzed the system presented above for heavy duty diesel engines, there is also a bypass valve on the turbocharger turbine (not drawn in schematic). This bypass valve is effectively a waste gate as discussed in the previous section. This system allows the same engine operation as that of the waste gate engine but reduces energetic losses that are inherited to the waste gate system. The waste gate allows for direct control on the power balance of the turbocharger and subsequently the boost pressure of the compressor. However, the wasted heat contained in the mass flow going through the waste gate of the turbocharger turbine can be utilized by the power turbine. Boretti [3] found that applying mechanical turbo compounding can increase the efficiency and thus reduce the specific fuel consumption of the entire engine system.

Leising et al. [10] further quantified the effects of mechanical turbo compounding with a long term experiment. They reported an average brake specific fuel consumption reduction of 4.7% for a 14.6L diesel engine performing a 50.000 miles extra-urban driving test in the United States of America.

It is clear that mechanical turbo compounding can improve the total efficiency of an internal combustion engine through further waste heat recovery. However, for improving the part load of an engine this system alone is not sufficient. It relies on a waste gate to improve the part load behavior and tries to minimize the inherited losses that come with the usage of a waste gate. To the author this seems like a "double end-of-pipe solution" where the solution to the primary problem (waste gate for low load) results in an extra problem (decreased efficiency) that requires a band-aid to function efficiently within the desired range.

2.3.4. Electrical turbo compounding

Similar to mechanical turbo compounding, electrical turbo compounding relies on a power turbine that is located downstream from the turbocharger turbine. However in this configuration, the power turbine is directly connected to an electric generator, see figure 2.6. This generator generates electrical power that can be fed into the vehicle's auxiliaries or into an electrical drive system in the case of hybrid vehicles. For the thermodynamic performance, this system is similar to the mechanical version with presumably some improvements on mechanical losses.

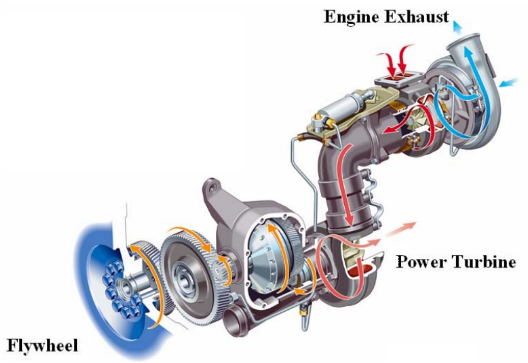

Figure 2.6: A electric turbo compounding system (source: www.scania.com/global/engines).

2.3.5. Hybrid turbocharging

In hybrid turbocharging, sometimes referred to as electrical turbocharging, an electric motor is fitted directly on the turbocharger shaft; this motor can also double as a generator depending on the desired operation. An example of this implementation is shown in figure 2.7.

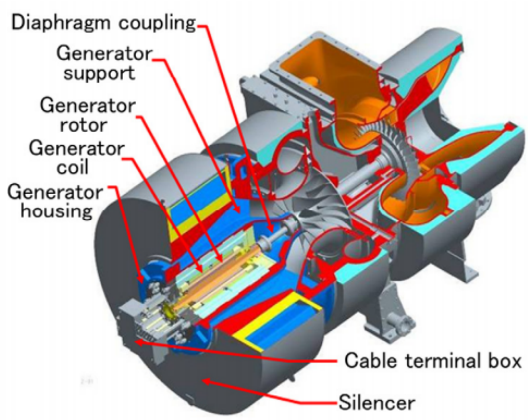

Figure 2.7: A hybrid turbocharger for marine application (source: www.mhi-global.com).

Other than with turbo compounding, this technique can directly influence the power balance of the turbocharger. If the power developed by the turbine exceeds the power absorbed by the compressor, the turbocharger can go into overspeed and the compressor can surge. The motor/generator in the hybrid turbocharger can function as a generator and absorb the extra available power preventing these unwanted effects. On the other hand when the turbine does not deliver enough power for the compressor to reach the desired boost pressure, the motor/generator can function as a motor and add the needed power for the compressor to reach its desired boost pressure.

Hybrid turbocharging has been extensively developed in Formula One racing since 2014 due to new restrictions on fuel usage and subsequent focus on energy recovery, more on this topic can be found in the article from race car engineering [14]. The automotive application is not further pursued in the scope of this report as it is very different from the marine application.

Ono et al. [13] performed a case study on the world's first marine application of a hybrid turbocharger (shown in figure 2.7) on a large commercial tanker vessel in 2012. They utilized the electrical generator of the hybrid turbocharger to supply all the required auxiliary power for the ship. This allowed the turbocharger to operate at a higher isentropic efficiency and improve the overall ship efficiency. They claim an efficiency gain of 5% due to optimized operation of the turbocharger.

Hybrid turbocharging has not yet been widely applied in shipping to resolve the issues concerning low load and transient behavior of the engine + turbocharger system. From the work done in Formula One it can be expected that hybrid turbocharging is able to provide better performance, both during low load operation and during transient operation. A hybrid turbocharger also allows for additional control strategies, giving the designer and operator more freedom in terms of a ship's operational profile.

A downside of hybrid turbocharging is the increased cost of equipment; the electric motor has to be able to cope with the high rotational velocities of turbochargers (10.000+ rpm). This requires an expensive and highly specialized permanent magnet motor/generator. It also requires extra equipment in terms of a large AC/DC converter and DC/AC inverter to make the turbocharger's electric motor out- and input compatible with the ships power grid. Ono et al. [13] had the ship outfitted with the frequency converters shown in figure 2.8 to be able to utilize the hybrid TC.

AC/DC converter (Calnetix, Inc.)   DC/AC inverter (Taiyo Electric Co., Ltd.)

Figure 2.8: Frequency converters used by Ono et al. (source: Ono et al. [13]).

The author believes that this technology poses many beneficial aspects and expects to see this technology be further developed in the coming years. Formula One and the commercial automotive industry are already doing thorough research into this technology. With the added benefits, it is only a matter of time before this technology sees it's application in the more conservative industry of marine Diesel engines.

3
Diesel engine simulation

Diesel engines have been extensively studied in both industry and academics. Their importance in the modern transport infrastructure drives the interest to gain a better understanding of their physical working. These efforts have resulted in a lot of different approaches to simulate the mechanical, thermodynamical and chemical processes that are present in a diesel engine.

3.1. Model classification

It is possible to make certain distinctions between modeling strategies used for modeling Diesel engines. Schulten et al. [16] proposed the distinction between analytical and empirical models.

Empirical models use a mathematical expression, usually a polynomial that bears little relation to the actual physical process. These expressions contain coefficients that can be fitted in such a way that the expression describes the particular solution to the chosen physical process at a specific operating point. However, these coefficients are no longer valid when the system variables change, they need to be fitted again to new experimental data. The advantages of empirical models are that they are quick to implement and quick to operate due to the fact that the calculations are less complex, using less intermediate calculations to compute the actual physical processes. The disadvantages are that they require data to fit coefficients for each particular solution making them very limited in terms of modular usage in overall systems.

Analytical models use expressions that are derived from physical processes. These models use physical relations and fundamental laws that are well studied in academic physics to accurately predict what the outcome will be. Here in lies the difference with empirical models: physical models are able to **predict** outcomes based on **proven theory**, whereas empirical models can **replicate** outcomes based on **experimental data**. It is evident that analytical models can provide more insight into the given problem, at the cost of requiring more effort to construct and operate.

An intermediate class of models exist that can be referred to as semi-empirical models. In this case physical properties are grouped together into groups of dimensionless numbers through the application of the Buckingham Pi theorem [4]. This provides a method for computing sets of dimensionless parameters from given variables when the form of the equation is unknown. These computations can be derived through experiments and be used to replicate those experiments. Because this method is based on dimensional number theory, it can be used to scale the models to work for components of different sizes.

Schulten et al. [16] proposed a further distinction in analytical models based on the field of application, in order of complexity:

- Computational fluid dynamics (CFD) models
- Phenomenological multizone models
- Crank angle models

- Mean value models
- Transfer function models

Mean value models are of particular interest to the author; the reader is referred to [16] for more details on the other types listed above.

3.2. Mean value engine models

Mean value engine models are models where the instantaneous cycle performance is averaged over the entire cycle. At every iteration of the simulation, the total cycle performance is calculated based on the instantaneous value of the input parameters. This modeling technique has been extensively studied at the TU Delft by Stapersma [18] and at the Dutch Naval College by Schulten [16]. The results of these studies have proven that this modeling technique is able to accurately predict the performance of turbocharged marine diesel engines.

3.3. Model choice

The TU Delft has developed two different models for simulating Diesel engines; these are called the Diesel A model and the Diesel B model. Both are classified as mean value first principle models, where the first principle name refers to the fact that it is based on analytical physical principals. The Diesel A model is simpler than the B model but has certain advantages over it. It requires less information of the physical engine and it requires less computational power to operate. However the turbocharger, the main interest of this thesis, is modeled with a very simple first order method. This meant that the Diesel A model was rejected early on for this particular the research assignment.

As mentioned above, the Diesel B model is more complex than the Diesel A model. It also requires a lot more information of the physical engine and its operating conditions to properly calibrate the model. This has always proven to be a big disadvantage of the Diesel B model since this data is very hard to come by. An alternative to the Diesel B has briefly been considered for this research assignment. This alternative model was constructed by the author and is based on the modeling techniques used in the Diesel B model. The goal was to use the advanced features of the Diesel B model but simplify certain components to make it easier to calibrate it to new engines; hence it is named the B-minus model. It was determined that the development of an entirely new Diesel engine model was too far outside of the scope of the thesis, the validation of the model was not performed but a functioning model has been produced and documented. A detailed description of the B-minus model can be found in appendix D.

In the end, the Diesel B model from the TU Delft was selected for this research assignment to see if it could be adapted to model an sequentially turbocharged engine. This choice was made because the Diesel B model has a proven track record and because there was a lot of data available for the Pielstick PA6B engine.

3.4. The TU Delft Diesel B model

The Diesel B model has two distinctly different processes: the closed cylinder process and the open cylinder process. As the name might suggest, these two processes are classified by whether the valves of the cylinder are open or closed. Figure 3.1 shows the pressure in the cylinder during 720 degrees of crankshaft rotation, in this figure the closed cylinder process runs from when the inlet valve closes(IC) until exhaust valve opens (EO). The open cylinder process, named gas exchange in figure 3.1, runs from EO until IC.

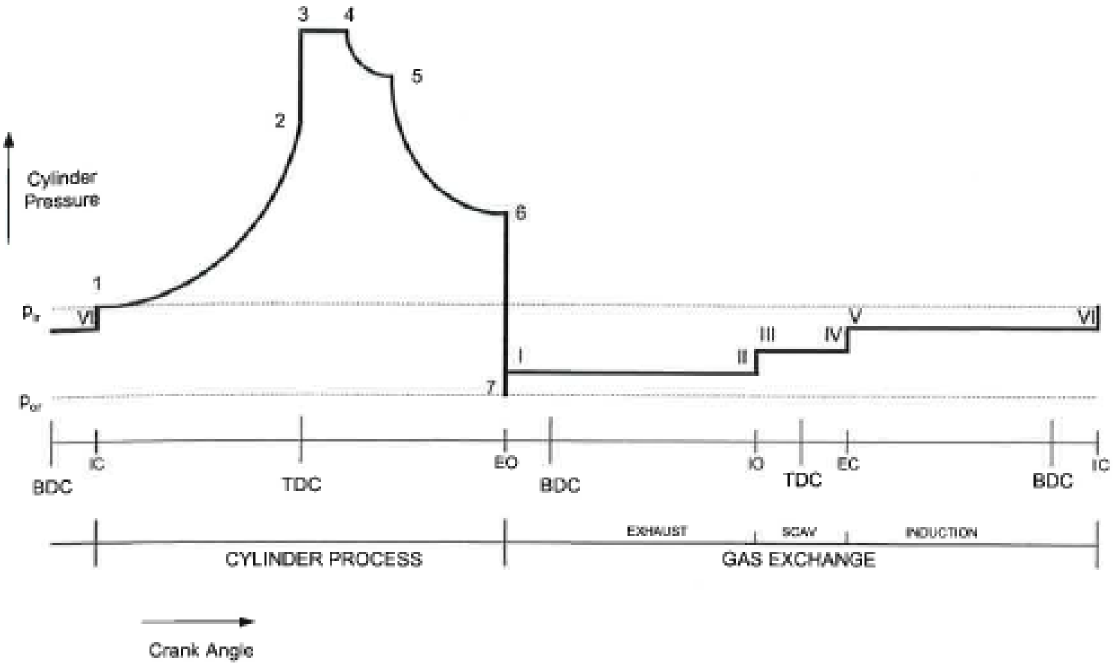

Figure 3.1: pressure in cylinder of a diesel engine (source: Schulten [16]).

The inclusion of the open cylinder process is what makes the Diesel B model different from the Diesel A model which basically only models the closed cylinder process. Looking at figure 3.1, one might suggest that the inclusion of the open cylinder does not increase the complexity of the model by much. It only makes up about half of the cycle time and the magnitude of the pressure is much lower than that of the closed cylinder process. However this is far from the truth, the Diesel B model is a vastly more complex model than the Diesel A model. This is illustrated by the model specifications given in table 3.1:

Table 3.1: An indication of the complexity difference between the Diesel A and B models.

	Diesel A model	**Diesel B model**
Input parameters	22	148
Continuous integrators	2	17
Memory blocks	0	14
Subsystems	22	291

Because of the complexity of the Diesel B model and because it was not created by the author, the reader is referred to [16] and [18] for a detailed description of each component in the model. However, for the scope of this research assignment it is important to explain certain concepts that the Diesel B model uses.

3.4.1. Volume and resistor elements

The Diesel B model tries to model a complete engine by combining sub-models of the physical sub components of an actual engine: inlet receiver, compressor, cylinders, etc. From a modeling perspective the engine components can be either a resistance element or a volume element, see figure 3.2:

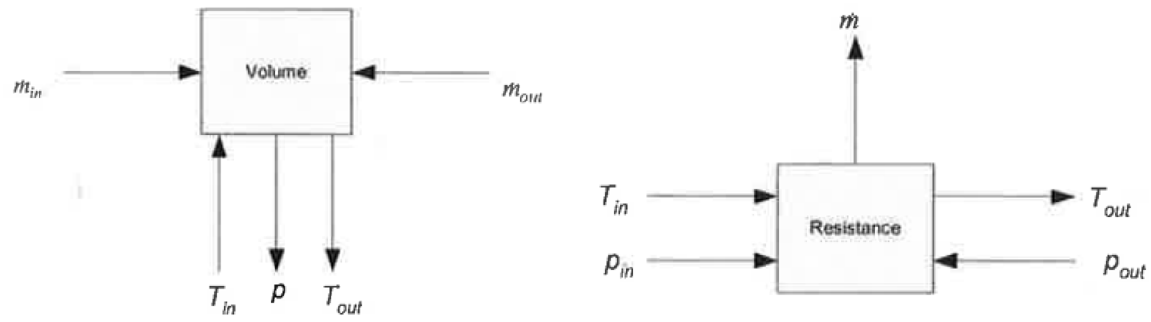

(a) volume element (b) resistance element

Figure 3.2: volume and resistor element with their respective in- and outputs (source: Schulten [16]).

These two basic elements have the following functions:

- Resistance element: These elements calculate the mass flow through the element as a function of the pressure difference over the element.
- Volume element: These elements calculate the internal state properties of the element as a function of the mass and energy leaving and entering the element.

The resistance elements used in the Diesel B model are not all using the same set of equations; rather they each have a custom set of equations to calculate the mass flow. The simplest resistance element is that of an orifice plate, for which the mass flow can be determined based on the conservation of momentum.

Whereas the restrictor elements each have custom sets of equations, all the volume elements are using the same set of equations. These are derived from the conservation of mass and the first law of thermodynamics. A full derivation of the equations used for the basic volume and orrifice plate resistor elements can be found in appendix E.

3.4.2. Volume and resistor network

The volume and resistor elements can be connected to form a volume-resistance network. This network bears resemblance to an electrical RC-type network, where the resistors (R) inhibit the current and the capacitors (C) store charge. In the volume-resistor network the resistors inhibit the flow of mass and the volumes store mass and energy. This theory to engine modeling is applied by both Jensen et al. [9] and Schulten et al. [16]. The model by Schulten et al. is shown in figure 3.3:

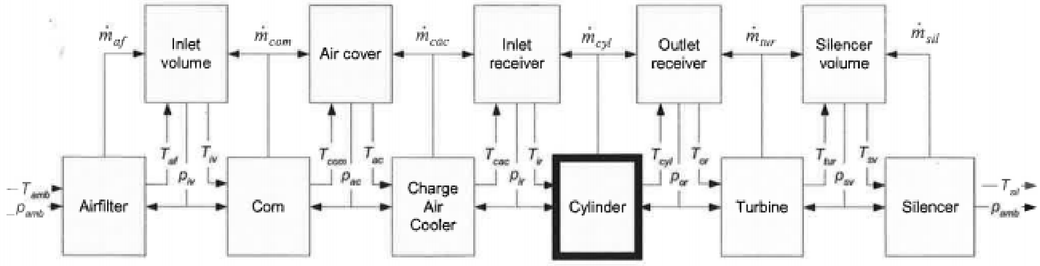

Figure 3.3: volume and resistor network of a turbocharged Diesel engine (source: Schulten[16]).

The components in the top row of figure 3.3 are the volume elements and those on the bottom row are the resistor elements. The cylinder is a special component because it also contains the closed cylinder process that is not part of the gas exchange. All the other components shown in figure 3.3 are there to facilitate the gas exchange. With the structure and concepts of the Diesel B model explained it is also important to have a look at how it can be used for engineering applications.

3.4.3. Model calibration

In its current form the Diesel B model requires a lot of parameters, see table 3.1, to be defined by the user in order to simulate a new type of engine. These parameters can be divided into different groups that have a distinct origin. According to Schulten [15] the parameters can be divided into the following sets:

- Physical parameters, exist regardless of the model
  - Dimensions
  - Physical properties
- Model parameters, exist only because of the model.

Schulten then redefined a more practical subdivision of the parameters:

- The known parameters
- The arbitrary parameters
- The unknown parameters

The known parameters are parameters that can be found in the engine specifications or academic literature, some examples are: cylinder bore, number of cylinders, gas properties, etc.

The arbitrary parameters are parameters that are not known for the specific engine but their trends can be captured by expressing them in dimensionless numbers. These parameters are invariant when expressed in dimensionless relations. For example, some dimensions of the engine components are not available in the specification but can be scaled in relation to the bore, stroke and number of cylinders. A specific example is the valve diameter, which can be determined in relation to the bore diameter.

The unknown parameters are a set of parameters that cannot be found in specifications or literature, nor can it be defined by set scaling relations. Finding these parameters is the most difficult aspect of modeling a new engine with the Diesel B model. Stapersma [19] proposes a combination of calibrating rules to find these unknown values for the Diesel B model. However this procedure requires a lot of trial-and-error through manual iteration. This procedure is very time consuming because the user has to spend considerable time and effort to analyze the outcome of each unique set of unknown parameters. This whole process complicates the usage of the Diesel B model, which in its operation is already quite complex.

The author has developed a procedure that partially automates the calibration of the unknown parameters. The method still depends on trial and error but rather than analyzing the outcome of each and every experiment, the outcome of multiple experiments is convoluted into a set of statistical indicators. This allows the user to run a large combination of unique parameter sets and analyze the outcome of all these simulations with only a handful of "quality of fit" indicators. This procedure has been derived from the "Design of Experiments method" as postulated by Fisher [7]. A full description of this method and its application to the Diesel B unknown parameters can be found in appendix F. This method has been used to evaluate in excess of 25.000 unique combinations of the unknown parameters for the Diesel B model.

Throughout this report there will be mention of observed data sets for the purposes of calibration, result comparison and validation. A detailed explanation of the data sets can be found in appendix H. Two separate data sets are used, each for a specific purpose:

- The Lloyds data set: This is a data set with a rich selection of observed parameters. This data set was constructed by measuring the average steady state operation of the engine on a water-brake bench test. Six operating points where recorded, these will be used to compare the steady state performance of the engine models. This set is also used in the calibration process of the Diesel B engine model.
- The Sea Trial data set: This set is recorded on board of the Indonesian TNI ship Diponegoro during continous operation. It captures transient operation of the ship where a load step is applied to accelerate the vessel from 0% propulsion load to 99% propulsion load. Unfortunately the set does not contain as much parameters as the Lloyds data set. This data set will be used to compare the transient performance of the engine models.

For the application of the Diesel B engine model it is not necessary for the reader to read the details of the calibration process. However, It is important for the reader to know that this method fits the unknown parameters in such a way that the model offers a solution for the minimal steady state average error in relation to the Lloyds data set. This is an arbitrary choice made by the author and the impact of this choice will be reflected upon later in the report during model validation.

During this calibration, it was found that the charge air cooler model in the original Diesel B model did not produce the trends that were expected. This has prompted the author to launch an investigation into an alternative charge air cooler model to better suit the performance trends. This model is discussed in the next chapter.

4 Alternative charged air cooler model

4.1. Observed problem with the original charge air cooler model

For the calibration process of the Diesel B engine model, the simulation results are compared to an observed data set from a bench test; the Lloyds data set. All of the components of the Diesel B model show the expected trends except for the charged air cooler.

The outlet temperature of the air leaving the charged air cooler does not comply with the expected trend. This gave reasonable cause for concern and justified a separate investigation into the charged air cooler sub model.

This chapter outlines the working principles of the charged air cooler model that is currently used in the Diesel B model, followed by an analysis on the output of this model. An alternative model based on a different heat exchange calculation method is presented afterwards. The report is concluded with a reflection on both models and a choice of which model will be used in the sequentially turbocharged Diesel model.

4.2. Diesel B charged air cooler model theory and application

The charged air cooler model in the Diesel B model consists of two sub models:

- Air mass flow model: a model to determine the mass flow of air through the charged air cooler.
- Heat exchanger model: a model to determine the heat exchange between the hot air and the cooling water and determine the resulting air exit temperature.

These sub models are explained in detail in the following sub sections.

4.2.1. Air mass flow model

The air mass flow model is based on the flow equation for subsonic flow through an orifice plate. This is a well-studied relation in the field of aerodynamics; the same method is used for other subsonic restrictors like the air filter and silencer volume. a detailed derivation of this relation is given in appendix E.

However, the erroneous trend in the charged air cooler model is the outlet temperature. Therefor it is likely that the problem is not the mass flow but the heat exchanger model.

4.2.2. Heat exchanger model

The heat exchanger model is based on a dual pass heat exchanger. In this type of heat exchanger the fluids pass each other multiple times with different intermediate temperatures to optimize the overall heat transfer effectiveness. A schematic overview of the heat exchanger model is given in figure 4.1.

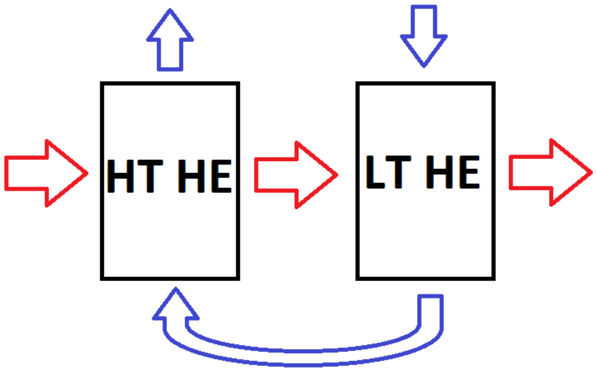

Figure 4.1: A schematic overview of the low and high temperature dual-pass heat exchanger.

This model provides a high level of detail for the charged air cooler, however this comes at a cost. The implementation of a multi pass system also brings the need to know the intermediate temperatures for calibrating the model. In most cases this data is not available and has to be estimated.

The heat transfer coefficient of each of the two heat exchangers is determined by calculating the Nusselt number. The Nusselt number is a dimensionless number that represents the ratio of convective to conductive heat transfer across the boundary of a fluid. For different types of heat exchangers, the Nusselt number can be determined by an empiric relation with other dimensionless flow groups: the Reynolds and Prandt numbers. For the low temperature and high temperature heat exchanger models (LTHE and HTHE), the following relations are applied [12]:

Dimensionless numbers, Nusselt, Reynolds, Prandtl:

$$\mathrm{Nu} = \frac{h \cdot L}{\kappa} \tag{4.1}$$

$$\mathrm{Re} = \frac{\rho \cdot V \cdot L}{\mu} \tag{4.2}$$

$$\mathrm{Pr} = \frac{c_p \cdot \mu}{\kappa} \tag{4.3}$$

Empiric Nusselt number relations:

$$\mathrm{Nu} = 0.023 \cdot \mathrm{Re}^{0.8} \cdot \mathrm{Pr}^{0.3} \tag{4.4}$$

$$\mathrm{Nu} = 0.023 \cdot \mathrm{Re}^{0.8} \cdot \mathrm{Pr}^{0.4} \tag{4.5}$$

With the Nusselt number it is possible to calculate the convective heat transfer coefficient of both fluids. The convective heat transfer coefficient determines the thermal resistance for heat to transfer from the bulk of the fluid to the wall:

$$h = \frac{\mathrm{Nu} \cdot \kappa}{L} \tag{4.6}$$

The transferred heat has to pass through a wall through conduction. The wall's thermal conductivity determines the thermal resistance over the wall itself. Together with the convective resistance of the fluids a thermal network can be constructed, see figure 4.2:

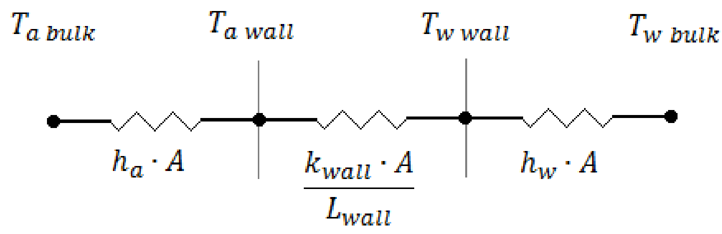

Figure 4.2: A thermal network for the heat transfer of fluids through a wall.

With this method it is possible to determine not just the bulk temperature but also the intermediate wall temperatures. As with the multi-pass HE system, this method provides a high level of detail at the cost of needing more data to determine the model parameters.

The water at the inlet has a constant temperature and the mass flow of water is dependent on the engine speed. The mass flow of water is given by:

$$\dot{m}_w = \dot{m}_{w\_nom} \cdot \left(\frac{n_{eng}}{n_{eng\_nom}} \right)^3 \tag{4.7}$$

4.3. Isolated model investigation of Diesel B charged air cooler model

The charged air cooler model has been taken out of the Diesel B model and tested in an isolated environment. The observed data points from the bench test are imposed on the model input and the output is compared to the same parameters in the data set.

A constant water inlet temperature is used in the original model. A correction has been performed on the inlet temperature, with a look-up table; the observed cooling water temperature is used instead of a constant value.

Several simulations with different model parameters have been evaluated with both a constant and a corrected cooling water entry temperature; the best result of these is presented in figure 4.3:

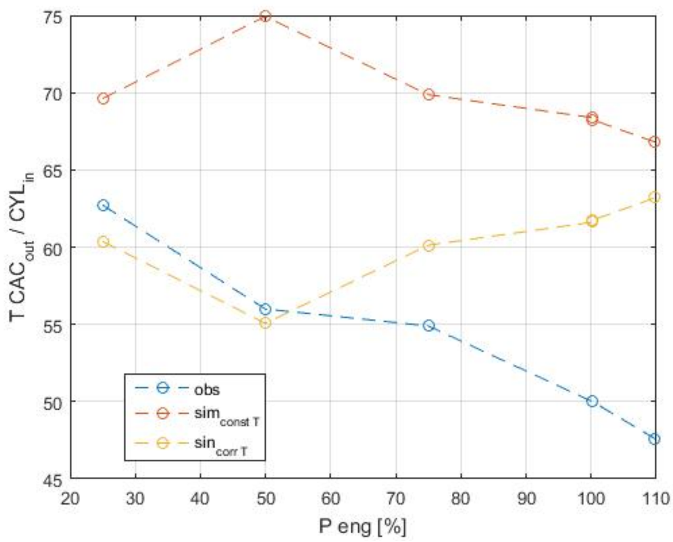

Figure 4.3: Charged air cooler outlet temperature, observed and simulated results for constant and corrected water inlet temperature.

Figure 4.3 shows that the model does not produce a satisfying result. An alternative model will be investigated instead of trying to fit all of the different model parameters. There are simply too many unknown parameters to justify the use of this model.

4.4. Alternative model

The proposed alternative charged air cooler model is a simpler implementation than the original air cooler model applied in the Diesel B model. It uses the same principle for the mass flow model, but the heat exchanger is modeled with a simpler method.

The charged air cooler model calculates the air temperature change as a result of the heat exchange between the hot compressed air and the cold cooling water. There are various ways to approach a solution when analyzing the thermal performance of a heat exchanger, the two methods of interest are the Log mean Temperature Difference (LMTD) and the effectiveness-Number of Transfer Units (NTU) methods [12]. Both share common parameters and concepts and will arrive at the same solution to a heat exchanger thermal capacity. In general terms, the LMTD method is used to calculate the geometry of a heat exchanger given certain end conditions and the NTU method is used to calculate the end conditions for a given geometry. Both methods and their application in the model will be explained in more detail.

4.4.1. The LMTD Method

The LMTD method is the most commonly known method to analyze heat transfer in heat exchangers, it is the logarithmic average of the temperature difference between the hot and cold fluid. It is applicable to both counter and co-current flow arrangements. The definition of the LMTD is:

$$\text{LMTD} = \frac{\Delta T_h ot - \Delta T_c old}{\ln\left(\frac{\Delta T_h ot}{\Delta T_c old}\right)} \tag{4.8}$$

The LMTD can be used to calculate the heat capacity of a heat exchanger as follows:

$$Q = U \cdot A_{HE} \cdot \text{LMTD} \tag{4.9}$$

To calculate the heat transfer duty it is necessary to know the geometry, the heat transfer coefficient and the temperatures at the entry and exit for both fluids. The exit temperature of the hot stream (air) is the parameter of interest, making the LMTD method inapplicable for continuous simulation. However, it is used to calculate the geometry of the heat exchanger by using the fact that the parameters in the nominal operating point are known or estimated. If the temperature change and the mass flow of the air are known in nominal operation, it is possible to calculate the amount of heat rejected by the air:

$$Q = \dot{m}_{air} \cdot c_{p\_air} \cdot \Delta T_{air} \tag{4.10}$$

The heat rejected by the air is absorbed by the water:

$$Q = \dot{m}_{water} \cdot c_{p\_water} \cdot \Delta T_{water} \tag{4.11}$$

This allows for the calculation of the mass flow or temperature change in the water. If one of these parameters is known the other can be calculated. With the heat transfer duty and all four temperatures known it is now possible to calculate the geometry and heat transfer coefficient by combining equations 4.8, 4.9 and 4.10:

$$U \cdot A_{HE} \cdot \text{LMTD} = \dot{m}_{air} \cdot c_{p\_air} \cdot \Delta T_{air} \tag{4.12}$$

$$UA = U \cdot A_{HE} = \frac{\dot{m}_{air} \cdot c_{p\_air} \cdot \Delta T_{air}}{\text{LMTD}} \tag{4.13}$$

The heat transfer area and coefficient are lumped together into one parameter: UA. Both of these values are constant values and are always used in conjunction. When designing a heat exchanger they offer information about the actual size of the heat exchanger. When analyzing the thermodynamic performance of the heat exchanger it is not necessary to know the individual contribution of the geometry and heat transfer coefficient to UA.

4.4.2. The effectiveness-NTU Method

The Effectiveness-NTU method takes a different approach to solving heat exchange analysis by using three dimensionless parameters: heat capacity rate ratio, heat exchanger effectiveness, and Number of Transfer Units (NTU). The relationship between these three parameters depends on the type of heat exchanger and the internal flow pattern.

The first dimensionless parameter is the heat capacity rate ratio, the ratio of the minimum to the maximum value of heat capacity rate for the hot and cold fluids. The heat capacity rate of a fluid is a measure of its ability to release or absorb heat. The heat capacity rate is calculated for both fluids as the product of the mass flow and the specific heat capacity of the fluid.

$$C = \dot{m} \cdot c_p \tag{4.14}$$

The heat capacity rate ratio is calculated by dividing the smaller heat capacity rate by the larger one, this ensures that R is defined between 0 and 1:

$$R = \frac{C_{min}}{C_{max}} \tag{4.15}$$

The second parameter, effectiveness, is defined as the ratio of the actual heat transfer rate to the maximum possible heat transfer rate for the given flow and temperature conditions:

$$\xi = \frac{Q}{Q_{max}} \tag{4.16}$$

The maximum possible heat transfer rate is achieved if the fluid with the lowest heat capacity rate experiences the maximum temperature difference across the heat exchanger:

$$Q_{max} = C_{min} \cdot \Delta T_{max} \tag{4.17}$$

$$\Delta T_{max} = T_{hot\_in} - T_{cold\_in} \tag{4.18}$$

The last dimensionless parameter, the Number of Transfer Units, is the ratio of the heat exchanger's ability to transfer heat to the fluid's minimum ability to absorb heat:

$$\mathrm{NTU} = \frac{UA}{C_{min}} \tag{4.19}$$

Notice that the value of UA is the same as calculated with the LMTD method in equation 4.13. The relationship between the three parameter groups of the NTU method is tabulated for different types of heat exchangers. For the air cooler model an unmixed cross-flow arrangement is considered, the effectiveness/NTU relation for this type of heat exchanger is given in figure 4.4:

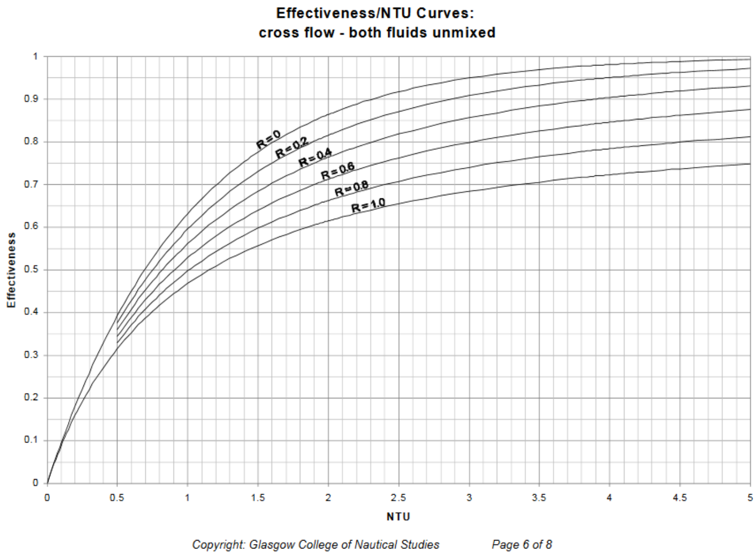

Figure 4.4: Effectiveness – NTU curves for a cross flow heat exchanger (source: Glasgow College of Nautical Studies).

The curves in figure 4.4 have been fitted to an asymptotic function:

$$\xi = 1 - \exp\left(A_1 \cdot \mathrm{NTU}^{A_2}\right) \tag{4.20}$$

$$A_i = a_{i1} + a_{i2} \cdot R + a_{i3} \cdot R^2, \qquad i = 1, 2... \tag{4.21}$$

The coefficients are fitted with Matlab's curve fitting tool and provide the following result, figure 4.5:

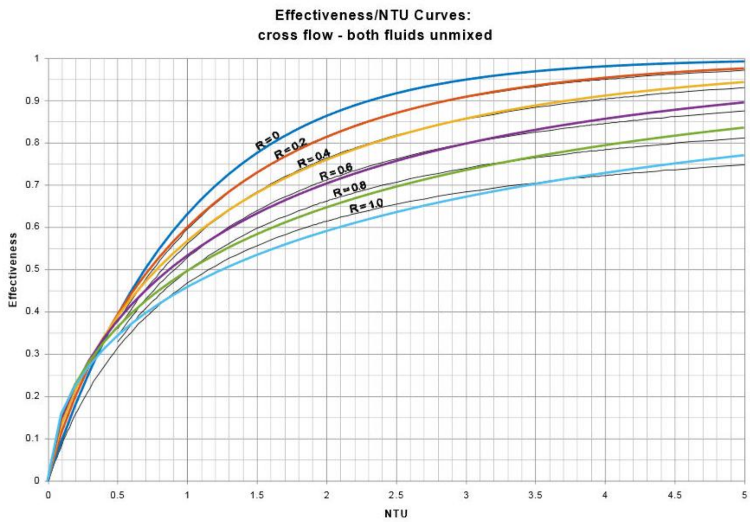

Figure 4.5: Comparison of proposed equation to the graphical data (source of underlying image: Glasgow College of Nautical Studies).

An asymptotic logarithmic function was chosen to reflect the logarithmic characteristic of the driving force in a heat exchanger, the LMTD. The quality of the fit degrades for higher heat capacity ratios. For typical air cooler arrangements the value of R is in the range of 0.01 to 0.3 and operates at a Number of Transfer Units higher than 1.5. For this region the proposed equation provides a very good fit to the original graph.

The Simulink model uses these NTU-curves to find the effectiveness corresponding to the current R and NTU. The amount of heat rejected by the air can be calculated with the effectiveness and the entry temperature of both the air and cooling water.

The Simulink model of the heat exchanger is shown in figure 4.6.

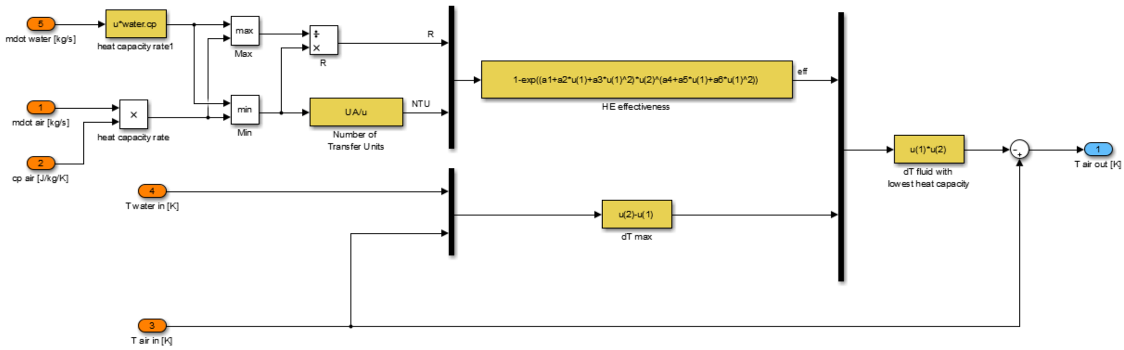

Figure 4.6: An overview of the air cooler sub-model

The mass flow of water is modeled the same as in the Diesel B charged air cooler, equation 4.7, and the temperature is corrected with the observed cooling water temperature, both dependent on engine speed.

4.5. Isolated model investigation of alternative charged air cooler model

The alternative model has been tested under the same external conditions as the regular diesel B model. The results of these experiments are presented in figure 4.7:

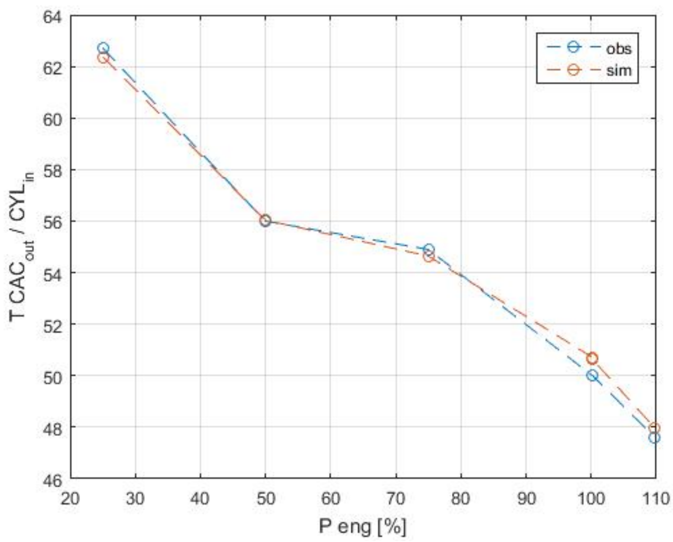

Figure 4.7: Results of the alternative charged air cooler model plotted with the observed data set.

Although the alternative model is much simpler, it provides much better results than the original charged air cooler model. This is surprising since one would expect the simpler model to capture the trend but not as accurate as is the case in figure 4.7. These results are further analyzed and compared to the Diesel B charged air cooler model in the sub-conclusion of this chapter.

4.6. Sub-conclusion

The two charged air cooler models presented in this report both have a useful application. The choice of which charged air cooler model to use is dependent on the required level of detail. The original charged air cooler model is much more encompassing than the alternative NTU model, however this comes at a price. The original model needs a lot more information to calibrate it correctly. An overview of the required calibration parameters is given in table 4.1:

Table 4.1: Listing of the required parameters for calibration.

Diesel B charged air cooler model	**Alternative charged air cooler model**
nom. T air at LTHE inlet	nom. T air at inlet
nom. T air at LTHE outlet	nom. T air at outlet
nom. T water at LTHE inlet	nom. T water at inlet
nom. T water at LTHE outlet	nom. T water at outlet
nom. T air at HTHE inlet	nom. p air at inlet
nom. T air at HTHE outlet	nom. p air at outlet
nom. T water at HTHE inlet	
nom. T water at HTHE outlet	
nom. p air at inlet	
nom. p air at outlet	
hydraulic diameter air side LTHE	
hydraulic diameter water side LTHE	
hydraulic diameter air side HTHE	
hydraulic diameter water side HTHE	
nom. Velocity air side LTHE	
nom. Velocity water side LTHE	
nom. Velocity air side HTHE	
nom. Velocity water side HTHE	
wall thickness LTHE	
wall material LTHE	
wall thickness HTHE	
wall material HTHE	

The alternative model uses an overall heat transfer capacity; it is not divided into smaller parts to see the individual contribution of each of the heat transfer modes (convection hot-side, conduction wall, convection cold-side). This makes the model a lot simpler to calibrate, it can be calibrated with the nominal point parameters. Whereas the original Diesel B model also requires material and geometric parameters to be known or estimated.

The results of the Diesel B charged air cooler model (with constant and corrected temperature) and the alternative model are shown together in figure 4.8:

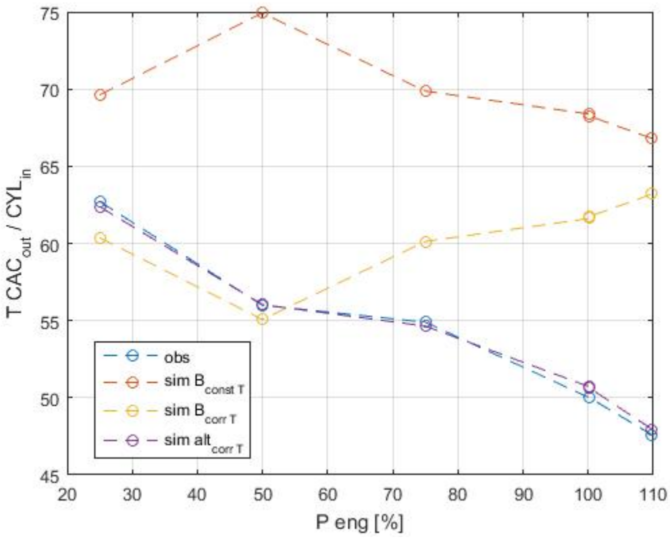

Figure 4.8: Results of all model evaluations.

From figure 4.8 it becomes clear that the alternative model is able to provide better results with the added benefit that it is much easier to calibrate and use.

The average error is calculated with the root mean square error (RMSE) and the normalized root mean square error (NRMSE), these statistical indicators are explained in detail in appendix F. These indicators are displayed in table 4.2

Table 4.2: Error indicators for both models.

	RMSE	**NRMSE**
Original model – constant temp	16.68 K	110.5 %
Original model – corrected temp	9.58 K	63.4 %
Alternative model – corrected temp	0.449 K	2.98 %

In light of the findings in this chapter, the alternative charged air cooler model will replace the current model for all Diesel engine models that are presented in this report. The simpler model has better results than the complex model, there is no justifiable reason to keep the current charged air cooler model and not use the alternative.

5

The Simple STC model

The Diesel B model with a single turbocharger was presented in chapter 3. Two models have been created based on the Diesel B model to simulate sequentially turbocharged engines: the "Simple STC model" and the "Full STC model". The Simple STC model is presented in this chapter and the Full STC model will be presented in the following chapter. The Simple STC model gets its name from the simple implementation in Simulink, which literally requires only 2 multiplication blocks to be added to the original Diesel B model.

5.1. Model hypothesis

The Simple STC model relies on the idea that the characteristics of both turbochargers can be modeled with the permanent turbocharger. When there is only one turbocharger active, this turbocharger is modeled in the same way as the original Diesel B engine. This comes as no surprise since the Diesel B model is constructed with a single turbocharger.

When the second turbocharger is connected in parallel, the two turbochargers each show the same characteristics in comparison to each other. This is due to the fact that they are of the same type and size and they are also connected to the same volumes, meaning they are operating under the same boundary conditions. As a result, both turbochargers are delivering an equal amount of mass of combustion air to the engine.

The statement above is captured in the following assumptions that are used to construct the model:

- In single turbocharger operation, a single turbocharger supplies the full air demand of the engine.
- In dual turbocharger operation, each turbocharger supplies exactly the half of the air demand.
- In dual turbocharger operation, both turbochargers operate on the same inlet and outlet conditions.
- In dual turbocharger operation, both turbochargers operate on the same speed, the two turbocharger shafts are virtually connected with a 1:1 ratio.

These assumptions will be evaluated in the sub conclusion section at the end of this chapter. By comparing the results of the model against the observed data sets of the real engine, it will be possible to present a qualitative analysis of the trends and a quantitative analysis of the absolute and relative error.

5.2. Model implementation

The assumptions that were postulated in the previous section can be used to define the mass flow of the compressor and turbine for both single and dual turbocharger operation. These relations and their derivations are explicitly stated in the following equations:

The total combustion air mass supplied to the engine:

$$\dot{m}_{eng\_in} = \dot{m}_{com\_A} + \dot{m}_{com\_B} \tag{5.1}$$

The mass flow through each compressor is a function of the speed at which it rotates and the state properties of the volumes it is connected to:

$$\dot{m}_{com\_i} = f(X_i) \tag{5.2}$$

$$X_i = (n_{tc\_i}, p_{out\_i}, p_{in\_i}, T_{in\_i}, x_{in\_i}) \tag{5.3}$$

For single turbocharger operation, equation 5.1 reverts to:

$$\dot{m}_{eng\_in} = \dot{m}_{com\_A} + 0 = 1 \cdot \dot{m}_{com} \tag{5.4}$$

For dual turbocharger operation, equations 5.1 and 5.2 are combined:

$$\dot{m}_{eng\_in} = \dot{m}_{com}(X_A) + \dot{m}_{com}(X_B) \tag{5.5}$$

Both compressors use the same algebraic function, meaning that they produce the same output if the same input is given. The assumptions stated that the boundary conditions for both turbochargers are the same in dual turbocharger operation. With this information, equation 5.5 reverts to:

$$X = X_A = X_B \tag{5.6}$$

$$\dot{m}_{eng\_in} = \dot{m}_{com}(X) + \dot{m}_{com}(X) = 2 \cdot \dot{m}_{com} \tag{5.7}$$

The same derivation is made for the turbine side, resulting in equation 5.8 for single turbocharger operation and equation 5.9 for dual turbocharger operation:

$$\dot{m}_{eng\_out} = 1 \cdot \dot{m}_{tur} \tag{5.8}$$

$$\dot{m}_{eng\_out} = 2 \cdot \dot{m}_{tur} \tag{5.9}$$

Equations 5.1 untill 5.9 show that the mass flow of the compressor and turbine can be multiplied by 1 or 2 for the same pressure ratio and turbocharger speed to simulate single or dual turbocharger operation. This doubles the mass flow of the compressor and turbine of the permanent turbocharger, in a way that it acts as if the mass flow of the switchable turbocharger is virtually imposed on the permanent turbocharger.

For calibration of the model, the compressor and turbine of the turbocharger have to be matched to provide only half of the required nominal engine air demand at their nominal operating point. In the standard Diesel B engine, the compressor and turbocharger are always matched to provide the full air demand.

In the Simulink model, the sequential turbocharging implementation is simple but very effective. Details of this implementation can be seen in figures 5.1a and 5.1b. The details of the overall model are not important, this figure is only shown to display the simplicity of the model implementation; the green outlined box shows the section that has been modified. In both cases the mass flow calculated by the mass flow sub-model is multiplied with a variable that takes the value 1 or 2, depending on the type of TC operation. With this simple implementation, the total mass flow is now captured in the permanent turbocharger.

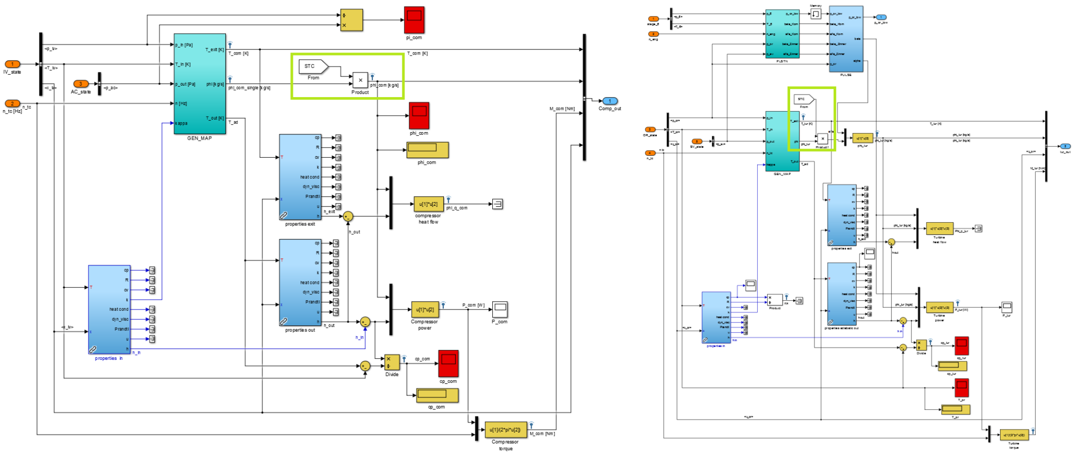

(a) compressor sub-model (b) turbine sub-model

Figure 5.1: A detail of the sequential turbocharger implementation in the Diesel B model.

The STC variable is a control parameter that is activated by comparing the engine speed and turbocharger speed to pre-set switch over points. Figure 5.2 shows the operating map of the Pielstick PA6 and the regions in which the type of turbocharger operation is defined, a larger version of this figure is available in appendix A. The blue and green regions are the regions where dual TC operation is used. When switching from 1 to 2 turbochargers, the green region is used to determine when to switch on the second turbocharger. When switching from 2 to 1 turbocharger, the blue region is used to switch off the second turbocharger. The different switching on and off regions create a hysteresis loop. This prevents unnecessary on and off switching of the turbochargers when traversing through this region. Figure 5.2 also shows the activation region of the bypass valve over the engine. This valve is open below approximately 80 % of the engine power and closes above this value. The bypass valve is installed to prevent "hunting" of the turbochargers. This is the effect that occurs when the engine is too restrictive for the air flow and the two turbochargers start discharging mass into each other which results in oscillating turbocharger performance. The by-pass valve offers a "path of least resistance" for the air flow, preventing this undesired effect. The by-pass valve is already part of the original Diesel B model.

Figure 5.2: Operating map of the Pielstick PA6B V20 engine on board the SIGMA corvettes (source: DSNS).

The control strategy for determining when to switch the turbochargers depends on three different variables:

- The amount of turbochargers currently in operation.

- The speed of the permanent turbocharger.
- The speed of the engine.

The control strategy depicted in figure 5.2 can be replicated with a set of logical relations between the control variables. These relations are given in the following pseudo-code:

if $STC = 1$ *(in dual turbocharger operation)*
    if *(n_eng <750 rpm* ***OR*** *n_tc <16000 rpm)*
        $STC = 0$ (set to single turbocharger operation)

else if $STC = 0$ *(in single turbocharger operation)*
    if *(n_eng >780 rpm* ***AND*** *n_tc >24500 rpm)*
        $STC = 1$ (set to dual turbocharger operation)

This control strategy is implemented in Simulink by using the same logical relations; the control sub system is shown in figures 5.3 - 5.5.

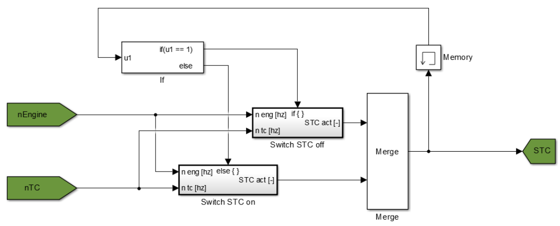

Figure 5.3: Top level of the turbocharger control sub system.

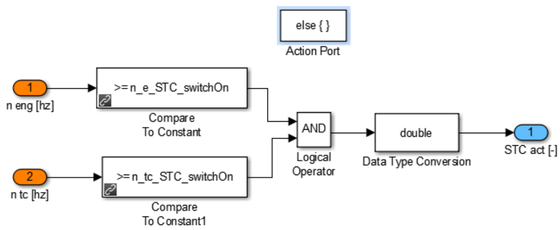

Figure 5.4: Subsystem for switching from single to dual turbocharger operation, logical AND operator.

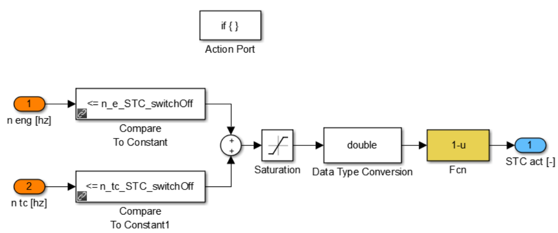

Figure 5.5: Subsystem for switching from dual to single turbocharger operation, logical OR operator.

This concludes the implementation of the Simple STC model, in the following sections the model will be evaluated and its outcome will be discussed.

5.3. Steady state analysis

First of all it is important to evaluate the steady state performance of the engine. For the mean value Diesel engine, steady state is defined as follows:

> *The model has reached steady state equilibrium if all the integrators of the time derivatives output a constant value that does not change over time.*

Evaluating the model at steady state removes many of the processes that are dependent on time, for instance the time delay in the interaction between the turbocharger and the engine. Removing the time dependencies of the model allows for the model output to be analyzed in comparison to certain indicative engine parameters instead of simulation time, some examples of these parameters could be:

- Engine power, absolute / relative
- Engine speed, absolute / relative
- Fuel rack, absolute / relative
- Boost pressure, absolute / relative

The benefit of relating engine parameters to, for example, the relative engine power is that the engine parameters can be easily compared to other engine types. Another benefit is that the engine parameters can be related to a practical indicator like the fuel rack. The position of the fuel rack can be easily monitored on board of the vessel during operation and can give the engine mechanic direct feedback on what the other parameters should look like.

Another benefit of steady state analysis is that it excludes the time dependent parameters that need to be calibrated. In the Diesel engine model, these parameters are: the masses of engine components, rotational inertia of shafts and volumes of the volume elements. These parameters act as a time delay on the integrators and since the integrators output a constant value at steady state, the time they take to reach this state is irrelevant.

5.3.1. Method

The top level of the diesel engine requires two inputs and produces one output; the inputs are: engine speed and fuel rack position; the output is engine torque. The fuel rack position input can be seen as an external input that is set by the operator. The engine speed input is the result of the interaction between the engine and the load that it is coupled to.

The engine speed can be calculated with the use of Euler's rotation equation for rigid bodies, equation 5.10:

$$M = I \cdot \dot{\omega} \tag{5.10}$$

The net resulting torque is a sum of the engine and load torque of which both are dependent on engine speed and only the engine torque is dependent on the fuel rack position, equation 5.11:

$$M = M_{eng}(n_{eng}, X_{fuel}) - M_{load}(n_{eng}) \tag{5.11}$$

Equations 5.10 and 5.11 are combined to form a first order differential equation that is dependent on the engine speed:

$$I \cdot \dot{\omega} = M_{eng}(\omega, X_{fuel}) - M_{load}(\omega) \tag{5.12}$$

Finding the engine speed for steady state becomes a Cauchy problem (initial value problem) and can be solved with ordinary differential equation solvers. This is done in the Simulink environment, where essentially the complete model is a very large differential equation with many states.

The fuel rack position can be either controlled directly or through a PID controller (governor). When controlled through the governor, the fuel rack position is set in such a way that the engine runs at a required engine speed. This is achieved by using a feedback loop where the engine speed is compared to a required set point. For the steady state analysis this controller is not needed and the fuel rack is controlled manually.

To simulate a large amount of operating points it is necessary to do equally large amounts of simulations. This is undesired and luckily there are ways to cope with this problem; by using a quasi-steady state method. This is achieved by changing the fuel rack very slowly over a large span of time, making it is possible to simulate a very gentle transition of one operating point to the next. This effectively creates an operating line of steady state operating points. For this simulation, the fuel rack is gradually reduced from 110% to 25% over 60000 seconds. This process is much slower than any of the other transitional effects in the engine, generally in the order of 6-60 seconds.

The steady state results are compared to the Lloyds data set, this data set was logged on a bench test where the engine was connected to a water brake. This water brake has the same characteristics as a fixed pitch propeller and operates on the so-called "propeller curve". This means that the torque of the load is scaled to the speed with the power of two, equation 5.13:

$$M_{load} = M_{load\_0} \cdot \left(\frac{n_{eng}}{n_{eng\_0}} \right)^2 \tag{5.13}$$

In appendix C, a steady state analysis is performed with a different load curve. Instead of the propeller law curve of equation 5.13, the maximum allowable torque from the manufacturer's torque envelope is used. This analysis provides some insight into how the engine performs when operating at the maximum limit.

5.3.2. Switching between single and dual turbocharger operation

An important aspect of the sequentially turbocharged engine is the process where the switchable turbocharger is switched on or off. This is what distinguished the sequentially turbocharging strategy from regular turbocharging. However, it is important to realize that this is a transient effect; as the turbocharger is switched on or off, the steady state operating point has to shift from one turbocharger operation to the other.

Even worse is the fact that the turbocharger switching on and off regions are also dependent on whether the load is increasing or decreasing. When the load is increasing, turbocharging operation goes from one to two turbochargers and vice versa when the load is decreasing. This creates a region where two possible solutions exist for steady state, this is shown in figure 5.6.

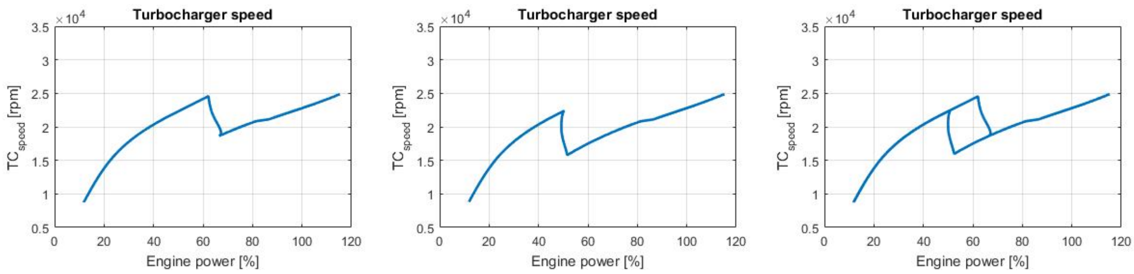

(a) Increasing load. (b) Decreasing load. (c) Both transitions.

Figure 5.6: Steady state turbocharger speed with switching for both increasing and decreasing load.

Figure 5.6 shows the turbocharger speed of the model, it can be witnessed that the switching strategy results in different switching points depending on the direction of the load. In figure 5.6a the switchable turbocharger is switched off at 67.3 % engine power. In figure 5.6b the switchable turbocharger is switched on at 50.5 % engine power. Figure 5.6c shows both lines in the same graph, it can be witnessed that three different regions can be defined:

- below 50.5 % engine power, a single turbocharger is in operation.
- above 67.3 % engine power, two turbochargers are in operation.

- above 50.5 % engine power and below 67.3 % engine power, the turbocharging mode depends on the current turbocharging mode.

These three regions are shown with vertical lines in figure 5.7a:

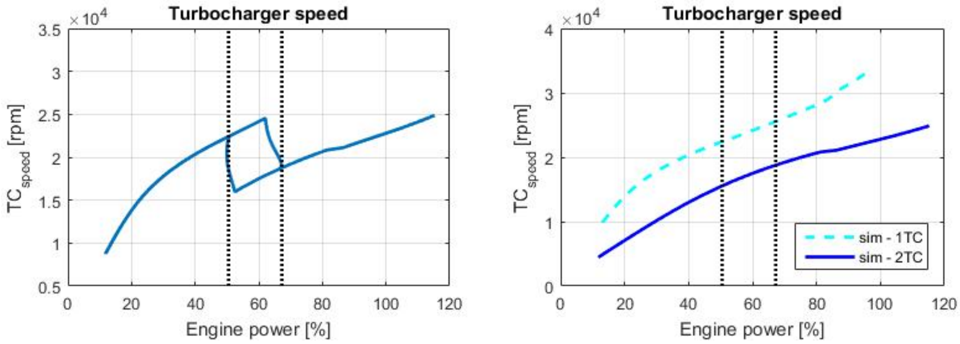

(a) With switching. (b) Without switching.

Figure 5.7: Three different regions of turbocharger modes.

Because of the transient effects when switching and the undefined area where both turbocharger modes can exist, an alternative method needs to be used to display the results of the steady state analysis.

The model is evaluated for both turbocharger operations across its entire operating spectrum. This achieved by simulating the engine with a single turbocharger (STC = 0) for the full range of the fuel rack, from 110% to 25%. The data is stored and the simulation is repeated but this time for dual turbocharger operation (STC = 1). The data from both sessions is presented in the format of figure 5.7b, where the result of both turbocharger modes is presented along with the dividing regions as defined above. This gives a clear insight into the benefits and drawbacks of each turbocharger operational mode. These results are presented and analyzed in the following section

5.3.3. Results

The steady state results of the Simple STC model simulation are plotted together with the six operating points of the Lloyds data set. Obviously this can only be done for the parameters that where recorded in this data set. The model also calculates other parameters that where not recorded but are interesting to analyze because they give more insight into the thermodynamical processes in the engine. These will be presented after the plots of the Lloyds data set. All plots are using the relative engine power in % for their x-axis, this is common practice for combustion engine analysis; it allows for the comparison of engine parameters of engines with different sizes.

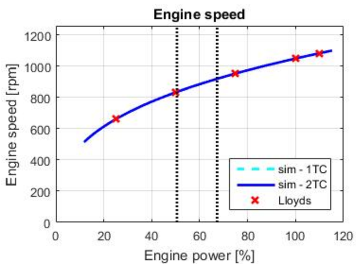

Figure 5.8: Steady state simulation result: engine speed.

The engine speed is a direct result of the propeller law that was given in equation 5.14. It comes as no surprise that the model follows this curve since the load is imposed on the engine model, however figure 5.8 does confirm that the Lloyds test bench water brake follows the same propeller curve.

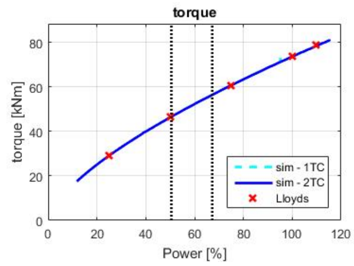

Figure 5.9: Steady state simulation result: engine torque.

The engine torque is on the propeller law as expected, the same conclusion holds as for figure 5.8, the Torque shown in figure 5.9 is a direct result of the propeller law from equation 5.13.

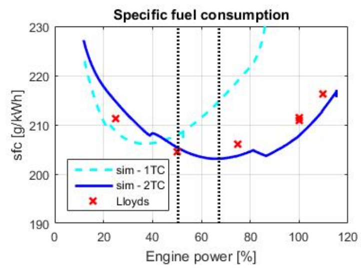

Figure 5.10: Steady state simulation result: specific fuel consumption.

The specific fuel consumption is a culmination of many different engine parameters. Ultimately it is determined by the total engine efficiency and the fuel properties. In the diesel B model, the total engine efficiency is built up of a collection of specific efficiencies. Unfortunately these weren't measured and this leaves the specific fuel consumption as an indicator for the engine efficiency. It can be seen that the trends are matching but that there is some error for both single and dual turbocharger operation. The transition at 80% engine power is a result of the by-pass valve closing/opening.

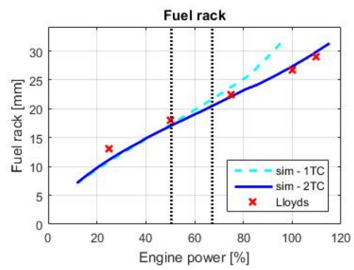

Figure 5.11: Steady state simulation result: fuel rack.

The fuel rack position is directly related to the fuel flow into the engine. Nothing peculiar can be seen in comparison to the recorded data other than the simulation for single turbocharger operation is slightly to low. Other than that the model follows the trends.

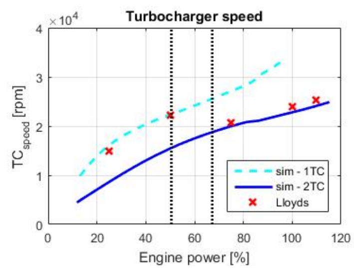

Figure 5.12: Steady state simulation result: turbocharger speed.

The turbocharger speed was already briefly shown in sub section 5.3.2, this time the Lloyds data is included. It can be witnessed that the simulated turbocharger speed is slightly to low for dual- and slightly to low for single turbocharger operation. The trends of both operational modes do seem to follow the expected behavior. This will be revisited in figure 5.25 where the compressor map is shown.

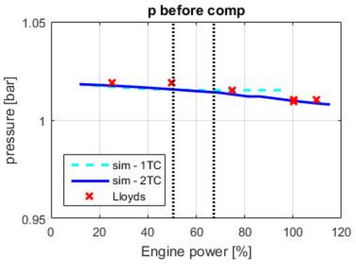

Figure 5.13: Steady state simulation result: compressor entry pressure.

The compressor entry pressure is a result of the combustion air mass flow drawn in by the compressor and the restrictive property of the air filter. Due to the sucking action of the compressor it is lower than ambient pressure. The absolute differences between the model and the Lloyds set are very small and the model follows the record trend.

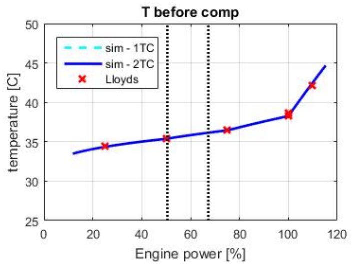

Figure 5.14: Steady state simulation result: compressor entry temperature.

The compressor entry temperature is the same as the ambient temperature because the air filter acts as an adiabatic nozzle. The ambient temperature from the Lloyds data set is imposed on the model through a look-up table to increase the accuracy of the comparison. The table performs linear interpolation on the values in between the recorded points. This explains the shape of the compressor entry temperature results.

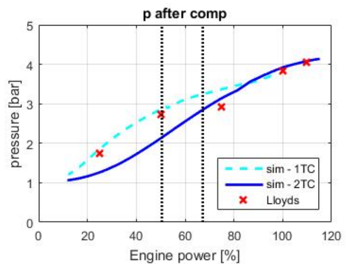

Figure 5.15: Steady state simulation result: compressor exit pressure.

The compressor exit pressure is slightly to high for both turbocharger modes. The trends are what is expected of a compressor on a turbocharged engine. It can be witnessed that the single turbocharger compressor is able to supply a much higher pressure in the low engine power range until it cuts off around 80 %. This has to do with the fact that the smaller turbocharger starts to choke at higher mass flows. This will become more apparent in figure 5.24.

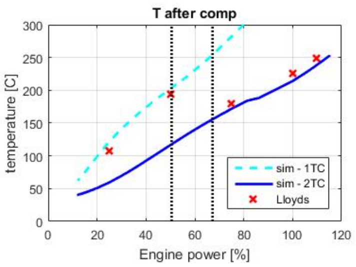

Figure 5.16: Steady state simulation result: compressor exit temperature.

The temperature of the air leaving the compressor is significantly hotter than the air entering it. The result for dual turbocharger operation is slightly to low where the results for single turbocharger operation is slightly to high. This effect was also seen in figure 5.12, the reason for these offsets will be explained in the validation of the steady state model. Single turbocharger operation results in a much higher temperature due to the higher pressure as seen in figure 5.15.

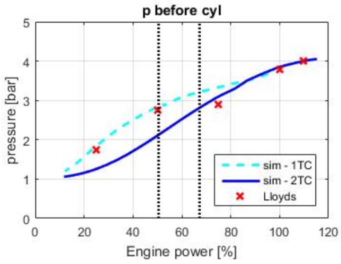

Figure 5.17: Steady state simulation result: charge pressure.

The charge pressure is the pressure of the gas measured in the inlet receiver after the air cooler and before the cylinder. It is practically the same as the compressor exit pressure from figure 5.15 but with the pressure loss over the air cooler included. This pressure loss is generally in the order of 100 mbar.

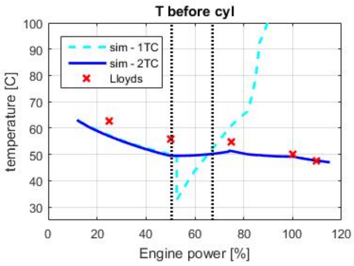

Figure 5.18: Steady state simulation result: charge temperature.

As with the charge pressure, the charge temperature is measured after the air cooler. Other than with the pressure, the air cooler has a significant effect on the temperature difference (this is its primary function after all). It can be seen that the alternative air cooler model presented in chapter 4 is able to produce the same trends as the Lloyds data set. The large spike in the single turbocharger operating line can be explained by the choked air mass flow, figure 5.24. The mass flow of the air is choked while the mass flow of water is still increasing, this makes the air cooler cool excessively (near 50% engine power). Above 65% the model operates in an unstable region, but normally dual turbocharging mode is used in this region, which does show the correct characteristic.

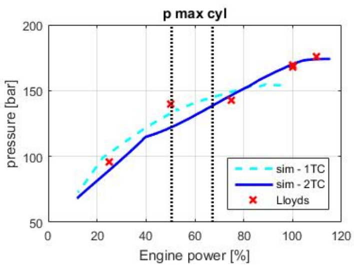

Figure 5.19: Steady state simulation result: maximum cylinder pressure.

The maximum cylinder pressure seems to match the recorded data points. The absolute error is very small and gives reason to believe that the trends are correct. Since this is the only in-cylinder measurement, not much can be said about it's accuracy because it cannot be directly related to other recorded values.

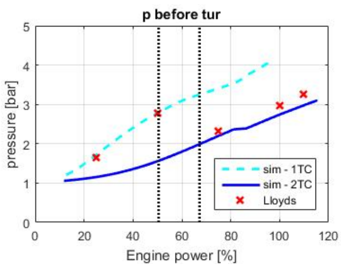

Figure 5.20: Steady state simulation result: turbine entry pressure.

The turbine pressure for single turbocharger operation is matching the recorded points almost perfectly, the simulation for dual turbocharger operation seems to be a bit too low. As with the compressor pressures, it can be witnessed that a single turbocharger is able to operate at higher pressures for low engine power.

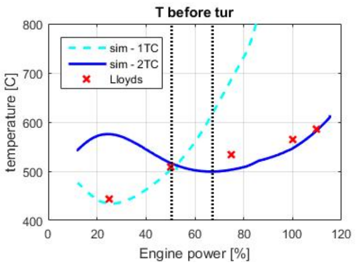

Figure 5.21: Steady state simulation result: turbine entry temperature.

The turbine entry temperature is heavily influenced by the combustion process of the engine. Normally this is coupled to the air excess ratio in the exhaust (lambda measurement) to make a detailed analysis of the combustion quality. Unfortunately the lambda measurement was not performed for the Lloyds data set. In general, it can be said that a lower turbine entry temperature is the result of a higher efficiency of the closed cylinder process. In figure 5.22 it can be witnessed that there is a cross-over point between the two operational modes. Below 50% engine power, using a single turbocharger results in lower turbine entry temperatures. Above 50% engine power this is true for dual turbocharger operation.

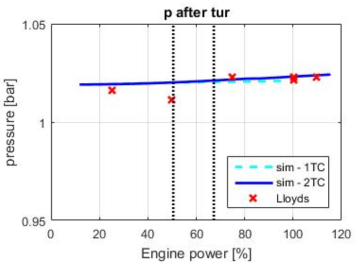

Figure 5.22: Steady state simulation result: turbine exit pressure.

As with the pressure that was measured before the compressor, figure 5.13, the turbine exit temperature is the result of the mass supplied by the turbine and the restrictive nature of the exhaust pipe. This time the volume has mass being blown into it, resulting in a pressure that is slightly higher than the ambient pressure.

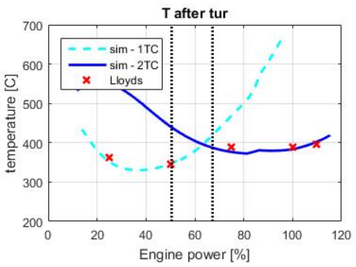

Figure 5.23: Steady state simulation result: turbine exit temperature.

The turbine exit temperature closely matches the recorder data points. This parameter also shows a cross-over point of the temperature in the turbocharger switching region; at a slightly higher power rating than for the entry temperature, 60% instead of 50 %. The lower exit temperature means that less heat is available in the exhaust gasses. This heat is used by the engine and thus the engine is more efficient.

This concludes all the parameters that where recorded in the Lloyds data set. The following figures are parameters that are calculated by the model but unfortunately not recorded. However they do provide insight and discussing them is vital to form a conclusion on the implementation of sequentially turbocharged engines.

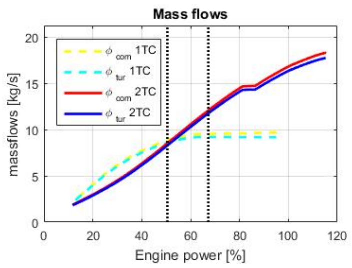

Figure 5.24: Steady state simulation result: mass flows.

The mass flow of the two different turbocharging operations give a very clear indication of why sequential turbocharging is applied to Diesel Engines. For low load, the single turbocharger is able to supply more air to the engine than two combined. However there exist a cross-over point where the single compressor is choking and the mass flow does not increase with an increase of the pressure ratio. Beyond this point the dual turbocharging strategy is able to supply more air to the engine.

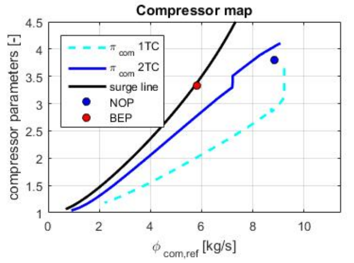

Figure 5.25: Steady state simulation result: compressor map.

The compressor map shows the same information as figure 5.24 but in figure 5.25 the mass flow is plotted in relation to the pressure ratio. In the map it can be witnessed that the single turbocharger operating line is indeed choking (no increase of mass flow for increasing pressure ratio). The dual turbocharger operating line does not go beyond the surge line but its surge margin (the distance between the operating line and the surge line) is much smaller than that of the single turbocharger operating line.

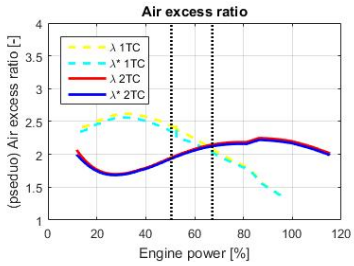

Figure 5.26: Steady state simulation result: air excess ratio.

The improved mass flow characteristic is also clearly shown with the air excess ratio. It can be witnessed that the air excess ratio is higher for a single turbocharger below 60% of the engine power and higher above that for two turbochargers. This increased air excess ratio theoretically means that more fuel can be injected before certain engine limits are reached (cylinder temperature, smoke formation).

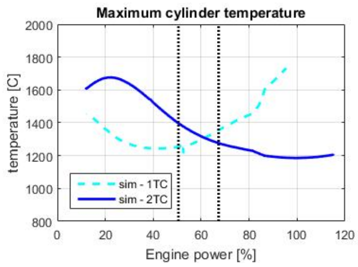

Figure 5.27: Steady state simulation result: maximum cylinder temperature.

The maximum cylinder temperature shows the same trends as the turbine entry and exit temperatures. There is a cross-over point and once again the single turbocharger outperforms the two combined turbochargers in the low engine load region. A lower maximum cylinder temperature for the same power rating means that there is less wear on the engine components and less formation of NOx. Emissions are outside the scope of this research but it is none the less interesting to know that sequential turbocharging can potentially reduce NOx emission in part load operation.

5.3.4. Validation

In the previous section the results of the simulation model where presented with the six data points of the Lloyds data set. In this section a quantitative analysis of the error of those results is performed. This is done by calculating the root mean square error (RMSE) which quantifies the average absolute error. Equation 5.14 is used to calculate the RMSE.

$$\mathrm{RMSE} = \sqrt{\frac{\sum_{i=1}^{n} (y_{sim(i)} - y_{obs(i)})^2}{n}} \tag{5.14}$$

Equation 5.14 offers an indication of how large the absolute error is of a certain parameter but it does not show how large that error is in relation to the normal condition. In order to have a comparative analysis it is necessary to normalize the absolute error. This can be done by relating it to a pre-set condition, for this the nominal condition is often chosen and the absolute error is divided by the nominal condition to provide the relative error. However it is of the authors opinion that this creates a biased outlook on the relative error.

For example when talking about temperature, would one divide the error by the nominal value in Celsius or Kelvin? Dividing by the nominal value in Kelvin would make the relative error appear smaller than if it where divided by the nominal value in Celsius. The same argument can be made for pressure (absolute or boost) and a hand full of other parameters.

To avoid this bias, the author has chosen to normalize the error with the values in the Lloyds data set. This is a logical choice because the data set is used as a reference for the absolute error as well. This achieved by dividing the absolute error for a certain parameter by the difference in the minimum and maximum value in the data set for the same parameter. This relates the absolute error to the spread in the measured set, it also removes the bias that was explained above. Because the error is related to the difference it is independent of the choice of units; for instance the difference between the minimum and the maximum measured charge temperature is the same in Celsius as in Kelvin. Normalizing the RMSE in this way creates a fair assessment of the relative error of the simulation model. Equation 5.15 is used to calculated the normalized root mean square error (NRMSE).

$$\text{NRMSE} = \frac{\text{RMSE}}{(y_{obs\_max} - y_{obs\_min})} \cdot 100\% \tag{5.15}$$

The RMSE and NRMSE are calculated for all parameters that where recorded in the data set. The results of these calculations is given in table 5.1.

Table 5.1: RMSE and NRMSE for the simulation results in comparison to the Lloyds data set

	RMSE		**NRMSE**	
turbocharger speed	1120	[RPM]	10,69	[%]
pressure at compressor inlet	0,00298	[bar]	30,43	[%]
pressure at compressor outlet	0,12816	[bar]	5,53	[%]
charge pressure	0,1262	[bar]	5,55	[%]
pressure at turbine inlet	0,21714	[bar]	13,38	[%]
pressure at turbine outlet	0,00828	[bar]	78,72	[%]
maximum cylinder pressure	4,6982	[bar]	5,87	[%]
temperature at compressor inlet	0,1854	[K]	2,41	[%]
temperature at compressor outlet	12,4018	[K]	8,73	[%]
charge temperature	3,5093	[K]	23,24	[%]
temperature at turbine inlet	15,9972	[K]	11,27	[%]
temperature at turbine outlet	4,8657	[K]	9,54	[%]

Table 5.1 gives a good indication that the simulation model is able to capture the steady state performance of a sequentially turbocharged Diesel engine. Most of the parameters are within acceptable error margins, less than 10% relative error. Some large outliers in relative error are the pressure before the compressor and the pressure after the turbine. This is a direct result of comparing them to the spread in the data, which is very small for these parameters. Their absolute error is very small, less than 10 mbar, so there is no cause for concern regarding these large relative errors.

The reason that all the parameters are showing errors is due to the complexity of the simulation model calibration. It was explained in section 3.4.3 that there are a lot of unknown parameters that have to be calibrated for the Diesel B model. The author has made the arbitrary choice of calibrating these unknown parameters in such a way that the total summation of the NRMSE of all the parameters in table 5.1 is at a minimum, see appendix F for a detailed explanation.

5.4. Transient analysis

The previous section has shown how the model is able to replicate the trends of a sequentially turbocharged engine for steady state operation. This section will go into the transient performance. For the mean value Diesel engine, transient performance is defined as follows:

> *The model is in transient operation if the time derivatives are not at rest and the output of the integrators is changing over time.*

Evaluating the model under transient conditions allows the user to replicate real world dynamic loading conditions of the engine. If the engine is used as a main propulsor on board of a ship, it will see a lot of dynamic use during its life time. This is less so the case for engine's that are running under near constant loads, for example: large merchant shipping vessels for container and bulk transport. The transient analysis of the Pielstick PA6B is of particular interest as the goal of this research assignment is to replicate and study the effects of this engine on board a SIGMA corvette during acceleration.

5.4.1. Method

As was explained in chapter 5.3.1, the Diesel engine model requires a load and a fuel rack position for its input. The method for these inputs is different from the method used in the steady state analysis. The goal is to replicate a load step from the sea trial and compare this data to the simulation results. To do so the model has to experience the same load and fuel input as the real engine experienced during the sea trial. It is important that the time occurrence of the input is the same for both model and data because the output is compared in the same time domain.

The fuel rack position is controlled by the engine governor. In chapter 5.3.1 it was explained that this governor receives an engine speed set point as its input and act likes a negative feedback controller. For the transient analysis, the governor speed set point recorded in the sea trial data is imposed on the model through a time-dependent look-up table.

The shaft torque and speed was recorded during the sea trial. The location of this measurement is somewhere between the gearbox and the propeller. At this location, the shaft power is calculated. The engine torque can be estimated by dividing the shaft power by the engine speed in [rad/s]. This can be done because the engine speed is also recorded. However, if the engine torque is determined in this way, the shaft and gearbox losses need to be taken into account. For now, all these losses are neglected. This choice is made because the engine model is in a test bench environment where these specific loading conditions are not modeled. In chapter 7, the engine model is placed inside an environment where the full propulsion train is modeled and the specific load contributions are more accurately modeled. For now, the analysis is done without taking these losses into account. This makes the engine run at a slightly lower load than the actual engine in the sea trial experienced. The choice to neglect these losses is reflected upon in the sub conclusion of this chapter.

The estimated shaft torque is imposed on the engine through a time-dependent look-up table. It is important that the load is time dependent and not speed-dependent (like the propeller law). Because the ship has experienced exterior loading like waves and wind, these are not correlated to the engine speed. But they are recorded in the same time domain that is used for comparison. Thus the imposed load on the model needs to be time-dependent.

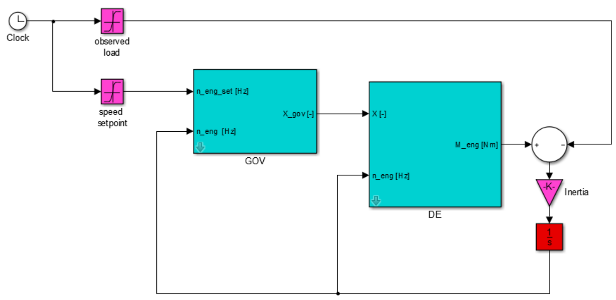

Figure 5.28: A schematic overview of the transient analysis modeling method.

figure 5.28 shows a schematic of how the engine model receives its input. Both the engine speed and engine load are imposed on the engine model through the time dependent look-up tables (magenta).

The acceleration starts when the engine is running at approximately 600 rpm and delivering about 25% of its nominal power. The Diesel B model has some problems with its scavenging model, this sub-model becomes very unstable in these low speed and power ranges. Therefor this region is excluded from all transient simulations in this report. Some discussion of the problems surrounding the exact causes of these issues are discussed in chapter 8.

5.4.2. Results

The results of the sea trial load step transient simulation are presented together with the recorded data. The parameters that where not recorded but are present in the simulation are presented afterwards. The steady state data was presented versus the relative engine speed. The transient simulation is presented versus time. The time scale starts at a little over 50 seconds, this is because the time scale matches the time scale of the sea trial data, which does not start at zero.

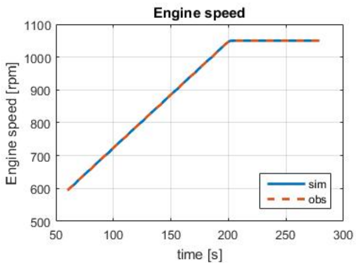

Figure 5.29: Transient simulation result: engine speed set point.

The engine speed set point is the same for both the speed trial and the simulation. This comes as no surprise as it was used as one of the inputs for the model.

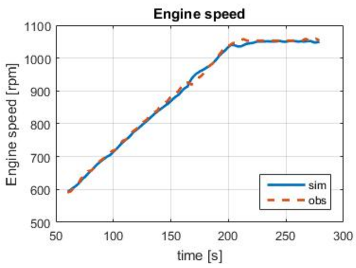

Figure 5.30: Transient simulation result: engine speed.

The actual engine speed follows the set point shown in figure 5.30. At approximately 160 seconds, the engine goes from single to dual turbocharger mode. The sea trial data shows that the engine speed drops very slightly at this point. The simulation model shows the exact opposite effect, it is not large in magnitude but the trend is unexpected.

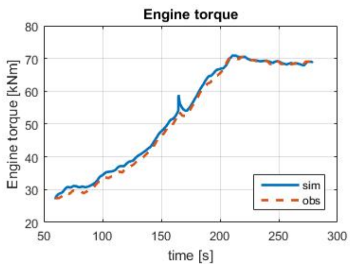

Figure 5.31: Transient simulation result: engine torque.

The engine torque shown in figure 5.31 closely resembles the observed sea trial data. At approximately 160 seconds the second turbocharger is switched in and the engine torque of the simulation model peaks, whereas the observed data set does not show this peak. Later in this chapter it will be explained that this is due to the fact that the assumptions that were used to construct the model do not hold up during this switching event.

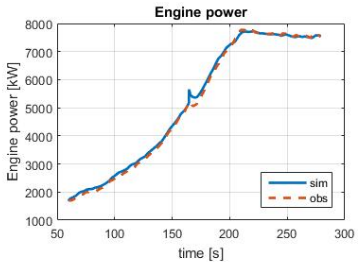

Figure 5.32: Transient simulation result: engine power.

The simulation follows the imposed load characteristics from the sea trial data. When the second turbocharger is switched on, the power momentarily increases instead of decreasing like in the sea trial data. This also explains why the speed in 5.30 was increasing instead of decreasing.

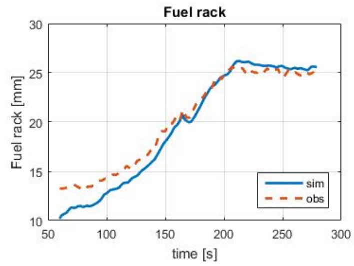

Figure 5.33: Transient simulation result: fuel rack position.

The fuel rack position follows the trends that are shown in the observed data set. When the second turbocharger is switched in, the fuel rack is held back momentarily by the governor. In the lower power range, the fuel rack position of the simulation is slightly to low.

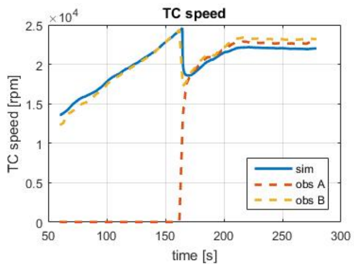

Figure 5.34: Transient simulation result: turbocharger speed.

The turbocharger speed of the Simple STC model is compared to the turbocharger speed of both turbochargers on the real engine. In the assumptions at the start of this chapter it was explained how the model only simulated the permanent turbocharger. This can be seen in figure 5.34; the simulation result closely resembles the recorded speed of the permanent turbocharger(B). When the second turbocharger is switched in, the turbocharger speed of the model does not "dip" as far as the real permanent turbocharger did during the sea trial.

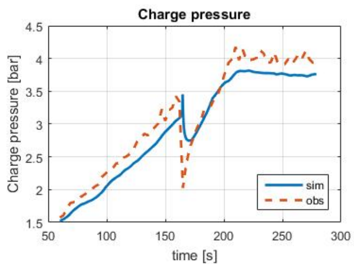

Figure 5.35: Transient simulation result: charge pressure.

The simulated charge pressure is slightly lower than the observed data. The same "dip" as in figure 5.34 can be witnessed. In the real engine, the charge pressure drops faster than in the Simple STC model.

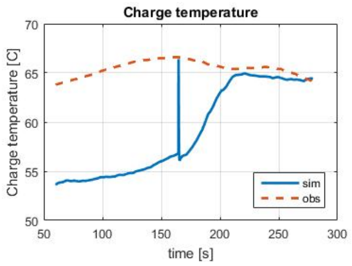

Figure 5.36: Transient simulation result: charge temperature.

The charge temperature shows a trend that does not match the observed data. After 200 seconds, the temperature does start to match the expected trend. It is important to note that at this point, the vessel acceleration has ceased and the system has reached near-steady state.

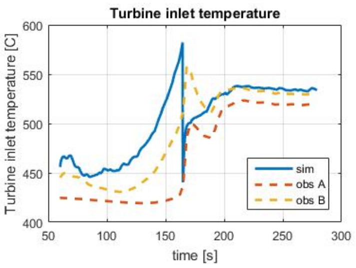

Figure 5.37: Transient simulation result: turbine entry temperature.

The turbine entry temperature is presented for the simulation and both turbochargers on the real engine. Up until the point of switching, the simulation follows the trend but shows a higher value. When switching occurs, the temperature drops in both the simulation and the real engine. However, the temperature in the simulation drops very violently. After switching, the simulation temperature slowly recovers and follows the expected trend again.

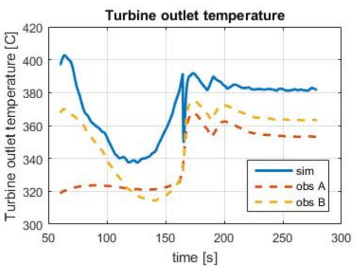

Figure 5.38: Transient simulation result: turbine exit temperature.

The turbine exit temperature shows some resemblance to the entry temperature in figure 5.38. The simulation follows the trend, although at a somewhat higher absolute value. The switching occurs very violently, as it did for the entry temperature.

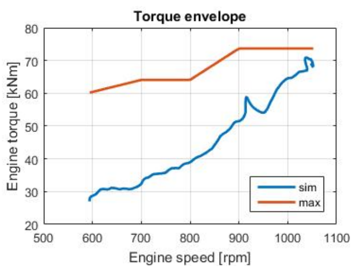

Figure 5.39: Transient simulation result: torque envelope.

The torque envelope shows that the engine is nowhere close to the maximum allowable torque during this acceleration. This effect forms one of the main reasons why these models have been constructed. The objective is to find out if it is possible to use the available torque during acceleration.

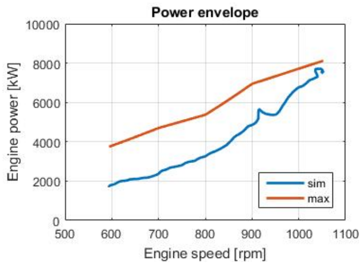

Figure 5.40: Transient simulation result: power envelope.

The power envelope shows the same effects as the torque envelope of figure 5.39. According to the envelope there is a lot of available power during acceleration which is not used.

This concludes all the parameters that where recorded in the sea trial data set. The following figures are parameters that are calculated by the model but unfortunately not recorded. However they do provide insight and discussing them is vital to form a conclusion on the implementation of sequentially turbocharged engines.

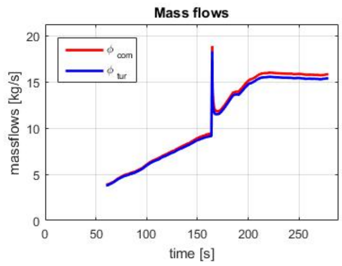

Figure 5.41: Transient simulation result: mass flows.

The mass flow of the compressor and turbine give a good indication of what is happening during switching. The whole principle of the Simple STC model is that the mass flow is multiplied with an integer value, one or two based on the turbocharger mode. Because this occurs instantly, the mass flow of the compressor and turbine is instantly doubled. This results in a transient effect during switching that is not representative of the real physical event.

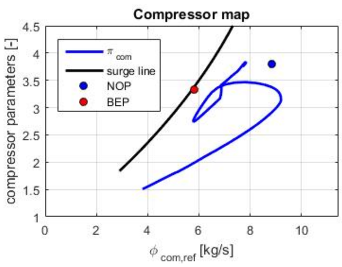

Figure 5.42: Transient simulation result: compressor map.

The compressor shows the transition from single to the dual turbocharger operation for the compressor on the primary turbocharger. However, as discussed above, this transition is somewhat questionable of whether it captures the true physical transition.

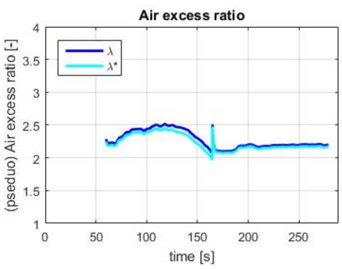

Figure 5.43: Transient simulation result: (pseudo) air excess ratio.

The air excess from the simulation model shows the same trends that where witnessed in the steady state analysis. When the engine is running at low speed the single turbocharger is providing more air to the engine. This results in a higher air-excess ratio.

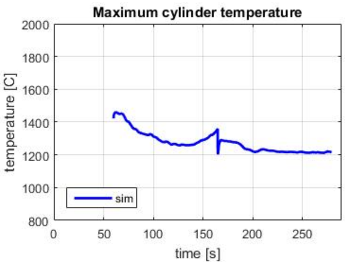

Figure 5.44: Transient simulation result: maximum cylinder temperature.

The maximum cylinder temperature does not rise to much during acceleration. Only for a very short time does the cylinder temperature get above 1400 degrees Celsius.

5.4.3. Validation

The validation of the transient model results has been evaluated with the same method that was used for the steady state analysis. The RMSE and NRMSE are calculated with equations 5.14 and 5.15. For the steady state analysis, only six data point were available. The load step in the sea trial data consist of a very large set of data points. This increases the resolution of the validation procedure and should result in a more accurate prediction of the average errors. The RMSE and NRMSE for the transient analysis are presented in table 5.2.

Table 5.2: RMSE and NRMSE for the simulation results in comparison to the Lloyds data set

	RMSE		**NRMSE**	
engine speed	7.6894	[RPM]	1.6404	[%]
engine power	110.44	[kW]	1.8128	[%]
fuel rack	1.2416	[mm]	9.8931	[%]
turbocharger speed	889.61	[RPM]	7.3533	[%]
charge pressure	0.2531	[bar]	9.7198	[%]
charge temperature	7.9417	[K]	283.63	[%]
temperature at turbine inlet	26.681	[K]	21.041	[%]
temperature at turbine outlet	22.437	[K]	36.903	[%]

5.5. Sub-conclusion

This section will discuss the sub conclusions on the Simple STC model after having presented the model hypothesis, the method and the results.

5.5.1. Answer to model hypothesis

The model hypothesis that was postulated at the start of this chapter was based on 4 assumptions:

- In single turbocharger operation, a single turbocharger supplies the full air demand of the engine.
- In dual turbocharger operation, each turbocharger supplies exactly the half of the air demand.
- In dual turbocharger operation, both turbochargers operate on the same inlet and outlet conditions.
- In dual turbocharger operation, both turbochargers operate on the same speed, the two turbocharger shafts are virtually connected with a 1:1 ratio.

These assumptions made it possible to make the implementation in Simulink very simple. The results have shown that the simulation model is indeed able to replicate the trends of a sequentially turbocharged engine. The output of the model bears a stark resemblance to the Lloyds data set for steady state and the sea trial data load step for transient performance. This has given the author the confidence to say that the assumptions where correct.

However there is an exception that cannot be overlooked. When the second turbocharger is switched in, both turbochargers are not operating on the same boundary conditions. This means that the third and fourth assumption are not true until both turbochargers have reached the same operating conditions again. The transient effect of switching turbochargers is not modeled correctly in the Simple STC model. The strange switching effect can be seen in the massflow in figure 5.41 which displays the direct cause of the Simple STC implementation. The compressor map in figure 5.42 shows a transition from single to dual operating mode that is unexpected. This trend should look more like figure 2.2, presented in section 2.2.

5.5.2. Devation of transient results

The results from the transient analysis show some deviation from the recorded data. There are multiple possible reasons for this deviation:

- As explained in section 5.4.1, the imposed load on the engine does not include any shaft losses. This makes the engine simulation model run at a lower load then the actual engine from the sea trial data.
- The deviation can also be a result of a measurement error.
- The simulation model is calibrated to match the Lloyds set as closely as possible. This is the same type of engine, but not the same physical engine. Both engines have experienced a different lifetime at the point in time where the test was recorded. this means that the effects of fouling, wear, installation, etc. are not the same for both engines, resulting in minor differences. These differences are quite large for the turbine temperatures. Figures 5.45 and 5.46 show the steady state performance of the simulation model compared to both the Lloyds and sea trial data. It can be seen that the simulation model closely resembles the Lloyds data, whereas the sea trial data deviates from both the model and the Lloyds data.

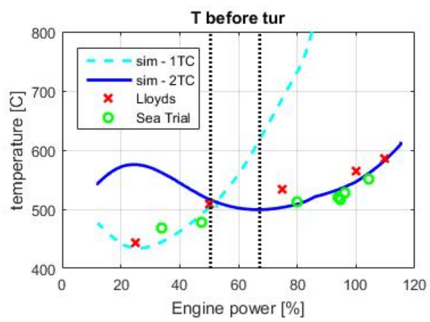

Figure 5.45: Transient simulation result: turbine entry temperature.

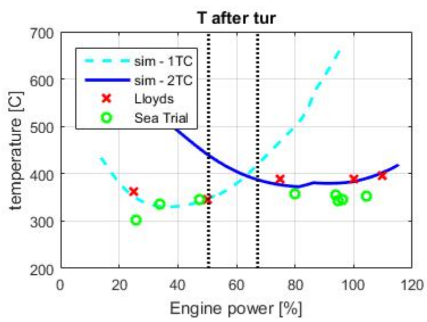

Figure 5.46: Transient simulation result: turbine exit temperature.

5.5.3. Transient charge air temperature

The charge air temperature is a result of the alternative air cooler model presented in chapter 4. It can be witnessed in figure 5.36 how the charge air temperature is lower than recorded during the transient operation but settles as soon as the engine settles. The new heat exchanger model does not take into account any dynamics, so the cause must be some other process. In figure 5.35 it can be seen that the charge pressure is lower than recorded, this means that the mass flow of air is lower than expected. In the air cooler model, the mass flow of air is cooled by the mass flow of cooling water. If the mass flow of air is lower than designed, the air is cooled more due to the longer residence time in the air cooler. This is what can be witnessed in figure 5.36. The problem is with the deviation in the gas exchange, not the new heat exchanger model.

5.5.4. Pro's and Con's of the Simple STC model

Finallly a list of pro's and con's of the Simple STC model is presented and discussed.

PRO: simple implementation in Simulink

Anyone familiar with the original Diesel B engine model should be able to work with this model without too much effort. It does not add any complexity to the existing model.

PRO: easily scaled up

The implementation of the Simple STC model is as simple as multiplying the mass flow with an integer value. For this thesis, the Pielstick PA6B is investigated which has two equally sized turbochargers. Only a single parameter has to be changed to scale up the model to three or more turbochargers, the Simulink model does not need to be altered to accomplish this.

PRO: no increase in computational load

The Simple STC model does not add any elements that take up computational power. Some examples of these types of blocks are: intergators, memory blocks and anything with zero-crossing detection. Running the Simple STC model takes up the same amount of computational power as running the standard Diesel B engine model.

CON: can only be used for equally sized turbochargers

The assumptions on which the model is built, state that the turbochargers are assumed to work under the same conditions. This assumptions only holds if the turbochargers are of the same type and of equal size. This model does not offer the possibility to investigate different sized turbochargers on the same engine.

CON: only simulates the permanent turbocharger

The Simple STC model only simulates the permanent turbocharger characteristics. The switchable turbocharger is imposed on the permanent turbocharger and the individual contribution is lost.

CON: switching effects are not modeled correctly Because of the simple assumptions, the model does not give a correct result when the turbocharger groups are switched in and out. At this time the turbochargers are not acting under the same boundary conditions and so the assumptions made to construct the model do not hold when switching occurs.

6
The Full STC model

The first attempt at modeling a sequentially turbocharged engine was presented in the previous chapter in the form of the Simple STC model. A second model has been constructed that takes a different approach at using the TU Delft Diesel B model to simulate a sequentially turbocharged Diesel engine. This second model is called the Full STC model, this name is derived from the fact the Diesel B model has been expanded in such a way that the full engine and all its components are modeled.

6.1. Model hypothesis

The Full STC model relies on the idea that the volume-resistor network of the Diesel B engine can be expanded by using the existing components. The Diesel B engine is built up out of different modular components with generic characteristics. By connecting these components in a different way, a new volume-resistor network can be constructed to model the gas exchange of the sequentially turbocharged engine. This method expands upon the work into the gas control valves that have recently been developed for the Diesel B model. These valves are implemented as restrictors that are connected in parallel with other restrictors, for instance: the waste gate valve is connected in parallel with the turbine. These statements are captured in the following hypothesis:

> *The following existing components can be used to expand the volume resistor network to model a new turbocharger strategy: compressor, turbine, turbocharger dynamics, gas control valves and generic volume.*

This hypothesis will be discussed in the sub conclusions of this chapter

6.2. Model implementation

The method that was presented in the previous section is used to adapt the Diesel B engine model in such a way that the contribution of each individual turbocharger is captured. The implementation is best explained through the use of a schematic overview of the existing Diesel B volume-resistor network, this is shown in figure 6.1.

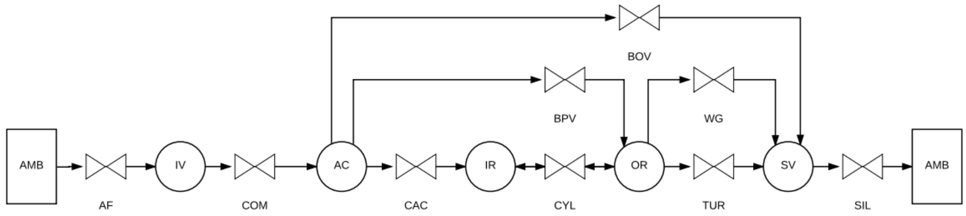

Figure 6.1: The volume-resistor network of the TU Delft Diesel B model.

In this figure, rectangles are the ambient volume elements. These elements have an infinite volume and constant temperature and pressure. The circles are the volume elements of the Diesel B model: IV is the inlet volume, AC is the air cover volume, IR is the inlet receiver volume, OR is the outlet receiver volume and SV is the exhaust silencer volume. The volume elements are connected by the restrictor elements: AF is the air filter, COM is the compressor, CAC is the charged air cooler, CYL is the cylinder process, TUR is the turbine and SIL is the exhaust silencer. The gas control valves that where added later, are connected in parallel with the original resistors. The gas control valve restrictor elements: BOV is the blow-off valve, BPV is the by-pass valve and WG is the waste gate.

It is important to note that the direction of the mass flow is not bi-directional for all restrictor and volume connections. The direction of flow is shown in figure 6.1 by the arrows. There is one path in the original flow model that does support a reversal of the flow, this is the cylinder. In the cylinder, negative scavenging can occur. This happens when the pressure in the outlet receiver is higher than the pressure in the inlet receiver. Because of the negative pressure difference, exhaust gasses flow back through the cylinder and by pass valve into the inlet receiver during scavenging.

The elements shown in figure 6.1 are rearranged to form a new network that is representative of the sequentially turbocharged engine gas exchange. The blow-off valve (BOV) and the waste-gate (WG) are removed because the Pielstick PA6B is not outfitted with these valves. This new network is shown in a schematic with the same style as before, figure 6.2.

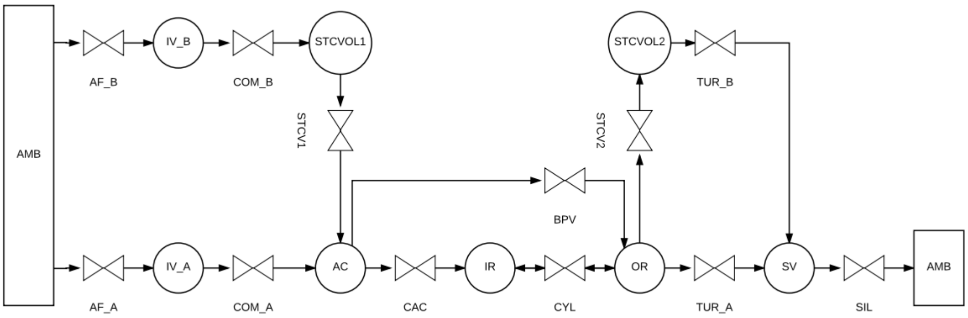

Figure 6.2: The volume resistor network for a sequentially turbocharged engine.

Figure 6.2 shows the proposed network for the Full STC model. The “bottom row” is the same as that of the Diesel B model. The Full STC model uses the existing components of the original Diesel B model with the addition of two extra volumes (STC VOL1 and STC VOL) and two extra restrictor valves (STCV1 and STCV2). STC VOL1 represents the volume between the compressor outlet and the STC inlet valve; STC VOL2 represents the volume between the STC exhaust valve and the turbine inlet. To get an idea of where these components are on the real engine, a picture (figure 6.3) of a sequential turbocharging group is shown with these components high-lighted.

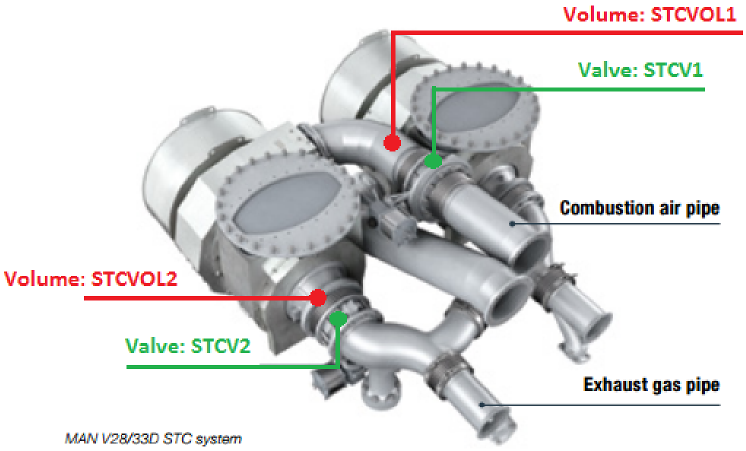

Figure 6.3: A picture of a sequential turbocharging group with the STC volumes and valves high-lighted.

The model implementation of the volumes is the same as all the other volumes in the Diesel B engine model, for a detailed derivation see appendix E. The implementation of the gas control valves is the same as the existing gas control valves of the original Diesel B model.

The flow through the switchable turbocharger is controlled by the STC valves (STCV1 and STCV2). In single turbocharger operation, STCV1 and STCV2 are closed and no mass passes through the valves. As a result there is no power developed by the turbine and the turbocharger shaft comes to rest. In dual turbocharger operation, STCV1 and STCV2 are opened and the valves connect STC VOL1 to the inlet receiver and STC VOL2 to the outlet receiver. This allows for the turbine to deliver power to the turbocharger shaft which starts to spin up.

During early testing of the model, it was found that the directional flow limits of the compressor were causing problems for the state properties in the STC VOL1 volume. When moving from dual to single turbocharger operation, the STC VOL volumes get disconnected from the overall gas exchange. For STC VOL1 this means that it is at a state of high pressure and temperature when STCV1 closes. Because the compressor mass flow is one-directional, this pressurized mass in STC VOL1 cannot escape the volume and it stays at a high pressure. In reality, this mass would flow back through the compressor but the mathematical model does not allow for this. To subvert this mathematical problem, a virtual valve has been installed in the model. This valve is shown as STCV3 in figure 6.4.

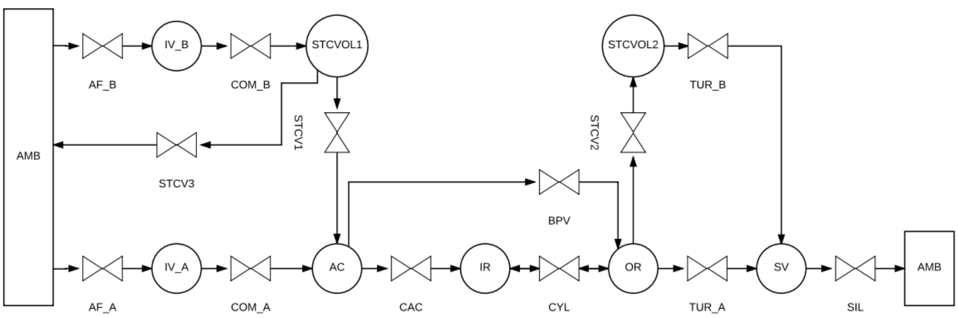

Figure 6.4: The volume resistor network for a sequentially turbocharged engine with virtual depressurization valve.

The virtual depressurization valve connects STC VOL1 to the ambient volume. This allows for the mass in STC VOL1 to escape and allow the volume to depressurize as it would in reality. Valve STCV3 is opened and closed opposite to the main control valves STCV1 and STCV2. This means that STCV3 is closed when STCV1 and STCV2 are open and vice versa.

The control scheme is the same as the control scheme that was presented for the Simple STC model. The same Simulink sub-systems are used as shown in figures 5.3-5.5. Only this time instead of sending a one or a two to the mass flow multiplication, it sends a one or a zero to the gas valve actuators which opens or closes the gas control valves.

Modeling the second turbocharger with its individual components has significantly increased the complexity of the Simulink model. Whereas the Simple STC only required the addition of two multiplication blocks in the Simulink environment, the Full STC model requires the complete gas exchange and turbocharger dynamics to be modeled in full. This makes the model less appealing for the purposes of practical application for other users, since it takes a lot of insight to get to grips with the model and its usage. An overview of how the schematic from figure 6.4 looks in the Simulink environment is given in figure 6.5. In this figure, the outlined area in red is what was added to the original Diesel B model. Figure 6.5 only serves to display the complexity of the Full STC model.

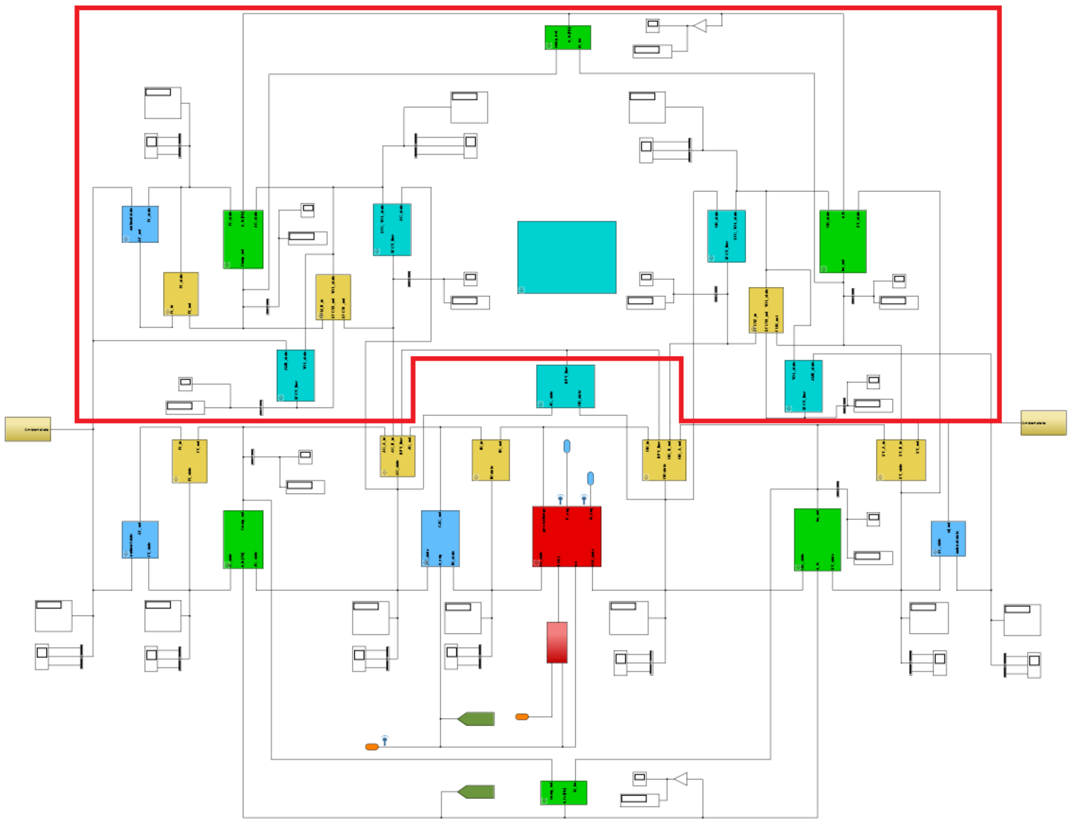

Figure 6.5: An overview of the Full STC model in Simulink.

6.3. Steady state analysis

The steady state analysis is performed under the same condition as was done for the Simple STC model, using the same definition for steady state for the Diesel engine model:

> *The model has reached steady state equilibrium if all the integrators of the time derivatives output a constant value that does not change over time.*

The results of the model are presented in the same manner as the steady state results of the Simple STC model. The engine parameters are analyzed in relation to nominal engine power, this is used for the x-axis of the plots. As before, the switching of the turbocharger group is not included as explained before, this is a transient effect that will be studied in the transient analysis.

6.3.1. Method

The same method for steady state analysis is applied as for the Simple STC model discussed in chapter 5.3.1:

- The fuel rack is decreased slowly over time to provide an operating line of semi-steady state operating points.
- The engine is loaded with a propeller law curve that is matched in the nominal point as shown in equation 5.13.
- The turbochargers are not switched, the analysis is done for both turbocharger operations and is divide into three regions of relative power. These three regions depict the area where single or dual turbocharging is used.

6.3.2. Results

The analysis of the steady state revealed that the results of the Full STC model and the Simple STC model are the same. This is not surprising since the assumptions made to model the Simple STC model are true during steady state operation. It is during the transient effect of switching the switchable turbocharger on or off that these assumptions are not valid. To illustrate the fact that the steady state results are the same, some figures with the results of both models are shown side by side in figures 6.6 - 6.10.

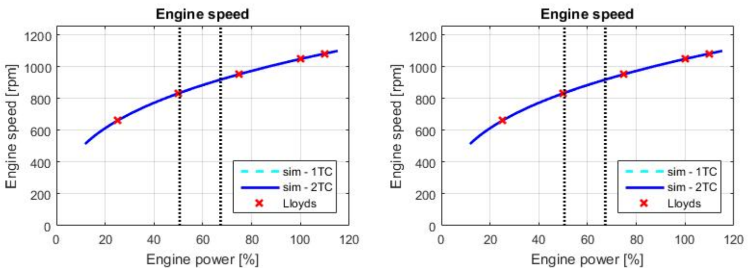

(a) Simple STC model. (b) Full STC model.

Figure 6.6: Steady state simulation result: engine speed.

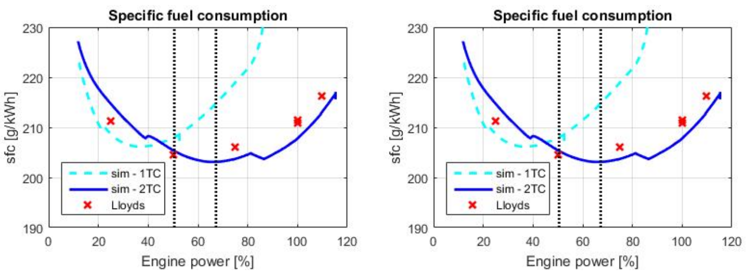

(a) Simple STC model. (b) Full STC model.

Figure 6.7: Steady state simulation result: specific fuel consumption.

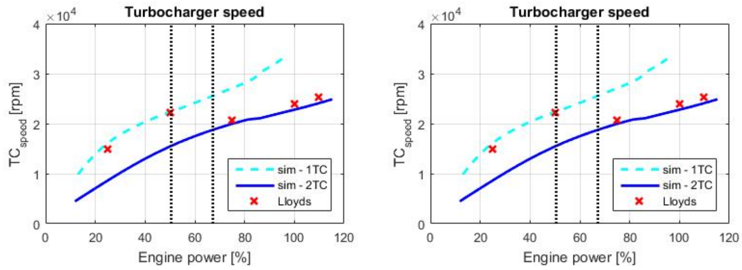

(a) Simple STC model. (b) Full STC model.

Figure 6.8: Steady state simulation result: turbocharger power.

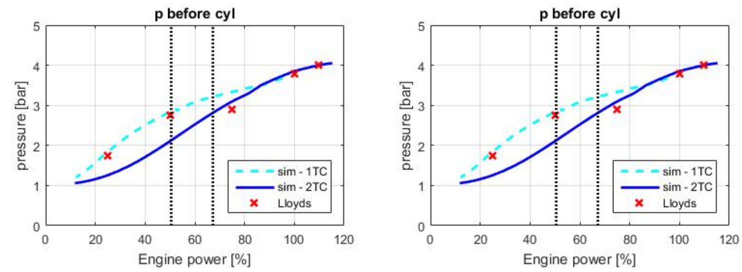

(a) Simple STC model. (b) Full STC model.

Figure 6.9: Steady state simulation result: charge pressure.

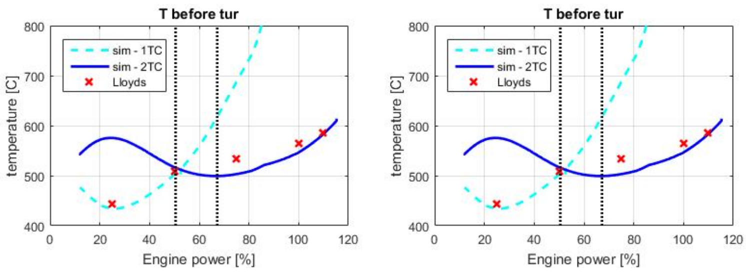

(a) Simple STC model. (b) Full STC model.

Figure 6.10: Steady state simulation result: turbine entry temperature.

6.3.3. Validation

Since the results are the same for both models, the quantitative validation is the same as for the Simple STC model. These results can be found in table 5.1.

6.4. Transient analysis

The transient analysis is performed under the same condition as was done for the Simple STC model, using the same definition for transient operation of the Diesel engine model:

> *The model is in transient operation if the time derivatives are not at rest and the output of the integrators is changing over time.*

The results of the model are presented in the same manner as the steady state results of the Simple STC model. The engine parameters are analyzed in relation to the recorded sea trial data. The results are presented in the same time domain as the sea trial data, with time for the x-axis of the plots.

6.4.1. Method

The same method for steady state analysis is applied as for the Simple STC model discussed in chapter 5.4.1:

- The observed speed set point is imposed on the engine governor, which determines the fuel rack position
- The observed shaft load is imposed on the engine to determine the engine speed through the use of Euler's law for motion of rigid bodies. Shaft losses are neglected, as a result the simulated engine torque is lower than the real engine torque.

It is expected that the Full STC model is able to capture the transient effects during switching of the switchable turbocharger more accurately. This is due to the fact that each turbocharger is modeled with its individual components. The results of the transient analysis are presented in the next section. The Full STC model is tested under the same conditions as the Simple STC model was in section 5.4, for more details see figure 5.28.

6.4.2. Results

As with the Simple STC model, the results of the sea trial load step transient simulation are presented together with the recorded data. The parameters that where not recorded but are present in the simulation are presented afterwards. The steady state data was presented versus the relative engine speed. The transient simulation is presented versus time, as before in section 5.4.2 with the timescale starting at a little over 50 seconds; the same time scale as the recorded sea trial data.

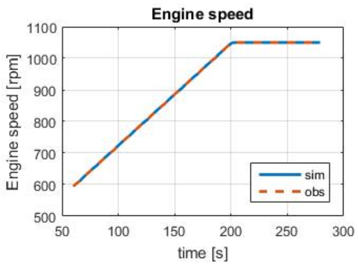

Figure 6.11: Transient simulation results: engine speed set point.

The engine speed set point in the simulation model is the imposed set point from the sea trial data set. Because of this, the fact that it shows exactly the same value is as expected.

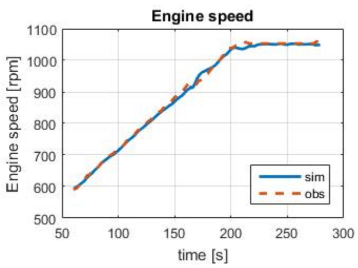

Figure 6.12: Transient simulation results: engine speed.

The actual engine speed of the engine is reaching the desired set point conditions for both the model and the sea trial. At around 160 seconds, the second turbocharger is switched in. It can be witnessed in figure 6.12 that at this point the engine speed is held back for a few seconds. This effect is seen in both cases, however it is more pronounced in the sea trial data set.

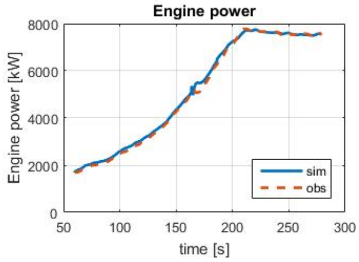

Figure 6.13: Transient simulation result: engine power.

The simulated engine power in figure 6.13 shows that when the switching of the second turbocharger occurs, the engine power decreases shortly until it stabilizes again. The sea trial data shows this effect and the model is able to replicate it. The same graph for the Simple STC model, figure 5.32, showed that the Simple STC model produced the opposite effect where the power increased instead of decrease.

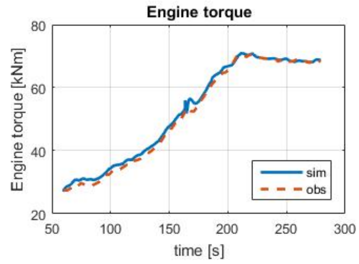

Figure 6.14: Transient simulation result: engine torque.

The engine torque shows the same effects as were witnessed for the engine power in figure 6.14. At the point of switching the engine torque overshoots slightly.

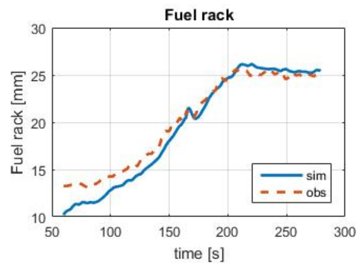

Figure 6.15: Transient simulation result: fuel rack position.

The fuel rack position shown in figure 6.15 follows the trend that is recorded in the sea trial data. When the turbocharger is switched in, the fuel rack is held back for a few seconds. The fuel rack is slightly higher after 200 seconds and slightly lower when operating in single turbocharger mode.

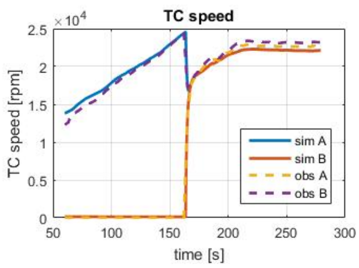

Figure 6.16: Transient simulation result: turbocharger speed.

The turbocharger results of the Full STC model shows the speed of both turbochargers on the engine, whereas the Simple STC model only modeled the permanent turbocharger. When compared with figure 5.34 it can be witnessed that during the transition from one to two turbochargers, the results of the Full STC model predict the turbocharger speed more accurately. In figure 5.34 the turbocharger speed did not decrease enough and the "valley" at 160 seconds was not as sharp as in figure 6.16.

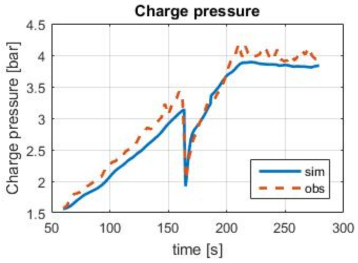

Figure 6.17: Transient simulation result: charge pressure.

The charge pressure in figure 6.17 shows the same effects as the turbocharger speed in figure 6.16. In comparison to the Simple STC results, figure 5.35, the results of the Full STC model appear to give a more accurate solution for the switching event at 160 seconds. The charge pressure from the model follows the recorded data in the sea trial very closely. Outside of the switching event, the simulated charge pressure is slightly to low.

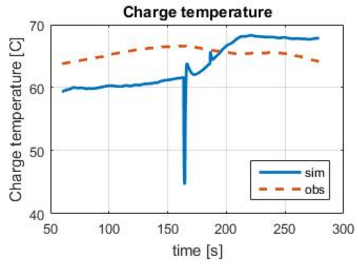

Figure 6.18: Transient simulation result: charge temperature.

The charge temperature shows a similar trend as it did in the Simple STC model, figure 5.36. The magnitude is about the same but the charge temperature is 5 degrees Celsius higher overall. This is caused because the mass flow of air through the air cooler is slightly different for both models. Since the restrictive property of the air cooler is relatively small, a small offset in pressure over the air cooler can result in a significant change in the mass flow through the model.

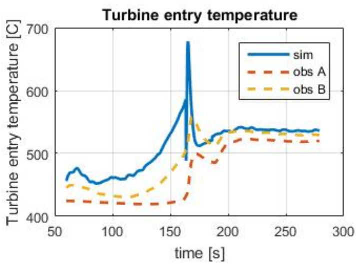

Figure 6.19: Transient simulation result: turbine entry temperature.

The turbine entry temperature in figure 6.19 shows a large offset at the moment the second turbocharger is switched in. This effect was also present in the results of the Simple STC model, figure 5.37. Outside of this switching region, the turbine entry temperature shows a large offset when operating on one turbocharger and almost no offset in dual turbocharger operation. The large peak is caused by the fact that the second turbocharger is not spinning fast enough when it is switched in, resulting in too little air for the engine. This causes the air excess ratio to decrease (figure 6.26) and cylinder temperatures to rise (figure 6.27). The increased cylinder temperature leads to a higher turbine entry temperature.

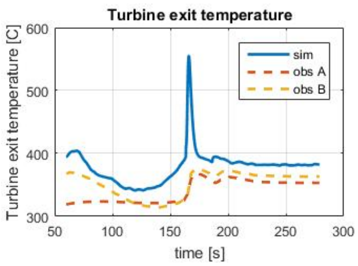

Figure 6.20: Transient simulation result: turbine exit temperature.

As with the turbine entry temperature, the turbine exit temperature shows a very large offset. This is partly caused by the fact that the turbine entry temperature is too high and partly due to the fact that the turbocharger is still spinning up. The slow speed of the turbocharger causes the turbocharger model to operate outside of the stable region, making the mathematical model results questionable during this event. The compressor map of the second turbocharger in figures 6.25 will prove that this is in fact true.

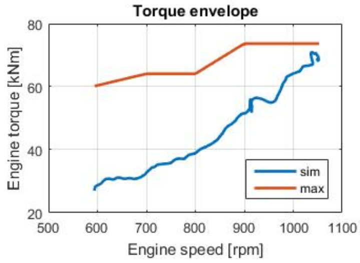

Figure 6.21: Transient simulation result: torque envelope.

The torque envelope in figure 6.21 shows that during the acceleration the full torque potential of the engine is not used. This was also shown in the results section of the transient analysis on the Simple STC model.

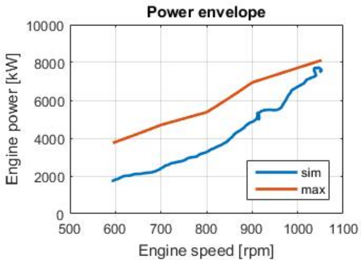

Figure 6.22: Transient simulation result: power envelope.

The power envelope shows the same development as the torque envelope in figure 6.21, there is a lot off potential power available that is not used during acceleration.

This concludes all the parameters that where recorded in the sea trial data set. The following figures are parameters that are calculated by the model but unfortunately not recorded. However they do provide insight and discussing them is vital to form a conclusion on the implementation of sequentially turbocharged engines.

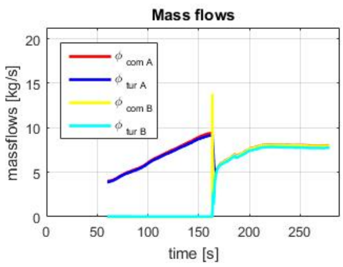

Figure 6.23: Transient simulation result: mass flows.

In figure 6.23 it can be witnessed how the Full STC model simulates the mass flow of each individual turbocharger. The compressor of the second turbocharger shows a large spike when switched in, this occurs for only a brief time. This is the results of the fact that the volume (STC VOL1) into which it discharges the air is at ambient pressure at that time. This effect only occurs for a very brief time, because the volume is relatively small to the inlet receiver volume. The high influx of mass causes the volume to pressurize rapidly and the mass flow reduces as a result of this.

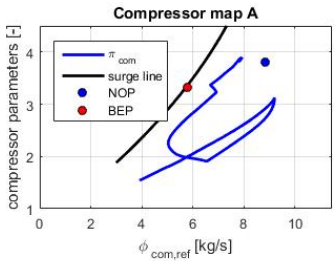

Figure 6.24: Transient simulation result: permanent turbocharger compressor map.

The compressor map of the permanent turbocharger is shown in figure 6.24. It shows the operating line of both single and dual turbocharger mode and the transition between them. The transition looks much more like the expected trend shown in figure 2.2 than the compressor map results of the Simple STC model, figure 5.42. When switching to dual turbocharger operation, both mass flow and pressure are decreasing more rapidly in the Full STC model than for the Simple STC model. This is the cause of the difference in the transient operating line shift in the compressor map. It is important to note that the map alone does not give enough information on this transient behavior as time is not recorded in this figure, it has to be analyses in conjunction with the displayed parameters versus time.

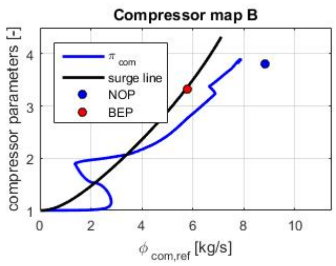

Figure 6.25: Transient simulation result: permanent turbocharger compressor map.

The compressor map of the switchable turbocharger is shown in figure 6.25. At the start of the simulation, the turbocharger is at rest and the pressure ratio over the compressor is unity. When the turbocharger is switched in, the mass flow rapidly rises for this compressor, see figure 6.23. This is pictured by the horizontal trend in figure 6.25 going from a mass flow of 0 [kg/s] to a little over 2 [kg/s]. As the mass builds up in the discharge volume, so does the pressure inside this volume. As a result the mass flow decreases again and the operation moves beyond the surge line. Shortly after, the turbocharger reached the operating line for dual turbocharging operation and continues under the same conditions as the permanent turbocharger.

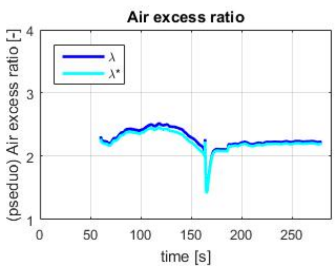

Figure 6.26: Transient simulation result: (pseudo) air excess ratio.

The air excess ratio in figure 6.26 shows that when switching of the turbochargers occurs, a large drop in the air excess ratio can be expected. The Simple STC model showed exactly the opposite trend in figure 5.43. For the Simple STC model, the air excess ratio showed a sudden peak in the air excess ratio instead of a sudden drop. This is a direct result of the different modeling approaches. The Full STC model provides a more accurate outlook on the events that occur during switching if the turbochargers.

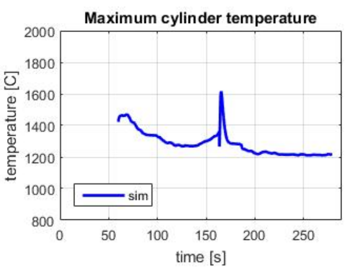

Figure 6.27: Transient simulation result: maximum cylinder temperature.

The maximum cylinder temperature in figure 6.27 also shows the opposite effect in comparison to the Simple STC model during the switching event. Because the cylinder temperatures are closely tied to the amount of combustion air available, it comes as no surprise that the witnessed result in figure 6.27 shows an increase in temperature during the switching event.

6.4.3. Validation

The validation of the transient model has been evaluated with the same method that was used for the steady state analysis. The RMSE and NRMSE are calculated with equations 5.14 and 5.15. In the previous chapter it was explained that for the steady state analysis, only six data point were available. The load step in the sea trial data consist of larger set of data points. This increases the resolution of the validation procedure and should result in a more accurate prediction of the average errors. The RMSE and NRMSE for the transient analysis are presented in table 6.1.

Table 6.1: RMSE and NRMSE for the simulation results in comparison to the sea trial data set.

	RMSE		**NRMSE**	
engine speed	7.7964	[RPM]	1.663	[%]
engine power	113.26	[kW]	1.8591	[%]
fuel rack	1.2182	[mm]	9.7067	[%]
turbocharger A speed	373.19	[RPM]	1.6324	[%]
turbocharger B speed	773.78	[RPM]	6.3960	[%]
charge pressure	0.1610	[bar]	6.1838	[%]
charge temperature	4.2416	[K]	151.49	[%]
temperature at turbine inlet	34.149	[K]	26.93	[%]
temperature at turbine outlet	35.639	[K]	58.617	[%]

6.5. Sub-conclusion

This section will discuss the sub conclusions on the Full STC model after having presented the model hypothesis, the method and the results.

6.5.1. Answer to model hypothesis

In the beginning of this chapter, the model hypothesis was postulated that was used to construct the Full STC model:

> *The following existing components can be used to expand the volume resistor network to model a new turbocharger strategy: compressor, turbine, turbocharger dynamics, gas control valves and generic volume.*

The results of the model bear a lot of resemblance to that of the Simple STC model and to the observed data sets. This leads to the conclusion that the volume resistor network can be expanded in the same way that an electrical RC-network can be expanded. As a proof of concept, the author has used this knowledge to adapt the Diesel B model for:

- Unequal sequential turbocharging.
- Two-stage turbo-compounding.

These models will not be treated further in this report, but they serve as an interesting starting point for anyone that want to investigate these turbocharging strategies. The models are available in the digital deliverables.

Expanding the volume resistor network has also shed some light on the limitations of the current implementation. Most of the volume and resistor elements are one-directional in terms of mass flow. The models either don't allow for mass flow in the other direction, like the compressor model, or they do allow for it but do not calculate the correct effects. An example of the incorrect calculation is in the volume elements, where the mass flow balance does account for mass flow in the opposite direction. But the energy balance does not correct the temperature of the mass flow in the opposite direction.

6.5.2. Switching of the turbochargers

The results from the transient analysis of both the Simple and Full STC model have shown that the major difference between them, in terms of output, is the effects that occur when the second turbocharger is switched in. It was reasoned that this switching was incorrectly modeled in the Simple STC model because the assumptions on which it is based do not hold during this event.

The results of the Full STC model do show the same trends as the recorded data during the switching of the turbochargers. The speed of both turbochargers in figure 6.16 show a clear comparison to the recorded data. This leads to the conclusion that the Full STC model is able to reproduce the trends during switching.

It can be witnessed in the massflow depicted in figure 6.23 that the engine is temporarily deprived of combustion air as the second turbocharger is switched in. As a result, the air excess ratio, figure 6.26, of the engine also degrades. This effect is not mentioned in the literature or by the manufacturers of sequentially turbocharged engines. The author believes that the results are representative of the reality; the KRI Diponegoro has experienced issues when switching the turbochargers, this was solved by limiting the fuel rack during this event. This solution gives an indirect confirmation that one of the problems for the real engines was a temporary starvation of combustion air during the switching of turbocharger groups. unfortunately there is no recorded data of the mass flow or the air excess ratio to confirm these suspicions.

There is another component that contributes to the switching effects of the turbo chargers that was not mentioned anywhere in the report and this is the Jet-Assist module. This is a pneumatic nozzle in the compressor housing that imparts momentum to the compressor wheel by expelling compressed air at high velocities tangential to the blades. This Jet-Assist module is used on the switchable turbocharger to spin it up externally when this turbocharger is switched on. Obviously the effects of this module affect the transient behavior of the turbocharger during spinning-up. However, there is no qualitative data available on the component and the characteristics. This component is ignored for the model since it's effects are only present for a very short time, in the order of a few seconds.

6.5.3. Compressor operating outside of the stable region

It can be witnessed in figure 6.25 that the switchable compressor is operating beyond the surge region of the compressor. In practice this operation would result in mass flowing in the opposite direction, in the model this does not occur. It can be imagined that this operation is realistic since, the second turbocharger's compressor suddenly gets exposed to a high pressure ratio while it is still spinning up. One could image that in this situation, mass would flow back through the compressor until it spins up fast enough to overcome the pressure ratio. The compressor map and characteristics are discussed in more detail in chapter 8.

6.5.4. Pro's and Con's of the Full STC model

Finally a list of pro's and con's of the Full STC model is presented and discussed.

PRO: able to capture the performance of each individual TC group.

Because both of the turbochargers are fully modeled in Simulink, the Full STC model can produce the contribution of each individual turbocharger. This has the added benefit of being able to create an engine that has two turbochargers that each have different characteristics.

PRO: gas control valves for STC are fully modeled.

The gas control valves that are controlling the mass flow of the switchable turbocharger are accounted for in the Full STC model. These valves help to accurately depict the engine performance during switching of the turbochargers.

CON: complex model, might take some time for a user to fully comprehend the model.

The model is far more complex than the simple STC model. Whereas the original Diesel B model already looks quite intimidating in Simulink, the Full STC model is even larger and it may take some time for new users to get acquainted with it.

CON:Increased number of integrators, thus increasing the computational load of the model.

The Full STC model requires 7 more integrators to be added to the original 17. This creates a significant increase in the computational load of this engine model.

CON: - Model does not scale in turbocharger groups

The Full STC model does scale well for a different number of turbocharger groups; a different number of turbocharger groups requires significant change of the Simulink model. This is not as simple as just changing some variables in the parameters files.

7

TNI Corvette model

The two previous chapters have demonstrated the two engine models that were developed for this research assignment. One of the goals was to gain insight into the physical processes that take place inside a sequentially turbocharged Diesel engine. Therefor the models were analyzed in a separate environment where the focus lay on the interaction between the engine and the turbocharger groups. Another goal of this research assignment was to provide an analysis of the engine performance on board a navy vessel. For this analysis the sequentially turbocharged engine model is placed inside an environment where all of the vessel's drivetrain components are modeled. This analysis will consist of two parts, in the first part the sea trial data is replicated with the model to form the validation of the total ship model. The second part of the analysis consists of an investigation into alternative control strategies with the goal of improving the vessel acceleration while maintaining engine limits.

7.1. Model description

The TNI Corvette model is based on the SIGMA corvette TNI Diponegoro, pictured in figure 1.4. In this model, the complete propulsion drivetrain of the ship and the propeller-hull interaction are accounted for. The model components that are used in this model are taken from an existing simulation model of the TNI Diponegoro, this model was supplied by DSNS. The author has chosen to divide the top level of model into two distinct sub systems:

- Bridge – this subsystem holds all of the control elements of the TNI Corvette model. It receives instantaneous physical values from the Ship system for feedback and issues new control signals to the Ship system for the actuation of physical components.
- Ship – this subsystem holds all of the models that represent the physical components and processes on board the vessel. This subsystem receives commands from the Bridge system and reacts accordingly.

Dividing the model into these two subsystems provides a clear distinction between the physical components and the control components. If the hardware on board of the physical ship is not changed, the Ship subsystem in the model remains the same. However, changing a control strategy on board of the real ship can be as easy as replacing some values in one of its computers. Separating the TNI Corvette model into these two systems gives future users the freedom to play around with the Bridge system without having to worry about remodeling the physical ship components.

This explains the top level model decision; in the following sections, the components of the Ship system are discussed in more detail.

7.1.1. Ship system

As explained before, the Ship system holds all the components that make up the propulsion drive train and the propeller hull interaction. An overview of the Ship sub system is given in figure 7.1.

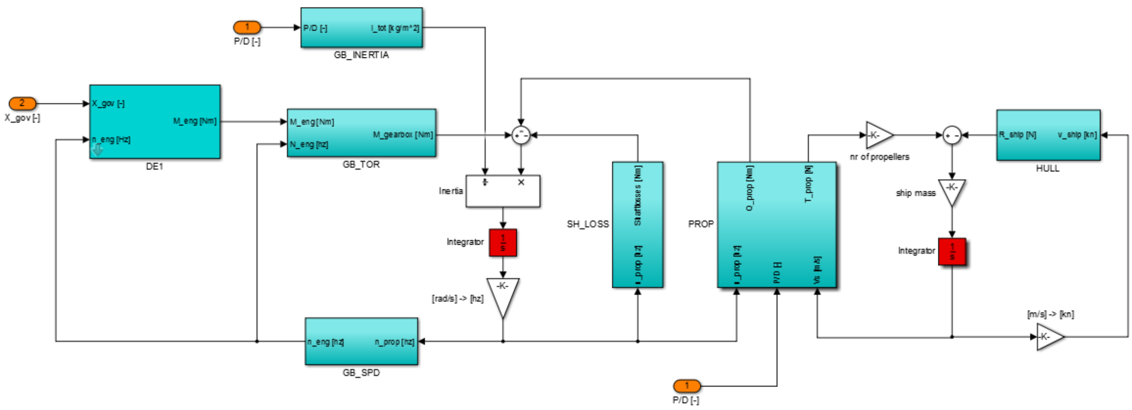

Figure 7.1: The Ship sub-system in Simulink.

In the Ship system there are two integrators that determine the velocity based on the laws of motion by Newton and Euler. The speed of the vessel is calculated with Newton's second law, equation 7.1.

$$m_{ship} \cdot \dot{v}_{ship} = 2 \cdot T_{prop} - R_{ship} \tag{7.1}$$

The propeller thrust and ship resistance force are treated in more detail in their respective sub sections. The other integrator calculates the angular velocity of the propeller shaft. Eulers law of motion for rigid bodies, equation 7.2, is used to calculate this velocity as was done in equation 5.10.

$$I_{tot} \cdot \dot{\omega}_{prop} = M_{eng} - M_{gb\_loss} - M_{shaft\_loss} - Q_{prop} \tag{7.2}$$

It can be seen that in equation 7.2 the losses of the gearbox and shaft are accounted for. These losses were not accounted for during the transient analysis of the engine itself in sections 5.4 and 6.4.

7.1.2. Engine sub system

The engine model in the Ship sub-system is the engine model that was treated in chapters 5 and 6. A choice had to be made to use the Simple STC model or the Full STC model. Based on the results of chapters 5 and 6, the author made the choice to integrate the Simple STC model into the TNI Corvette model. The arguments for this choice are as follows:

- The Simple and Full model show the same trends for the majority of their operation. The main difference is the switching effects that occur when the turbocharger groups are switched, however these effects only occur for a few seconds. When this transient has settled, both models give the same results.
- The computational load of the Simple STC model is lower than that of the Full STC model. This makes it possible to do more experiments with the TNI Corvette model due to the lower simulation time requirements.
- The switchable turbocharger components can sometimes cause converging problems for the model when this turbocharger is switched off. The mathematical model has some problems running below the minimum speed of the turbocharger. This causes some instability in the gas exchange components, preventing them from converging to a solution for the model.

7.1.3. Gearbox sub system

The gearbox system is split up into three different components, figure 7.1. The simplest sub system is the speed sub system; here the propeller speed gets multiplied by the gearbox ratio to output the engine shaft speed, equation 7.3. The torque subsystem translates the engine torque to the torque experienced on the propeller shaft.. In this subsystem the gearbox torque losses are also calculated. These are dependent on the engine speed and torque, the relation is given by the manufacturer, equation 7.5. The resulting torque on the output shaft of the gearbox is given in equation 7.6. The final sub system of the gearbox calculates the inertia as experienced by the propeller shaft. This is a sum of all the parts of the drive line where the inertia of the propeller is also dependent on the pitch of the propeller blades to account for the mass of the trapped water, equation 7.7.

$$n_{eng} = n_{prop} \cdot i_{gb} \tag{7.3}$$

$$M_{prop} = M_{eng} \cdot i_{gb} \tag{7.4}$$

$$M_{gb\_loss} = f(n_{eng}, M_{eng}) \tag{7.5}$$

$$M_{gb\_out} = M_{eng} - M_{gb\_loss} \tag{7.6}$$

$$I_{tot} = \left(I_{eng} + I_{gear\_eng} + I_{gear\_inter}\right) \cdot i_{gb}^2 + I_{gear\_prop} + I_{gear\_prop}(pitch) \tag{7.7}$$

7.1.4. Shaft Losses

The shaft losses are modeled with a look-up table that is dependent on the speed of the shaft. The data for these losses is supplied by the manufacturer. The losses are corrected for the direction of rotation to ensure that the shaft losses always act as a loss of power and never as a gain. The speed dependency of the losses is summarized in 7.8.

$$M_{gb\_loss} = \text{abs}\left(f(n_{prop})\right) \tag{7.8}$$

7.1.5. Propeller sub system

The propeller is a controllable pitch propeller; it is modeled with the use of the well-known open water diagram method. This method uses dimensionless coefficients to capture the propeller characteristics for different operating points. The different operating conditions are.

- Advance ratio (J)
- Propeller blade pitch

The propeller is the component that couples the two equations of motion to each other. On the one side it supplies a (negative) torque to the Eulers equation and on the other side it supplies a (positive) force in the Newton equation. The propeller torque and propeller thrust (force) are calculated with equations 7.9 and 7.10 respectively.

$$Q_{prop} = K_Q \cdot \rho \cdot n_{prop}^2 \cdot D_{prop}^5 \tag{7.9}$$

$$T_{prop} = K_T \cdot \rho \cdot n_{prop}^2 \cdot D_{prop}^4 \tag{7.10}$$

The coefficients K_Q and K_T are the dimensionless coefficients that where mentioned before. These are related to the dimensionless advance coefficient, J and the pitch of the propeller blades. Advance coefficient J is calculated with equation 7.11. The relation between the 3 dimensionless coefficients and the propeller pitch is measured under different conditions and tabulated for use in calculations. In the Simulink model, the K_Q and K_T coefficients are calculated with a 2D look-up table that depends on both the advance coefficient J and the propeller pitch, equations 7.12 and 7.13.

$$J = \frac{v_{ship} \cdot (1 - w)}{n_{prop} \cdot D_{prop}} \tag{7.11}$$

$$K_Q = f(J, pitch) \tag{7.12}$$

$$K_T = f(J, pitch) \tag{7.13}$$

The wake fraction in equation 7.11 and the thrust deduction factor in equation 7.10 are corrected for ship speed. These relations are based on model test of the ship's hull by MARIN.

7.1.6. Hull sub system

The hull system holds the total ship resistance. This ship resistance is derived from measurements on model test by MARIN. The implementation in Simulink is rather simple, a look-up table dependent on the ship velocity, equation 7.14.

$$R_{ship} = f(v_{ship}) \tag{7.14}$$

This concludes the description of the Ship system that holds all the machinery of the propulsion drive train. Before moving on to the application of the model, the Bridge system is shortly discussed. This system holds all the controls of the simulation. It consists of three components:

- Telegraph
- Combinators
- Engine governor

The telegraph is representative of the lever on the bridge that controls the load of the propulsion system. This lever goes from 0% to 100%, which is transferred to the combinators for the propeller pitch and the engine speed. The telegraph also has the ability to select two different propulsion modes: maneuvering and transit.

The combinators relate the lever position of the telegraph to a desired engine speed and propeller pitch set point. There are two different combinator settings, one for maneuvering and one for transit. Depending on the lever position and telegraph mode, the combinators send a speed set point to the engine governor and a pitch set point to the propeller pitch controller. The propeller pitch controller is not modeled as a dynamic component with feedback. In the model, the actual propeller pitch is a result of the set point and a rate limiter that limits the adjustment speed of the pitch.

The engine governor consists of two different sub systems, a PID controller and a set of limiters. The PID controller is the component that determines the fuel rack position. It does this by means of negative feedback on the actual engine speed and the engine speed set point. The limiters are evaluated after the PID controller; these limiters limit the fuel rack position from the PID controller based on pre-determined engine limits. For instance, the manufacturer specifies a fuel rack limit based on the engine speed and the number of active turbochargers to avoid overrating of the engine.

7.2. Steady state analysis of the load

The previous section gave a description of the components in the TNI Corvette model. The extra components in the TNI Corvette model provide a more accurate simulation of the engine load than the simulations that were performed in chapters 5 and 6 where the engine was either loaded with a perfect propeller law or the recorded shaft load. In this chapter the engine load is analyzed separately to provide some more insight into the steady state performance of the load. This will also provide some insight into the different combinator modes and vessel characteristics.

7.2.1. Method

As mentioned before, the interest of this steady state analysis is focused on the load and not the engine. The interaction of the engine is removed by removing the engine from the TNI Corvette model. In the full TNI Corvette model, the engine determines the shaft speed based on the experienced torque and delivered fuel rack position. This relation can be replaced by imposing the desired set-point speed of the combinator directly onto the engine shaft. Because the model is evaluated very slowly (semi-steady state) the transient interaction of the engine is not important and the model would reach the desired steady state speed set point anyway in this situation. Removing the engine just makes the analysis a lot faster.

The analysis is performed by first initializing the model dynamics at 0% of the telegraph lever. Afterwards the lever is moved to 100% very slowly over the course of 6000 seconds. This ensures that the model dynamics are neglected and the steady state characteristics are captured

7.2.2. Results

The results of the steady state load analysis are presented against the lever position. This provides insight into the relation of the sailing conditions and the input that is given from the bridge. Figures 7.2 and 7.3 form the exception, these figures show the steady state operating lines of the two different combinator modes in the torque and power envelopes of the engine.

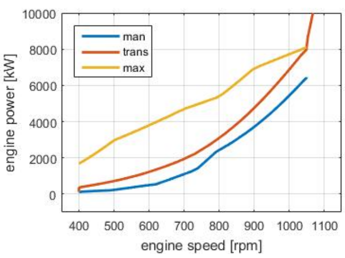

Figure 7.2: Steady state simulation result: power envelope of the engine, the two combinator modes and the maximum power rating.

Figure 7.2 shows the steady state operating modes of the two combinators. It can be seen that both operating modes are chosen very conservatively in relation to the maximum available power. Both are relatively low, especially in the low power range. The maneuvering operational line is lower than the transit line, presumably to have more available power for extra loading effects that occur during maneuvering (effects like increased wave resistance). Another interesting effect that can be witnessed is the sudden rise in power of the transit operation at the very high end of the speed range. This is done to ensure that the engine is always operating at the maximum engine rating when the lever is in the maximum position. The engine is over-rated and the load is controlled by reducing the pitch in such a way that the maximum engine load is attained trough different sea state and weather conditions. The pitch-reduction scheme is not modeled in this TNI Corvette model so this area must be avoided. In this TNI Corvette model, the engine would be severely over-rated if the lever is set to this position.

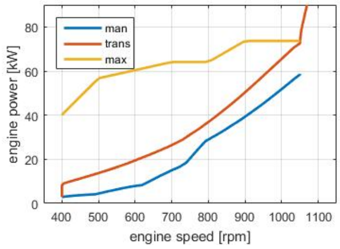

Figure 7.3: Steady state simulation result: torque envelope of the engine, the two combinator modes and the maximum torque rating.

The same effects can be seen in the torque envelope as could be seen in the power envelope of figure 7.2. This comes as no surprise as the power and torque envelope are closely related trough the x-axis: engine speed.

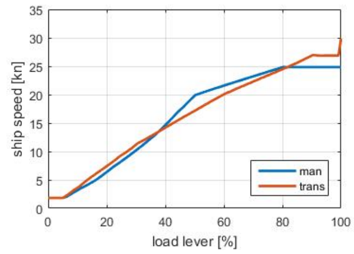

Figure 7.4: Steady state simulation result: ship speed of the TNI Corvette.

The steady state ship speed is related to the telegraph lever position for both combinator modes. It can be witnessed that the vessel speed is gradually increased with the lever position, for transit mode the vessel speed is almost linear to the lever position. This linear relation is desirable since it allows the operator on the bridge to set the speed of the vessel by only looking at the control lever. For transit mode, the final velocity settles at 27 knots and for maneuvering mode at 26 knots.

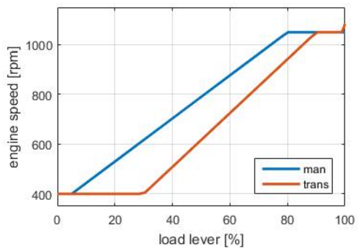

Figure 7.5: Steady state simulation result: engine speed.

The engine speed depicted in figure 7.5 is a direct result of the combinator set point. As explained before, the engine is not present in the model and the speed set point is directly imposed on the drive shaft of the propulsion line. Therefor figure 7.5 shows the direct output of the combinator modes in relation to the telegraph lever.

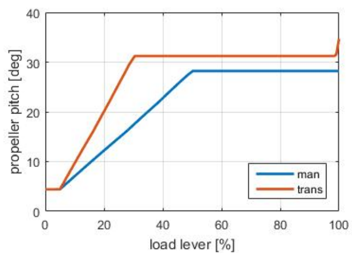

Figure 7.6: Steady state simulation result: propeller pitch.

Figure 7.6 show the pitch of the propeller. As with the engine speed in figure 7.5, there is no dynamic interaction on the actual pitch and the desired pitch. As a result, the propeller pitch shown in figure 7.6 shows the direct output of the combinator modes.

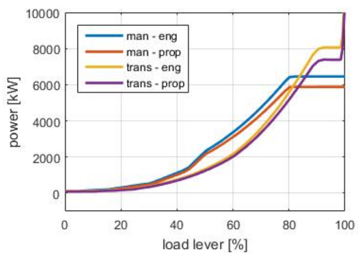

Figure 7.7: Steady state simulation result: power requirement.

In figure 7.7 the power of the propeller and the power experienced by the engine are shown in relation to the telegraph lever position. One of the interesting aspects of this figure is that it shows the losses of the shaft and gearbox combined. The difference between the propeller power and engine power is caused by these losses. These are also the losses that are neglected during the transient analysis of the isolated engine models in sections 5.4 and 6.4.

The results of the steady state load analysis provide some insight into the different loading conditions as a result of the telegraph lever position. These can be used to evaluate the choice of the combinators and potentially select new values for the combinator modes. For the scope of this report, these results are presented to provide the user with a clear understanding of the loading conditions on board the real vessel. The combinator modes will not be changed for this report, but they remain in interesting topic for the purposes of control optimization of the total propulsion system. This chapter will continue with the transient analysis of load.

7.3. Transient analysis of the load

In this chapter, the dynamics of the entire naval vessel are analyzed whereas in the previous two chapters the engine was analyzed separately. Before looking into the effects of the engine-load interaction it is wise to look at the load separately as to get a better understanding of the limits of the load itself.

7.3.1. Method

To test the dynamic limits of the naval vessel and the control strategies, all of the dynamics in the engine are removed and the engine torque is calculated directly by the fuel rack position with a linear relation. Figure 7.8 shows a schematic on how the engine speed and torque are determined.

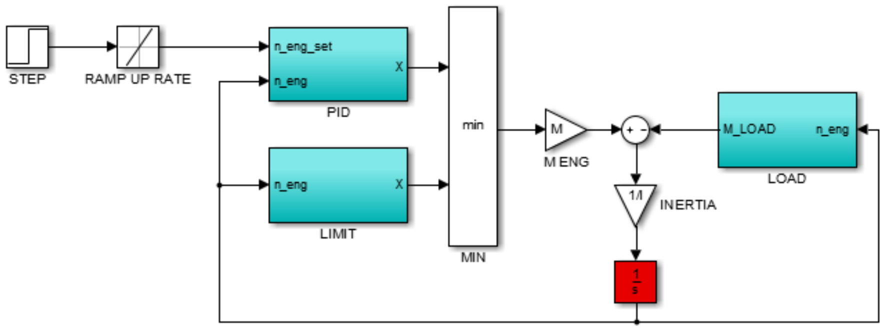

Figure 7.8: A schematic overview of how the engine torque is determined.

With the model shown in figure 7.8, the dynamic limits of the load are tested for several different ramp-up rates of the engine shaft speed. A step is applied to the PID controller; this step is limited in ramp up rate by the rate limiter. The PID controller itself is very quick to respond, it has a rise time of 3.8 seconds to go from 0% to 100%. The rate limiter is much slower, the default setting that is used in the recorded sea trial data is 3.2 $[rpm/s]$. This relates to a rise time of 203 seconds to go from 0% to 100%. The results will show the impact of increasing this rate limiter.

7.3.2. Results

In this section, the results from the dynamic load limit are shown against time. The simulation is performed for different ramp-up rates; 100%, 400%, 1000%, 5000% and 1e15% of the default rate limit of 3.2 $[rpm/s]$. As before in chapters 5 and 6, the acceleration begins at 600 rpm. For the TNI Corvette model this relates to a lever position of 45% and the acceleration is done with the transit combinator mode. Because the simulation starts at 45% lever load, the ship is already sailing at a significant speed, in this case 16 [kn]. The results will be plotted against simulation time, for consistency the same timescale is used as was done in previous chapters; starting at 50 seconds.

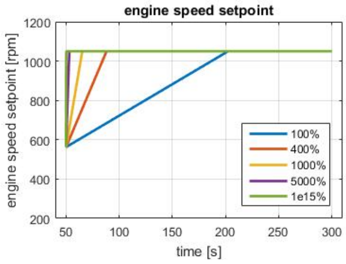

Figure 7.9: Transient analysis of the load: engine speed set point.

The engine speed set point is the result of the ramp-up rate limiter. The blue line for 100% shows the current limit that is placed on the engine in terms of acceleration. Increasing this limit will provide some insight in whether it is possible to utilize the full available power and torque based on the operating envelope.

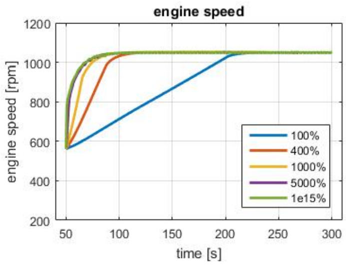

Figure 7.10: Transient analysis of the load: engine speed.

The actual engine speed follows the engine speed set point, however the inertia of the shaft and mass of the vessel limit the actual engine speed to ramp up as fast as the set-point.

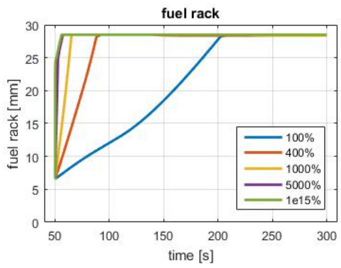

Figure 7.11: Transient analysis of the load: fuel rack position.

The fuel rack is the result of the difference in actual and set point engine speed that the PID controller uses to calculate the governor fuel rack position. It is limited by the governor limiter if the value calculated by the PID controller exceeds the accepted value for the current engine speed.

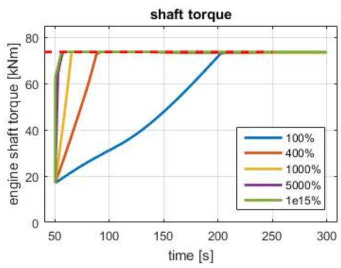

Figure 7.12: Transient analysis of the load: engine torque.

As explained in the previous section, the engine torque is a direct linear result of the fuel rack. This was done to remove the dynamics of the engine. Therefore the engine torque from figure 7.12 shows the same progression as the fuel rack from figure 7.11 only with a different magnitude.

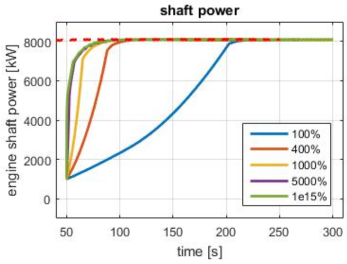

Figure 7.13: Transient analysis of the load: engine power.

The shaft power is the result of the torque and the speed of the engine. Whereas the torque was able to increase almost unrestricted, the engine speed still has to cope with the dynamics of the shaft. The power shown in figure 7.13 shows the same trend as the engine speed in figure 7.10.

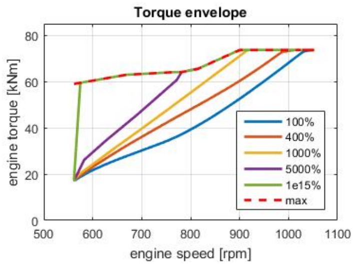

Figure 7.14: Transient analysis of the load: torque envelope.

The torque envelope of figure 7.14 gives some very important results, it can be witnessed that the available torque at lower engine speeds is only used by the limit of 1e15%. This limit is so high that it can hardly be seen as a ramp and more like a step. The second highest limit, 5000%, is also very high compared to the original 100% yet it does not provide a significant increase in utilized torque based on this operating envelope. Therefore it seems as if the load (propeller-vessel resistance) is in itself a limiting factor for the acceleration of the vessel and it would take and engine that can ramp up as fast as a step function to utilize the available torque at the beginning of the acceleration.

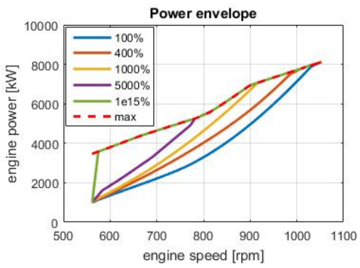

Figure 7.15: Transient analysis of the load: power envelope.

The power envelope shows the same effect as the torque envelope; the available power at the beginning of the acceleration is not fully used. To use this power the engine would have to ramp up almost instantly.

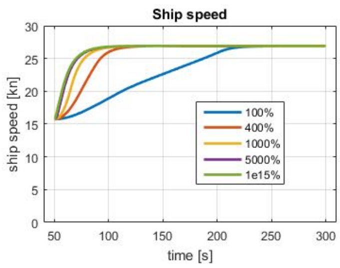

Figure 7.16: Transient analysis of the load: ship speed.

As a result of the faster engine acceleration, it can be seen that the vessel reaches its final velocity earlier. This comes as no surprise as this was the objective of the analysis.

7.4. Transient analysis – replicating the sea trial data

In this section the TNI Corvette model will be analyses during a transient load step that was recorded in the sea trial data. This is essentially the same analysis that has been performed for the Simple STC model and the Full STC model in sections 5.4 and 6.4 and differs from the analysi in the previous section because this time the engine dynamics are included. For this simulation, the components for torque losses are not neglected in the analysis because the shaft an gearbox losses are modeled in the simulation. This should provide a more realistic loading pattern of the engine and give a more accurate comparison to the sea trial data than the results from sections 5.4 and 6.4.

7.4.1. Method

The method is the same as before in chapters 5.4 and 6.4, the model is given the same input as the real vessel experienced during the sea trial. This time the input is provided through the telegraph lever which directly controls the set-point of the engine speed.

The analysis is performed in the time domain and the same domain is used for simulation as was recorded in the sea trial data. The individual results are discussed in the following section

7.4.2. Results

The results of the transient analysis for the TNI Corvette model are presented in the same manner as the results of chapters 5.4 and 6.4. All parameters are plotted in the time domain with time in seconds on the x-axis.

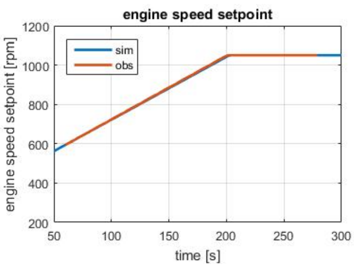

Figure 7.17: Transient simulation result: engine speed set point.

The engine speed set point is practically the same in the simulation as in the recorded sea trial data. The constant slope in figure 7.17 is a result of the rate limiter that limits the acceleration of the engine shaft.

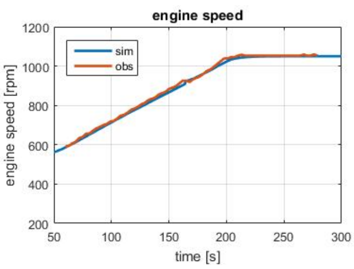

Figure 7.18: Transient simulation result: engine speed.

The engine speed of the model results and the sea trial data bears a close resemblance to each other. There is a noticeable deviation at approximately 160 seconds. Here the second turbocharger is switched in and the power of the engine increases due to the sudden increase in mass flow to the engine, as discussed in chapter 5.4.

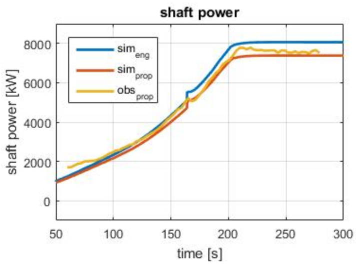

Figure 7.19: Transient simulation result: engine torque.

Figure 7.19 shows the recorded propeller shaft torque and the simulated shaft torque. The re and yellow lines follow each other closely, this means that the model is experiencing the same load as the physical engine did on board of the vessel.

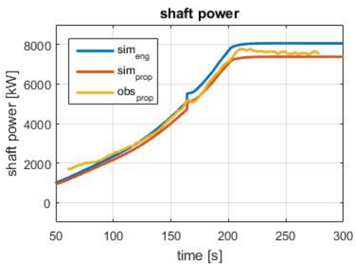

Figure 7.20: Transient simulation result: engine power.

Figure 7.20 shows the recorded propeller shaft power and the simulated shaft power. The engine power is also pictured in figure 7.20 and it can be seen that it is slightly higher than the propeller power; this is because the engine has to compensate for the losses in the gearbox and shaft. Including these losses should provide a more accurate comparison than the simulations of chapters 5 and 6, where these losses were neglected.

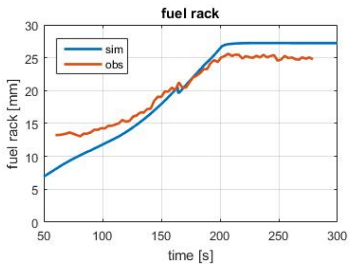

Figure 7.21: Transient simulation result: fuel rack position.

The fuel rack position in figure 7.21 shows the same trends as the fuel rack did during the transient analysis of the isolated engine models. It is interesting to see that the fuel rack tends to have the same trends towards the peaks in the data set but it deviates quite far in magnitude, especially in the beginning and end of the acceleration.

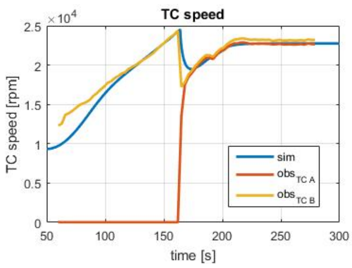

Figure 7.22: Transient simulation result: turbocharger speed.

The turbocharger speed in figure 7.22 shows the acceleration of the permanent turbocharger in the model and both turbochargers on the real engine. The simulation follows the trend closely with the exception of the switching behavior at 160 seconds. The behavior in the beginning of the acceleration also shows some minor deviation in magnitude but the trend does comply.

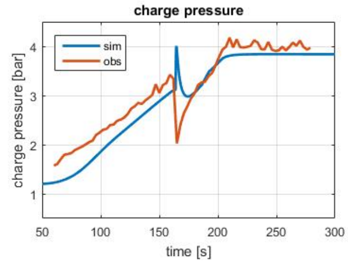

Figure 7.23: Transient simulation result: charge pressure.

Earlier in chapter 5.4 the transient analysis of the Simple STC model was presented. In this chapter the results of the charge pressure showed a similar but less pronounced peak in charge pressure during the switching of the turbochargers. The conclusion on the Simple STC still holds in the sense that it is able to replicate the trends of a sequentially turbocharged engine fairly well with the exception of the switching event itself.

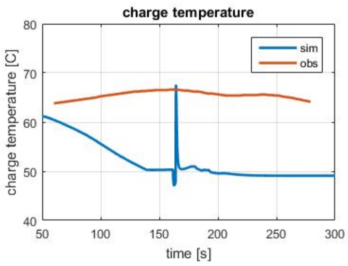

Figure 7.24: Transient simulation result: charge temperature.

The charge temperature in figure 7.24 shows the same average deviation as it did for the analysis in the previous chapters; this deviation is in the order of 10 degrees Celsius.

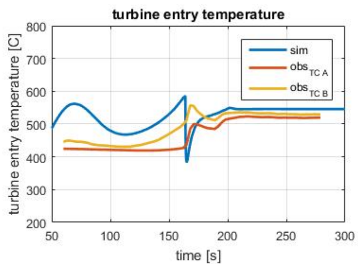

Figure 7.25: Transient simulation result: turbine entry temperature.

The turbine entry temperature in figure 7.25 shows the same trends as in the previous chapters, the trend is correct but there is a slight bias of approximately 30 degrees Celsius. The switching region shows the same trends as in chapter 5.4 where the Simple STC model was analyzed. During this switching event the simulated turbine entry temperature is off by a very large margin and the simulation results are not representative of the real process.

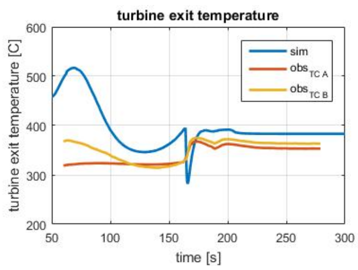

Figure 7.26: Transient simulation result: turbine exit temperature.

The turbine exit temperatures in 7.26 show the same issues as the turbine entry temperature in figure 7.25. The trends are replicated fairly well with the exception of the switching event.

This concludes all the parameters that where recorded in the sea trial data set. The following figures are parameters that are calculated by the model but unfortunately not recorded. These parameters will provide a more in-depth understanding of the processes in the engine.

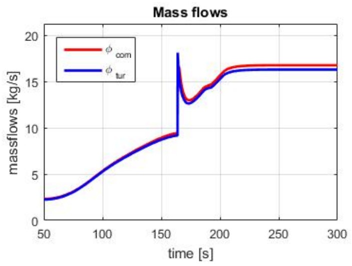

Figure 7.27: Transient simulation result: mass flows.

The mass flows shown in figure 7.27 show a similar trend to the results from the isolated Simple STC model in figure 5.41. When the second turbocharger is switched in, the mass flow is instantly multiplied by two. The resulting large peak in mass flow leads to a large error for the mass flow, this inaccurate modeling behavior settles after a few seconds.

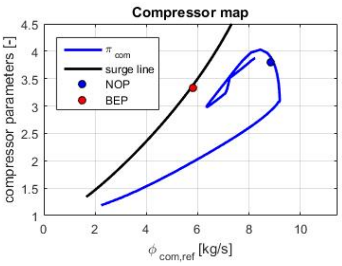

Figure 7.28: Transient simulation result: compressor map.

Figure 7.28 shows the compressor map of the permanent turbocharger. The same transient line from single to dual charger operation can be seen in figure 5.42. As was explained in chapter 5.4, this transient line is inaccurate.

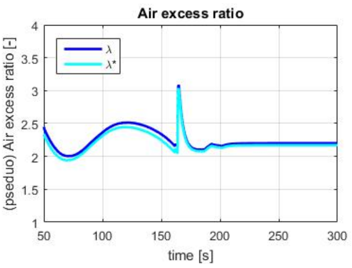

Figure 7.29: Transient simulation result: (pseudo) air excess ratio.

At the start of the acceleration, the air excess ratio is decreasing due to the increased loading of the engine. The increased loading means that more fuel needs to be injected and the turbocharger needs to keep up with the thermal load of the engine. At the start of the acceleration, the turbocharger is lagging behind and so the air excess ratio decreases. The high mass flow caused by the switching of the turbochargers is also producing a large error in the air excess ratio during the switching event.

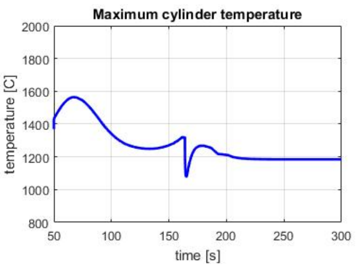

Figure 7.30: Transient simulation result: maximum cylinder temperature.

The maximum cylinder temperature in figure 7.30 is a result of the air excess ratio shown in figure 7.29. The decreased air excess ratio causes the cylinder temperatures to rise because there is less air to adsorb the heat of combustion.

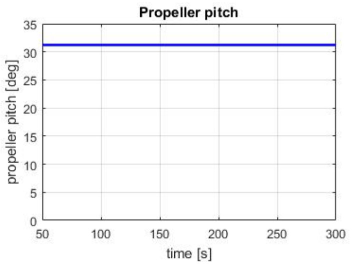

Figure 7.31: Transient simulation result: propeller pitch.

The propeller pitch is shown in figure 7.31, it can be witnessed that the pitch is at a constant pitch of 32 degrees for the entire acceleration.

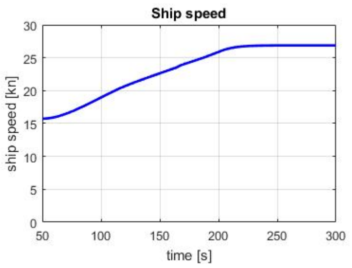

Figure 7.32: Transient simulation result: vessel speed.

Figure 7.32 shows the vessel speed. The goal of the load step on the telegraph lever was to accelerate the vessel; the model shows that the vessel is indeed accelerating. The vessel accelerates from 16 knots to 27 knots in little more than 200 seconds.

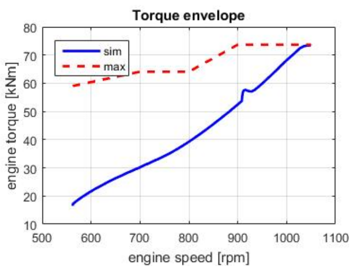

Figure 7.33: Transient simulation result: torque envelope.

The torque envelope of the engine during the acceleration is compared to the maximum allowed torque. It is apparent that this maximum is not reached except for the end when the full load of the lever is attained. Considering the engine margin in figure 7.33, there is a lot of theoretical torque available during the acceleration.

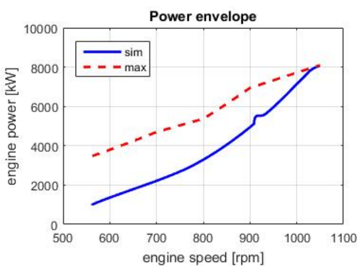

Figure 7.34: Transient simulation result: power envelope.

For the power envelope in figure 7.34, the same effects can be witnessed that were seen in the torque envelope of figure 7.33. The maximum available power is not utilized at the beginning of the acceleration when one would expect it to be used.

7.4.3. Validation

The validation of the TNI Corvette model will make use of the same method as presented in chapter 5.3.4 relying on the RMSE and the NRMSE (equations 5.14 and 5.15). This will give the average absolute and average relative error.

Table 7.1: RMSE and NRMSE for the simulation results in comparison to the sea trial data set

	RMSE		**NRMSE**	
engine speed	9.3181	[RPM]	1.9879	[%]
engine power	347.73	[kW]	5.7077	[%]
fuel rack	2.2357	[mm]	17.8138	[%]
turbocharger speed	1282.1	[RPM]	10.5972	[%]
charge pressure	0.3617	[bar]	13.8902	[%]
charge temperature	14.1395	[K]	504.98	[%]
temperature at turbine inlet	54.7495	[K]	43.1778	[%]
temperature at turbine outlet	58.5139	[K]	95.2399	[%]

7.5. Sensitivity analysis of the speed set point rate limiter

The results from section 7.4.2 have shown that the engine speed is able to closely follow the engine speed set point during acceleration, see figure 7.17 and 7.18. During this acceleration the required engine power does not approach the maximum available engine power as shown in figure **??**. In section 7.3 it was shown that the engine speed rate limiter acts as a restriction for utilizing the available torque during acceleration. It was found that the rate limiter needs to be severly increased to utilize this are of the operating envelope. However, the engine dynamics were not taking into account. This section will look at the engine limits that occur during acceleration with an increased engine speed rate limiter. This is done with a sensitivity study to show the effects of increasing the slope of the rate limiter in increments.

7.5.1. Method

The model acceleration is performed several times each time with a different slope for the rate limiters. The existing rate limit is 3.2 [rpm/s], this will be raised by 150%, 250%, 400% and 1000%. As before, the acceleration will take place under the same conditions as presented in section 7.4.2. For this analysis the load lever is moved from 45% to 95%.

7.5.2. Results

The results of the sensitivity analysis for the TNI Corvette model are presented in the same manner as the results of previous sections. All parameters are plotted in the time domain with time in seconds on the x-axis, the time domain is the same as that for the sea trial data.

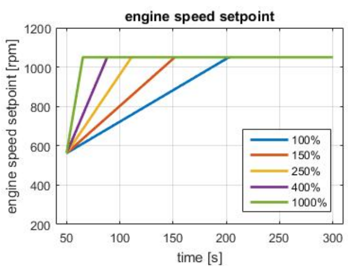

Figure 7.35: Sensitivity analysis result: engine speed set point.

Figure 7.35 shows the speed set point. The rate at which the speed set point increases is the variant parameters of this sensitivity analysis. The 100% case is the base case from section 7.4.2. The next figures will show the effects that this increased rate limit has.

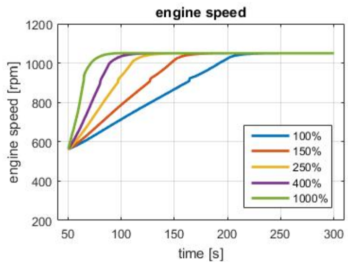

Figure 7.36: Sensitivity analysis result: engine speed.

The engine speed follows the trends that are requested by the speed set point. The small kink that is visible in all of the speed lines is the switching of the turbochargers. The higher the rate limit, the faster the engine reaches its required speed. The highest rate limit shows a small overshoot, this is caused by the I-gain in the PID controller in the governor.

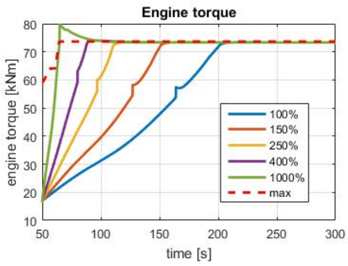

Figure 7.37: Sensitivity analysis result: engine torque.

The engine torque increases faster for the higher rate limiters. This is not surprising, because the governor is allowed to inject more fuel in a shorter amount of time.

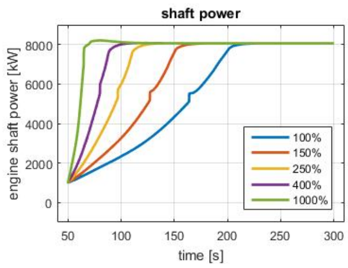

Figure 7.38: Sensitivity analysis result: engine power.

The engine power shows the same trends as the engine speed, the increased load limit makes the engine accelerate faster and there is a small overshoot for very large rate limits. The kink created by the switching of the turbochargers is more pronounced in the power than in the speed. For the highest rate limit, the effects from switching are not visible.

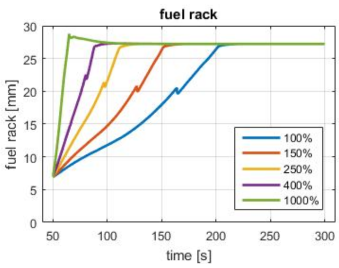

Figure 7.39: Sensitivity analysis result: fuel rack.

The results of the fuel rack position also show the overshoot for the highest rate limit. The other selected rate limit values each reach the desired fuel rack without any overshoot. At 95% load lever, all the simulations show the same results; the acceleration rate does not affect the final steady state conditions.

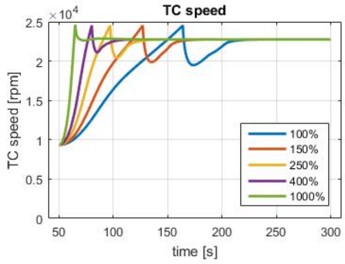

Figure 7.40: Sensitivity analysis result: turbocharger speed.

The turbocharger speed shows some interesting results. With an increased engine speed acceleration limit, the turbocharger speed needs to spin up faster as well. This is clearly witnessed in figure 7.40, where the increased acceleration causes the turbochargers to spin up faster. The increased rate limit also causes the turbochargers to switch over later in the acceleration (relative to the total time for acceleration). This is due to the time delay of the turbochargers; in the case for 1000% rate limit, the acceleration is done completely on a single turbocharger and the second turbocharger is only switched on at the end of the acceleration, in other words, turbo lag is occurring.

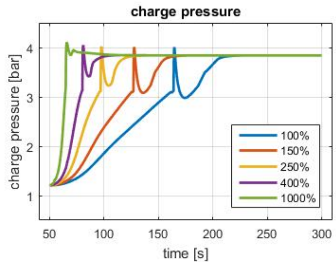

Figure 7.41: Sensitivity analysis result: charge pressure.

The charger pressure of the engine is relatable to the turbocharger speed. For the previous parameter, turbocharger speed, it was shown how an increased rate limit also increases the duty of the primary turbocharger. This effect can also be witnessed in figure 7.41 where the charge pressure is shown, this is again the result of turbo lag: where the turbocharger dynamics are out of sync with the engine dynamics.

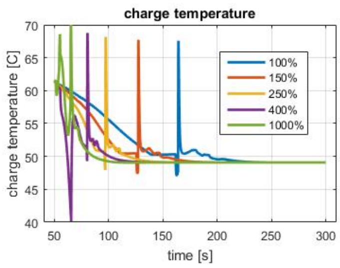

Figure 7.42: Sensitivity analysis result: charge temperature.

Charge temperature shows the same peek during switching as was witnessed earlier in figure 7.24. The overall differences in magnitude in charge temperature for the different rate limits are not significant. All the simulations show the same maximum values, only occurring faster or slower in time.

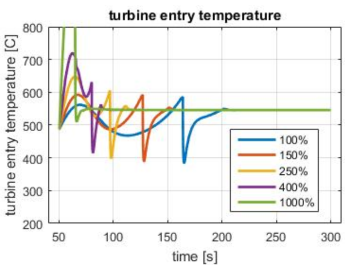

Figure 7.43: Sensitivity analysis result: turbine entry temperature.

In the beginning of the acceleration, the increased rate limit simulations show a higher turbine entry temperature. In later figures it will be shown that this higher entry temperature is a result of the decreased air excess ratio for the engine.

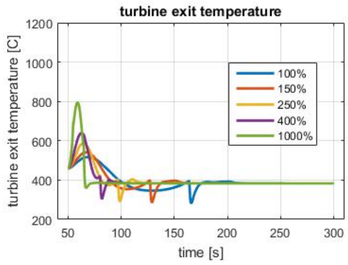

Figure 7.44: Sensitivity analysis result: turbine exit temperature.

As with the turbine entry temperature, the turbine exit temperature is significantly higher at the start of the acceleration for the simulations with an increased rate limit. In the case of 1000% rate limit increase, the exit temperature reached 800 degrees Celsius. This is of course very high for the gasses entering the exhaust silencer.

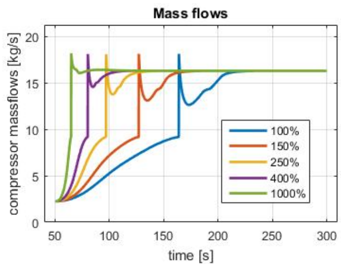

Figure 7.45: Sensitivity analysis result: compressor mass flow.

The results of the mass flow show the error that is introduced by the Simple STC model, the large peak that occurs when the second turbocharger is switched in. for the larger rate limit simulations, this problem becomes more significant. For the base case it was decided that the time scale of the switching effect was small enough in comparison to the total simulation length. Since the higher rate limit simulations take up less time, the effects of the switching are creating a larger error.

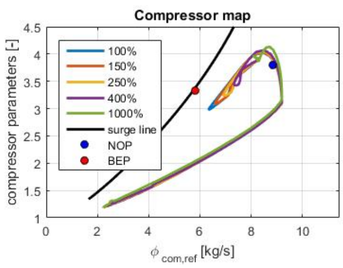

Figure 7.46: Sensitivity analysis result: compressor map.

The compressor map shows that the rate of acceleration has no impact on the operating lines in the compressor. What can be witnessed is that with higher acceleration, the compressor spends less time in dual charging operating mode. This is shown by the length of the upper operation line; this gets increasingly shorter for the higher acceleration simulations.

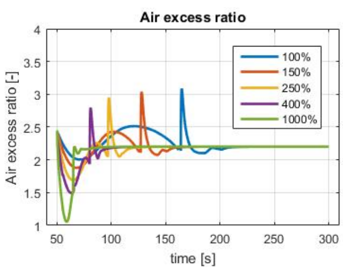

Figure 7.47: Sensitivity analysis result: air excess ratio.

The air excess ratio from figure 7.47 shows that it decreases during acceleration with an increased magnitude for higher acceleration rates. This was already hinted at for the explanation of the turbine temperatures. This effect is unwanted and the values shown for 1000% are exceeding the safe limits for thermal loading of the engine. The 400% simulation shows a minimum of 1.5 for the air excess ratio, this is deemed as the minimum accepted value for the air excess ratio. This choice is made arbitrarily by the author, based on common limits for this type of engine.

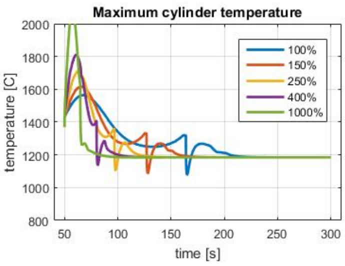

Figure 7.48: Sensitivity analysis result: maximum cylinder temperature.

With the decreased air excess ratio, comes a higher thermal loading of the engine. The exhaust gas temperatures were higher as showing in figure 7.43. This is of course a direct result of the fact that the cylinder temperatures are increasing significantly. The 1000% line shows cylinder temperatures in excess of 2000 degrees Celsius, this is extremely high and most likely above the continuous engine limits.

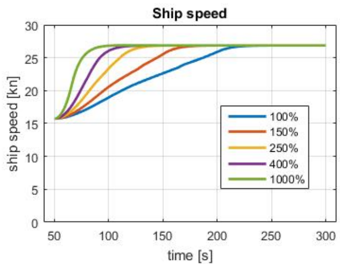

Figure 7.49: Sensitivity analysis result: ship speed.

The ship speed reaches the same final value for all simulations but the time in which it does is very different. This comes as no surprise since improving the acceleration was one of the objectives for raising the rate limiter.

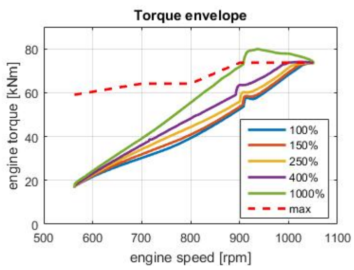

Figure 7.50: Sensitivity analysis result: torque envelope.

The torque envelope in Figure 7.50 shows how the available torque at the start of acceleration is not used. This was already shown in section 7.3, where the dynamic limits of the load were investigated. In this simulation, the maximum rate limiter is much smaller than in section 7.3 but it already exceeds the thermal limits of the engine (air excess ratio).

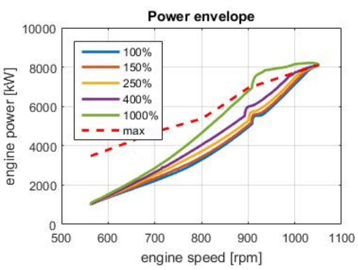

Figure 7.51: Sensitivity analysis result: power envelope.

Figure 7.51 shows the power delivered by the engine in the power envelope of the maximum allowable power. It can be witnessed that increasing the rate limit does not do much for the lower speed ranges; the difference between the simulations is very small here. At higher speed ranges the difference becomes more noticeable and even exceeds the maximum for the 1000% case.

7.6. Alternative control strategies

The models that are created for this research assignment can be used to investigate alternative control strategies. If other user would want to implement any control strategies to the model, this would be very easy due to the top-level division of control and machinery systems. For this research assignment one such strategy was suggested and this is briefly discussed.

7.6.1. Limiting fuel rack based on air excess ratio

As discussed before, the current limiting factor in the acceleration is the rate limiter on the engine speed set point. In the proposed alternative control strategy the rate limiter is removed and the maximum speed set point is given from the start of the simulation. With the alternative control strategy,a feedback loop on the air excess ratio limits the fuel rack in such a way that a minimum air excess ratio is attained. This control strategy is often applied in automotive applications where the air excess ratio is measured in the exhaust with a lambda probe. It can be more accurate as a control strategy than charge pressure based limits. This is due to the fact that lambda control relies on feedback whereas charge pressure control relies on feed forward.

The results are presented in the following figures:

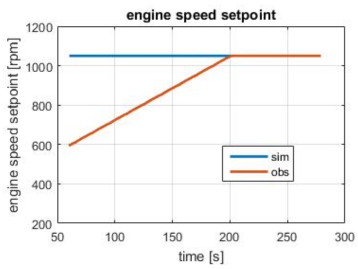

Figure 7.52: Alternative control result: engine speed set point.

The engine set point is unlimited, the final speed set point condition is given at the start of the simulation. In the observed data set the speed set point is gradually increased.

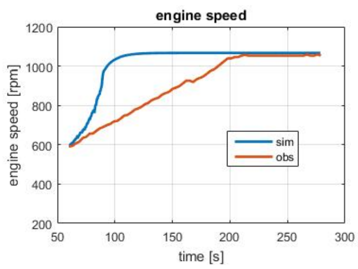

Figure 7.53: Alternative control result: engine speed.

The engine speed shows the effect of the new governor strategy. The engine is slowly accelerating due to the fact that the governor is limited by the air excess ratio.

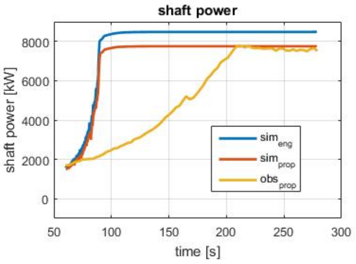

Figure 7.54: Alternative control result: engine power.

The engine power shows how the acceleration is performed faster than the with the original control strategy. It can also be seen how the engine power is higher during acceleration than in steady state. After reaching the desired speed, the engine power settles to the same steady state value.

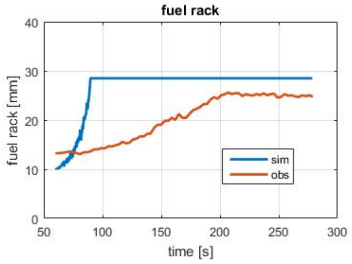

Figure 7.55: Alternative control result: fuel rack.

The fuel rack shows the same trends as the engine power. In figure 7.55 it can be seen that the control strategy is affecting the fuel rack.

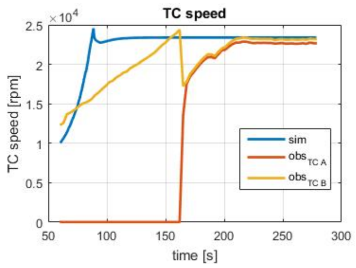

Figure 7.56: Alternative control result: turbocharger speed.

The turbocharger speed shows the same effects that where present during the increased rate limiter experiments. The turbocharger is spun up faster but the operation is mostly done on a single turbocharger. Near the end of the acceleration, the turbochargers are switched over to dual operation.

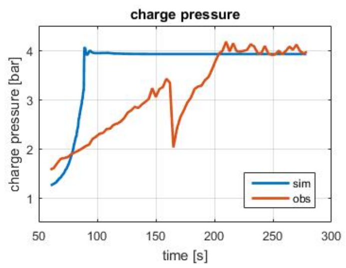

Figure 7.57: Alternative control result: charge pressure.

The effect of the late-switching are also witnessed in figure 7.57. The charge pressure is supplied by a single turbocharger during acceleration and only near the end is the second turbocharger switched in.

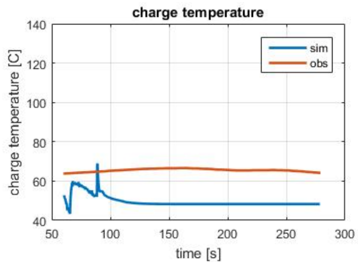

Figure 7.58: Alternative control result: charge temperature.

The charge temperature shows a similar trend to the earlier models. The simulation value is slightly lower than the observed value.

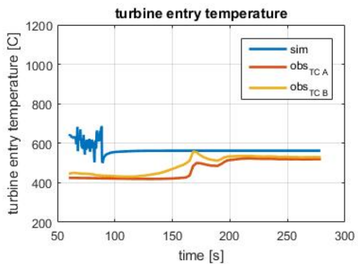

Figure 7.59: Alternative control result: turbine entry temperature.

The turbine temperatures show a very unsteady behavior when the control strategy is active. This is due to the fact that the control of the lambda value directly affects the turbine temperatures. Later it will be shown that the implementation of the control strategy does not result in a smooth behavior of the engine.

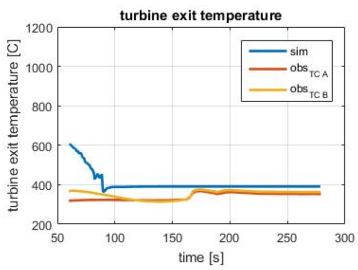

Figure 7.60: Alternative control result: turbine exit temperature.

The same effects for the turbine entry temperature can be witnessed for he turbine exit temperature.

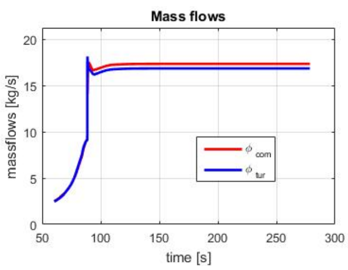

Figure 7.61: Alternative control result: mass flows.

For the mass flow in figure 7.61 , the same can be said as was said for the mass flow in figure 7.27. The results of the mass flow show the error that is introduced by the Simple STC model, the large peak that occurs when the second turbocharger is switched in. This problem is significant, for the base case it was decided that the time scale of the switching effect was small enough in comparison to the total simulation length. Since this simulations take up less time, the effects of the switching are creating a larger error.

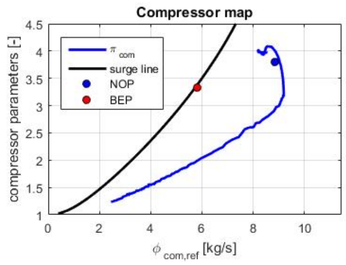

Figure 7.62: Alternative control result: compressor map.

The compressor map shows what was already stated for the turbocharger speed and charge pressure: during most of the acceleration, the engine operates on a single turbocharger.

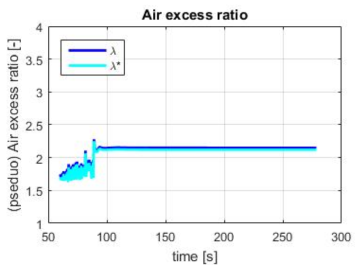

Figure 7.63: Alternative control result: air excess ratio.

The air excess ratio shows the effects of the control strategy, the control strategy starts to limit the fuel rack if the air excess ratio drops below 2. The fuel rack is then gradually limited until the air excess ratio drops below 1.6, after this the fuel rack is fully restricted.

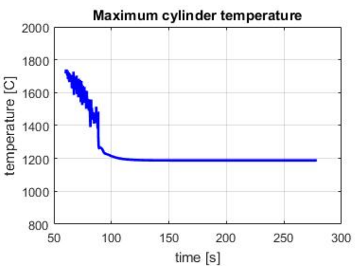

Figure 7.64: Alternative control result: maximum cylinder temperature.

The maximum cylinder temperature is getting very high in the range where the air excess ratio is low. The temperatures approach 1800 degrees Celsius, which is deemed too high for safe operation.

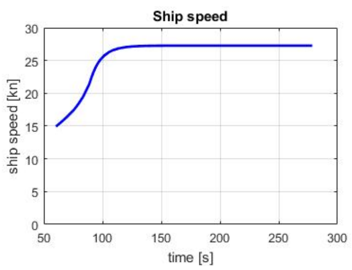

Figure 7.65: Alternative control result: ship speed.

The ship speed is show in figure 7.65, it can be seen that the acceleration occurs smoothly. The new control strategy seems to provide a smooth acceleration performance for the vessel, but not for the engines.

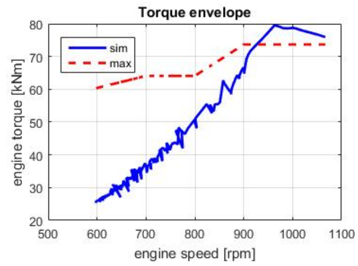

Figure 7.66: Alternative control result: torque enevelope.

The torque envelope shows that the control strategy is very noisy, this is most likely due to the simple implementation. However, if one were to image a smooth line through the blue line in figure 7.66, this line would represent the maximum acceleration that the engine can perform whilst still maintaining an air excess limit higher than 1.6. This provides some interesting insight into the fact that the available torque at the start of acceleration cannot be used and that the engine is limited by its thermal loading.

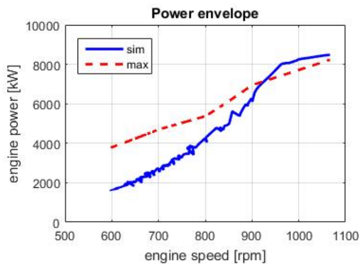

Figure 7.67: Alternative control result: power enevelope.

The power envelope shows the same effects as discussed for the torque envelope

7.7. Sub-conclusions

This section will discuss the sub conclusions on the TNI Corvette model after having presented the model implementation, the method and the results.

7.7.1. TNI Corvette acceleration

The application of the Simple STC model inside of the larger ship simulation has proven that is able to replicate the sea trial acceleration. For the lower speed and load combinations, the engine model results produce a large deviation in comparison to the sea trial data. This large deviation is caused by the errors produced by the scavenge model, this low load are is excluded from all of the presented simulation results and a more detailed discussion on this error is given in chapter 8.

7.7.2. Available power at the start of the acceleration

One of the supporting research questions was whether the available power at low speed, based on the operating envelope, could be utilized during acceleration. Section 7.3 has presented the dynamic limits of the load (ship and propeller). Here it was shown that to utilize the available power, the engine speed has to increase almost instantly to the desired set-point. If the acceleration of the engine is limited only slightly, the utilization of the available power decreases quickly. This analysis has shown that the selection based on the operating envelope alone is not sufficient to predict the availability of power during transient operation.

7.7.3. Dynamic propeller characteristics

The ship model does not include any dynamic model for the propeller pitch. In reality the propeller pitch is actuated by a hydraulic cylinder with its own dynamic characteristics. The dynamics of this system are ignored and the propeller set point is directly imposed on the propeller. However, the propeller pitch does not change during operation for all of the performed simulations. The dynamic response of the propeller is outside the scope of this research assignment, which focuses on the engine. To get a more complete picture of the load in the drive train, the propeller characteristics can be modeled more accurately. This would allow for more options on the control strategy and would be a good basis for a new research assignment that looks at the acceleration problem from a drivetrain level of detail.

7.7.4. Rate limit sensitivity analysis

The sensitivity analysis of the rate limiter has shown that in the current situation, the engine speed rate limiter is the limiting factor to the vessel acceleration. If this limit is increased the following trends can be witnessed:

- The air excess ratio is lowered
- The cylinder temperatures are increased
- The turbine temperatures are increased
- The turbocharger does not catch up fast enough, operates longer on a single turbocharger.

The lower air excess ratio is the results of the air supply to the engine. During increased acceleration, there is not enough air being supplied to the engine because the turbocharger is not spinning up fast enough. The same amount of fuel is injected but there is not enough fresh air moving through the engine. This air has to absorb the heat of combustion and its temperature is higher as a result. These high temperatures are an important limit to the engine operation. The actual limits are unknown and can be only be determined by an extensive material or (health) condition study of the engine. For the sake of argument, the author has arbitrarily selected the minimum air excess ratio to be 1.5. This is the minimum air excess ratio that occurs when the rate limit is increased by 400%. This low air excess ratio is only maintained for 5-10 seconds and is accompanied by very high temperatures. It is assumed that the mass of the engine components is sufficiently high not to reach a homogeneous temperature of this magnitude. Based on the results of the sensitivity analysis, the author would recommend a maximum increase in the rate limit of 400% for emergency situations.

7.7.5. Alternative control strategy

One alternative control strategy was analyzed, the strategy was to remove the engine speed rate limit and instead limit the governor fuel rack based on the actual air excess ratio. This strategy has shown to be lacking in its implementation. The control strategy is too simple in its implementation, looking at the air excess ratio alone is not sufficient for a smooth control strategy. In automotive applications, the air excess ratio is also used to determine the amount of fuel to be injected. However, it is often applied in the form of 3-d maps that relate the air excess ratio and the engine speed to a maximum limit for the amount of fuel to be injected. These control maps are created by tuning the engine on an engine-bench or inside the vehicle on a rolling road. This allows for a lot of flexibility on different operating regions of the engine, but also requires extensive research and testing to create these maps. This is outside of the scope of this research assignment and this alternative control strategy is deemed insufficient for its current implementation. However this control strategy has provided some insight into what the maximum acceleration rate is at which the air excess ratio does not drop below 1.6. Accelerating any faster than with this control strategy would surely result in damaged engine parts.

8

Discussion

In this chapter, a short discussion is provided on the results that were presented in the previous chapters. It offers room to discuss some of the findings and clarify some of the author's suspicions before drawing hard conclusions in the next chapter.

8.1. The generic Diesel B compressor and turbine maps

The Diesel B model uses semi-empiric relations for the compressor and turbine components. This has proven to be a sufficient method in the past as it was used for single turbocharger Diesel engines. The compressor and turbine map can be scaled to any size turbocharger and the map shape can be adjusted within certain limits to better present a given turbocharger. However, these options do leave much to be desired in terms of adjustability. The shape parameters have relatively small ranges for which the model is viable. This shortcoming has proven to be quite a large problem for this research assignment.

The emphasis of this research assignment is on the turbocharger components. Therefor it is important that the compressor and turbine maps are modeled correctly. Since these maps are not available, the shape parameters have been adjusted with the DOE method, appendix F. This has resulted in a solution for the generic compressor and turbine maps that provides a best-fit solution in comparison to the Lloyds dataset. This does not mean that the models are representative of the real performance; it means that the generic models have been parameterized in such a way that they approach the real performance as much as possible.

The problem with these maps is even worse for sequentially turbocharged engines because they have to account for multiple operating lines. This means that the full map has to be modeled correctly and not just a single operating line, as is the case with a single turbocharged engine.

8.2. Uncertainty in mass flow parameters

In the previous section it was explained how there is some uncertainty in the generic compressor and turbine maps. These maps hold the relations for the four governing parameters of the compressor and turbine models, these four parameters are:

- turbocharger speed
- pressure ratio
- mass flow
- isentropic efficiency

Of these four parameters, the turbocharger speed and pressure ratio are recorded in the Lloyds data set. The isentropic efficiency can be calculated based on the temperature and pressure ratio, both of which have been recorded in the Lloyds data set. This leaves the mass flow as the only unknown parameter. This is in fact one of the most important parameters in the gas exchange model, since its primary function is to model the mass flow through the different components. Not being able to compare the mass flow of the simulation to any real world data set is a big problem for the validation of the model output. For the calibration process, the model has been tuned to best represent all the recorded parameters. Since the mass flow was not recorded, no quantitative conclusion can be drawn regarding to whether the mass flow is modeled correctly throughout the model.

8.3. The Diesel B scavenge model

The Diesel B model was presented in chapter 3, here it was explained that the model has a high level of detail and many different processes are calculated in this model. One of these processes is scavenging of the cylinder. This occurs when both in and outlet valves are open; a difference in pressure causes the mass to flow from the inlet receiver to the outlet receiver. The reverse can also occur, this is called negative scavenging. This entire process is governed by the scavenging sub model in the Diesel B model.

For the work on this research assignment, many errors where encountered during the simulation sessions. The origin of a large portion of these errors can be traced back to the scavenging model. This scavenge model is based on the equations postulated by Stapersma [18]. Problems arise for this model when the engine is operating in very low speed regions. The scavenge conditions are dependent on the relative scavenge time. For these very low speed regions, the relative scavenge time goes to infinity, or rather the inverse (1 divided by the relative scavenge time) goes to zero. This means that the scavenge flow becomes infinitely large, something that is obviously not representative of the real process. The large error in the scavenge model leads to all sorts of other problems in the model, for instance the high scavenge temperatures which propagate to other temperature variables. The simulation results in these low speed regions have been excluded from this report.

The scavenge model itself is outside of the scope of this research assignment but it deserves to be mentioned for the reasons stated above. It was assumed that the proven track record of the Diesel B model would guarantee a correct representation of the Diesel engine and the gas exchange of the engine itself (air swallow demand). The problems encountered with the scavenging model have proven that the Diesel B model still has some internal issues that need to be resolved.

8.4. The Direction of flow

The direction of mass flow is limited to one direction for most components in the Diesel B model. This was already briefly touched upon in section 6.2 where the need for a virtual decompression valve is discussed. The limits for the directional flow are different for each restrictor element:

- The compressor and turbine restrictor models are both single-direction mass flow producers, these models will need a thorough remodeling to make them compliant with a bi-directional system.
- The cylinder model does allow for bi-directional mass flow, this is the negative scavenging model.
- All the other restrictors are based on the sub-sonic orifice plate model, which is also able to produce a bi-directional mass flow

The direction of flow is also a problem for most of the volume elements. As discussed in appendix E, the volume elements contain two balances; mass and energy. The mass balance is relatively simple, just a summation of all the masses in the model. Since a mass flow in the opposite direction is accompanied by a change in sign, the mass balance is correct even if the direction of the flow switches. However, the energy balance is not correct when the flow reverses. When mass leaves the volume, it is modeled in such a way that the energy leaving the volume is related to the mass flow and the temperature of the volume itself. If mass enters the volume, it is modeled in such a way that the energy entering the volume is related to the mass flow and the temperature of the mass entering the volume. If a mass flow that would normally leave a certain volume enters the volume (reversal of flow), the wrong temperature is used to calculate the energy balance.

This is the case for all of the volumes in the Diesel B model, with the inlet receiver as the exception. The inlet receiver is adjusted in such a way that it switches the temperature when negative scavenging occurs.

9 Conclusion

The previous chapter offered some discussion on the uncertainties in the simulation model and the problems arising from them. However it is still possible to drawn valid conclusions based on the research assignment. This chapter will provide hard conclusions on the main and supporting research questions. The main question of this research assignment given in chapter 1.4 and repeated here:

> *What are the effects on part-load and transient performance when sequential turbocharging is applied to marine Diesel engines?*

9.1. Answer to the main research question

The manufacturers claim that a sequentially turbocharged engine has a better part-load performance than a standard single turbocharged engine [6] [2]. The steady state performance of the simulation models, section 5.3 confirms this claim. The part load performance is better because of a higher quality of the air supply. This higher quality is the result of the following effects:

- The charge pressure for a single turbocharger is higher in part load than for the configuration of the dual turbocharger operation, this can be witnessed in figure 5.17. It is important to note that for the flow characteristics in steady state, the dual turbocharger operation mode acts in the same way as a large single turbocharger.
- The higher charge pressure at part load results in a higher mass flow supplied to the engine, this can be seen in figure 5.24. The single smaller turbocharger is able to supply more air to the engine at part load than the combination of two of the same turbochargers. This is only valid up to the point where the smaller turbocharger starts to choke, beyond this point the dual turbocharger operation is better.
- The higher mass flow into the engine also has the beneficial result of increasing the air excess ratio, figure 5.26. In part load, the air excess ratio is much higher for the smaller turbocharger. This allows for more fuel to be injected; the maximum available power is higher in part load for a sequentially turbocharged engine than for a single turbocharged engine.
- The increased air mass being drawn into the cylinder helps keep the process temperatures lower for the same power rating. This can be seen in figures 5.27, 5.21 and 5.23 where respectively the cylinder temperature, turbine entry temperature and turbine exit temperature are shown. All of these temperatures are significantly lower for the single smaller turbocharger; this means that the engine operation is further away from the physical temperature limits in the engine.

The points mentioned above show that under steady state conditions the sequentially turbocharged engine provides some significant benefits to the part-load operation of the engine

The transient analysis of the engine models has provided some interesting results on the effects that occur during the transition from one turbocharger to two turbochargers. These conclusions are based on the Full STC model, as presented in chapter 6.

When switching occurs, the turbocharge speed and charge pressure drop very rapidly to stabilize at a new operating point in the compressor and turbine map, figures 6.16 and 6.17. The transition in the permanent compressor map, figure 6.24, shows how the operation shifts from the single turbocharger operating line to the dual turbocharger operating line. The transition in the switchable compressor map, figure 6.25, shows how the switchable turbocharger shifts its operation from being inactive to matching that of the permanent turbocharger. The switchable turbocharger crosses the surge line during this transition, in the sub-conclusions of chapter 7 it was reasoned that this is a logical effect due to the sudden change in pressure ratio and speed of the second turbocharger.

The switching of the turbochargers has some negative impact on the engine performance; the supply of mass flow to engine is severely reduced during this transition. This effect can be witnessed in both the mass flow and air excess ratio, shown in figures 6.23 and 6.26 respectively. This negative effect is not mentioned by the manufacturer or any other literature on sequentially turbocharged engines. However, the author has reason to believe that this effect occurs on the actual physical engine, the manufacturer has built in a limiter in the governor that severely limits fuel injection during the switching of the turbochargers. The reason for this limit could very well be explained by the witnessed mass flow starvation effects in the simulation model.

In appendix B it was proven with the help of geometric scaling laws that the relative acceleration of a smaller turbocharger is higher than that of a larger turbocharger. A small turbocharger that provides half the air of a large turbo charger has a relative acceleration that is twice as high. Unfortunately there was no test data available of the same engine fitted with two different turbocharging strategies to confirm these findings. But thus far the scaling laws have given some merit to the claims that the engine manufacturers make on the improved dynamic performance of sequentially turbocharged engines.

No other mentionable transient effects have been witnessed in the model results. The transient performance is limited by the engine speed rate limiter. Because of this, there are no specific benefits in terms of acceleration for the application of sequential turbocharging. This conclusion is based on the transient analysis of chapters 5.4 and 6.4 where the rate limiter is not changed from the settings on board the actual vessel. A more in-depth conclusion on the transient effects related to the application of sequential turbocharging itself is given in the next section of the conclusions.

9.2. Answers to the supporting research questions

In this section, the answers to the supporting research questions are given based on the results of the research assignment.

Can the TU Delft Diesel engine models be adapted to simulate sequentially turbocharged engines?

For this research assignment, the TU Delft Diesel B has been adapted to form two different models: the Simple STC and Full STC models. The theory and application of these models has been discussed in great detail in chapters 5 and 6 respectively. Both models have certain benefits and drawback that are discussed in the sub-conclusions of these chapters, section 5.5 and section 6.5. The differences between these models are only visible in the transient analysis; for steady state, both models produce the same output. For transient analysis, the Full STC model captures the transient effects that occur during switching of the turbochargers more accurately. The Simple STC model is not able to capture this effect because the assumptions on which the model was built do not hold up during this switching event.

Both models are able to capture the trends of the real Pielstick PA6B STC engine within acceptable accuracy, the exact error values are listed in the validation sections of each individual analysis. In the prior chapter, a discussion on the accuracy of the adaption of generic components is given. Because the Diesel B model uses generic components, such as the compressor, it is not possible to fit the components in such a way that they offer an exact representation of the real components. This is a compromise that has to be made because exact specific models are not modular and there is not enough data to construct them.

This leads to the conclusion that the adaption of the Diesel B model is able to replicate the trends in a sequentially turbocharged engine accurately enough that it is suitable for application in larger systems, such as a marine vessel. However, it is not possible to adapt the model in such a way that all of the relevant engine parameters are modeled with a very high accuracy, making the model insufficient for a detailed engine study.

Can a simulation model be used to better predict/understand the transient behavior of a sequentially turbocharged engine on board of a naval vessel?

The Simple STC model has been integrated into a full model of one of the TNI Corvettes. Several acceleration tests have been performed with this model and have given some insight into the different limits that are present during acceleration.

First the dynamic limits of the load were tested to see if the available torque in the operating envelope could be utilized. For this analysis the engine dynamics were removed and the engine torque was based directly on the fuel rack position. With this analysis it was shown that the engine speed rate limit needs to be severely increased to utilize the available power during acceleration. To fully utilize the available power, the engine needs to ramped up almost instantaneously. This is of-course not possible since the engine has all sorts of internal mechanical and thermodynamical processes that are dependent on time. These processes present certain limits and have been analysed with a sensitivity analysis in section 7.5.

Currently the acceleration is limited by the rate in which the engine speed increases. This limit has been set by the manufacturer and it is somewhat conservative. A sensitivity analysis of the rate limit has shown how the engine limits are not met in the current situation. When the rate limit is increased, the turbocharger is increasingly starting to lag behind the acceleration of the engine. This results in lower air excess ratios and consequently higher cylinder and turbine temperatures. An increase of 400% of the rate limit was chosen as the maximum safe increase of the rate limit. In this situation, the minimum air excess ratio is low (1.5) but this only occurs for a brief time. A more in-depth study on the actual physical limits is needed to quantify the safety margins.

The combination of the transient load analysis and the rate limit sensitivity analysis have shown that the load itself is limited in how fast it can absorb power and that the engine is limited at a much lower acceleration limit. The original selection based on the operating envelope gives the wrong impression when predicting the transient performance. The high torque at low speed is available in steady state conditions, as shown in appendix C, but during acceleration the engine is limited in how fast it can reach this maximum load.

Can vessel performance be improved by changing the control strategy with the same hardware?

A single alternative control strategy was introduced in this report, a limit on the air excess ratio. This strategy has shown that the resulting machinery operation is not very smooth but this is mostly due to the simple application of this control strategy, as discussed in more detail in section 7.7.5. This research assignment has mostly focused on the engine as an isolated component to get a good understanding of the effects of sequential turbocharging. The implementation of different control strategies needs a more in-depth analysis to come to any meaning full conclusion regarding alternative control strategies. At the start of this thesis it was assumed that the analysis of alternative control strategies would be more plug-and-play. The model implementation is indeed plug-and-play due to the separation of the BRIDGE and SHIP model. However the reasoning and analysis of different control strategies needs sufficient attention to come to a meaningful conclusion of its application on board a real vessel.

The analysis of this particular control strategy has given some insight into what is the maximum rate at which the engine may accelerate. By limiting the air excess ratio and not the engine speed rate limiter, it has been shown what the theoretical acceleration limit of the engine is. This theoretical limit is nowhere near the maximum available torque in the operating envelope. This leads to the same conclusion as the previous question, that the application of a sequentially turbocharged engine as a main propulsor has a lot less power available during acceleration than is expected based on the operating envelope.

10
Recommendations

After the discussion and conclusion of the research assignment, there are still some interesting topics that can be investigated. This chapter will present some of the recommendations by the author based on this report.

10.1. Scavenging model

As discussed in chapter 8, the scavenging model has some serious limitations in the low speed ranges of the engine. The results that the simulation model produces are deviating strongly from the measured data in this region. A detailed study into the limitations of this scavenge model can resolve a lot of the problems associated with the Diesel B engine model. This work would require a detailed set of measured parameters that are significant to the scavenging process. Since most of these measurements have to take place inside cylinder, this research would require significant cooperation of one of the engine manufacturers. Alternatively a shipyard can be approached that is willing to make a significant investment into adding sensor equipment to an engine that is in operation on board a vessel.

10.2. True modular volume elements

The volume elements solve two different balances, the mass and energy balance. As discussed in chapter 8, the mass balance is working in both directions in its current implementation. The energy balance is not correctly modeled for bi-directional mass flow. This is due to the selection of the temperature, this is not corrected for in- or outflow. The temperature is only defined in the default flow direction. The construction of a truly modular volume model would be very beneficial to the expansion of the volume resistor network for alternative turbocharging strategies. If the volume model is created as a custom Simulink block through the use of S-functions, the number of in and output channels can be defined through top-level block parameters. In the current situation, the addition or removal of a mass flow channel requires significant modeling work in Simulink to change the inner workings of the individual volume elements.

10.3. Compressor and turbine model behavior outside of the stable operating region.

For the Full STC model, the switchable turbocharger is brought to rest when it is not active. When it does, it operates outside of the stable turbocharger operating region. For the compressor, there are four limits that bound the stable operating region. The direction for these boundaries are given in relation to the compressor map, example in figure 2.1. The four limiting factors are:

- Bounded on the left side by the surge line
- Bounded on the right side by the choking line

- Bounded on the top by the maximum turbocharger speed
- Bounded on the bottom by the minimum turbocharger speed

The mathematical model for the compressor is able to operate outside of these regions, but there is no validation study to confirm its accuracy in this region. Studying this effect can shed more light on the requirements for spinning up the turbocharger from rest. This can also add to the study into the effect of the jet-assist module that is present on the real engine but is not modeled in the simulation.

10.4. Diesel Bminus model

The author has created a simplified Diesel B model, full details in appendix D. This model was rejected early on because its performance was deviating very strongly for low speed ranges. For this reason the validation of the model was never performed and it was chosen to continue the development of the existing Diesel B model. This study has shown that the Diesel B model is severely limited by the scavenge model, as discussed above. This is quite interesting because this same limitation was witnessed in the Bminus model. It was assumed that this was a result of over simplifying the scavenging process, but now the author suspects that the actual theory used to construct this model is somewhat limited. Both the Diesel B and the Bminus model are based on the same physical principles that are postulated by Stapersma [**?**]. The author does not claim that this theory is completely wrong, but rather that its implementation is somewhat limited for mean value Diesel engine modeling.

The coincidal regions of error for both the Diesel B and Bminus models gives the author the confidence to state that the Bminus model is not as bad as it was presumed in the beginning of this research assignment. A complete validation study of this model has the potential to yield a trustworthy mean value Diesel Engine model that fills the niche in complexity between the Diesel A and Diesel B models.

10.5. Confirm the mass flow results with real data

As stated in the discussion of chapter 8, there is a lot of uncertainty regarding the actual values of the mass flows in the real engine and simulation model. If mass flow measurements can be performed on a sequentially turbocharged engine, these measurements could be used to further quantify the error of the model. As with the study on the scavenge model, this would require significant cooperation of either an engine manufacturer or an operator that is willing to invest in the sensory equipment.

10.6. Using the STC models for comparison studies

In this report the focus was on the sequentially turbocharged Diesel engine. Since there was little information available on this type of engine, there was room to look at the processes that occur in this type of engine. There was not enough room in the scope of the thesis to also look at other propulsion concepts and see how they stand up against the sequentially turbocharged engine. With the work presented in this report, the model or modeling techniques can be used by others to do a comparative studies with other propulsion concepts such as: gas-turbines, electric motors, regular diesel engine or any combination of the aforementioned.

A

Specifications of the Pielstick PA6B V20 STC

The detailed specifications of the Pielstick PA6B V20 STC are presented in this appendix. The following data is available:

- Table A.1, General engine geometry and operating specifications
- Figure A.1, General operational envelope of the PA6B, presented in: relative power vs. speed.
- Figure A.2, Specific operational envelope for the SIGMA corvettes with switching strategy included, presented in: power vs. speed.
- Figure A.3, Consumption curves, presented in: power per cylinder vs. speed.
- Figure A.4, A schematic overview of the air/gas circuit.
- Figure A.5, A technical drawing of the exterior of the engine for installation purposes.

These are presented on the following pages in the order listed above.

A.1. General specifications

Table A.1: General engine geometry and operating specifications.

TABLE REMOVED - CONTAINS CONFIDENTIAL INFORMATION

A.2. General operating envelope

Figure A.1: General operational envelope of the PA6B, presented in: relative power vs. speed.

A.3. Operating envelope for TNI corvettes

Figure A.2: Specific operational envelope for the SIGMA corvettes with switching strategy included, presented in: power vs. speed.

A.4. Consumption curves

Figure A.3: Consumption curves, presented in: power per cylinder vs. speed.

A.5. Air circuit diagram

Figure A.4: A schematic overview of the air/gas circuit.

A.6. Technical drawing of exterior

Figure A.5: A technical drawing of the exterior of the engine for installation purposes.

B

Turbocharger inertia

The inertia of the turbocharger shaft is an important parameter when investigating the dynamics of such a system. Unfortunately, there is very little information available from the manufacturers and because the compressor and turbine wheels have such irregular shapes; it is hard to estimate the actual inertia of the turbocharger shaft. None the less, this appendix will provide a method to estimate the inertia based on the cross-section of the turbocharger shaft. Prior to this, a discussion on different sized turbochargers is presented based on geometric scaling laws.

B.1. Turbocharger scaling laws

One of the important questions for the dynamics of the sequentially turbocharged engines is whether two small turbochargers spin up faster than a single large turbocharger. A comparison study would require the same engine to be fitted with both turbocharging systems and this was unfortunately not available for this study. However, the difference will be investigated with the help of scaling laws. In the following equations, the subscripts 0 and 1 represent two turbochargers of different size with the same relative shape.

The scaling factor S is defined as the ratio of the radius of the compressor wheel between the two turbochargers:

$$\frac{r_1}{r_0} = S \tag{B.1}$$

Because the relative shape is the same, the length scales linear with the radius:

$$\frac{L_1}{L_0} = S \tag{B.2}$$

The compressor has the same relative shape, therefore it is assumed that the tip velocity, $r \cdot \omega$, remains the same, solving the equation for the speed ratio:

$$r_0 \cdot \omega_0 = r_1 \cdot \omega_1 \tag{B.3}$$

$$\frac{\omega_1}{\omega_0} = \frac{r_0}{r_1} = \frac{1}{S} \tag{B.4}$$

Again, because the relative shape stays the same, the degree of reaction (ratio of axial and tangential velocity) stays the same. Combing this relation with the speed and radius ratio gives a solution for the ratio for the axial velocity at the entrance of the compressor:

$$\frac{C_{a\_1}}{2 \cdot r_1 \cdot \omega_1} = \frac{C_{a\_0}}{2 \cdot r_0 \cdot \omega_0} \tag{B.5}$$

$$\frac{C_{a\_1}}{C_{a\_0}} = \frac{r_1 \cdot \omega_1}{r_0 \cdot \omega_0} = \frac{r_1}{r_0} \cdot \frac{\omega_1}{\omega_0} = \frac{1}{S} \cdot S = 1 \tag{B.6}$$

The mass flow ratio depends on the axial flow velocity, the density and the cross sectional area at the inlet. For the same inlet conditions, the mass flow ratio is defined as:

$$\frac{\dot{m}_1}{\dot{m}_0} = \frac{\rho_1 \cdot C_{a\_1} \cdot A_{CS\_1}}{\rho_0 \cdot C_{a\_0} \cdot A_{CS\_0}} = \frac{\rho_1}{\rho_0} \cdot \frac{C_{a\_1}}{C_{a\_0}} \cdot \frac{A_{CS\_1}}{A_{CS\_0}} = 1 \cdot 1 \cdot \frac{\pi \cdot r_1^2}{\pi \cdot r_0^2} = \left(\frac{r_1}{r_0}\right)^2 = S^2 \tag{B.7}$$

The compressor and turbine power scale with the mass flow, specific heat and temperature difference. If both turbochargers are operating under the same conditions, the power ratio becomes:

$$\frac{P_1}{P_0} = \frac{\dot{m}_1 \cdot c_{p_1} \cdot \delta T_1}{\dot{m}_0 \cdot c_{p_0} \cdot \delta T_0} = \frac{\dot{m}_1}{\dot{m}_0} \cdot \frac{c_{p_1}}{c_{p_0}} \cdot \frac{\delta T_1}{\delta T_0} = \frac{\dot{m}_1}{\dot{m}_0} \cdot 1 \cdot 1 = \frac{\dot{m}_1}{\dot{m}_0} = S^2 \tag{B.8}$$

The torque ratio follows from the power and speed ratio:

$$\frac{M_1}{M_0} = \frac{\frac{P_1}{2 \cdot \pi \cdot \omega_1}}{\frac{P_0}{2 \cdot \pi \cdot \omega_0}} = \frac{P_1}{P_0} \cdot \frac{\omega_0}{\omega_1} = S^2 \cdot S = S^3 \tag{B.9}$$

The complex shape of compressor and turbine wheel can be approached as a series of finitely small disk elements that vary in radius across the length of the shaft, this is explained in more detail in the next section. For each of these disk elements their mass ratio can be defined with:

$$\frac{m_1}{m_0} = \frac{\rho_1 \cdot V_1}{\rho_0 \cdot V_0} = \frac{\rho_1 \cdot L_1 \cdot \pi \cdot r_1^2}{\rho_0 \cdot L_0 \cdot \pi \cdot r_0^2} = \frac{\rho_1}{\rho_0} \cdot \frac{L_1}{L_0} \cdot \left(\frac{r_0}{r_1}\right)^2 = 1 \cdot S \cdot S^2 = S^3 \tag{B.10}$$

For each of these disk elements, their inertia can be defined with the mass and the radius, leading to the following ratio for inertia:

$$\frac{I_1}{I_0} = \frac{0.5 \cdot m_1 \cdot r_1^2}{0.5 \cdot m_0 \cdot r_0^2} = \frac{m_1}{m_0} \cdot \left(\frac{r_1}{r_0}\right)^2 = S^3 \cdot S^2 = S^5 \tag{B.11}$$

Combining the inertia and torque, it is possible to evaluate the rotational acceleration ratio of the turbocharger:

$$\frac{\dot{\omega}_1}{\dot{\omega}_0} = \frac{\frac{M_1}{I_1}}{\frac{M_0}{I_0}} = \frac{M_1}{M_0} \cdot \frac{I_0}{I_1} = S^3 \cdot \frac{1}{S^5} = \frac{1}{S^2} \tag{B.12}$$

Equations B.1 to B.12 are evaluated to see if a single turbocharger that supplies the full mass flow is slower than two turbochargers that each supply half of the air demand. For this application, subscript 0 belongs to the smaller turbocharger, as such S is determined with equation B.7: $S^2 = 2$. The results of this analysis are shown in table B.1.

Table B.1: Scaling analysis, 1 vs 2 turbochargers for the same total mass flow, $\dot{m}_1 / \dot{m}_0 = S^2 = 2$.

ratio	scaling factor	value
radius	S	$\sqrt{2}$
length	S	$\sqrt{2}$
speed	$1/S$	$1/\sqrt{2}$
mass flow	S^2	2
power	S^2	2
torque	S^3	$(\sqrt{2})^3$
inertia	S^5	$(\sqrt{2})^5$
acceleration	$1/S^2$	$1/2$

Table B.1 shows the scaling relations for the large turbocharger in relation to the smaller turbocharger. It can be seen that the mass flow is twice as large, this was the arbitrary chosen value in order to find a value for S. The relative acceleration of the larger turbocharger is only 50% of the smaller turbocharger. However, the speed of the larger turbocharger is also lower but the speed does not scale with the same relation as the acceleration. The speed of the larger turbocharger is only 71% of the smaller turbocharger. This leads to the conclusion that the two smaller turbochargers are in fact able to spin up faster than a single large turbocharger based on these simple scaling relations.

B.2. Calculation of the turbocharger inertia

The inertia of the turbocharger is not known or given by the manufacturer. However, the project guide of the compressor is available and it provides a cross-sectional view of the turbocharger shaft. This cross section is shown in figure B.1:

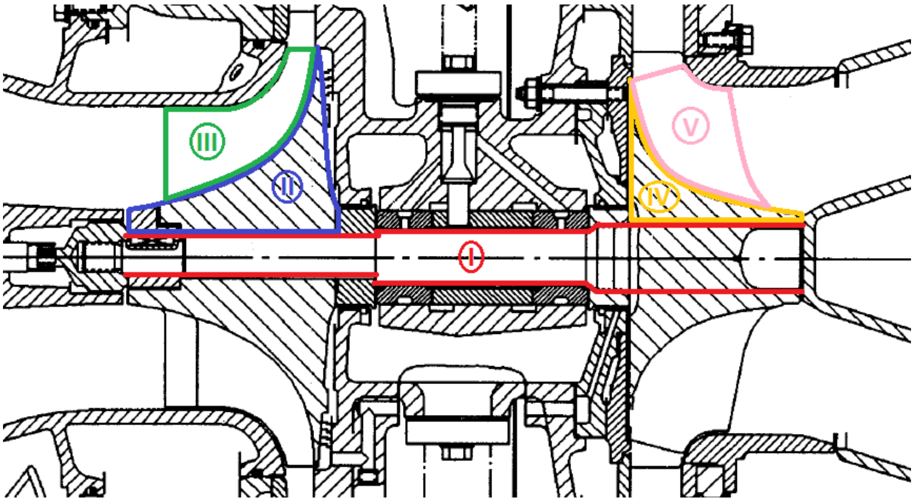

Figure B.1: A cross-section of the turbocharger shaft with its various components.

In this figure there are 5 different areas that can be defined:

- I - shaft
- II - compressor wheel solid core
- III - compressor wheel blades
- IV - turbine wheel solid core
- V - turbine wheel blades

The shaft is made out of steel with a density of 7900 $[kg/m^3]$, the compressor wheel is made out of aluminum with a density of 2720 $[kg/m^3]$ and finally the turbine wheel is made out of a special nimonic alloy with a density of 8100 $[kg/m^3]$. These materials were found in the project guide and can be used for the solid parts.

For the bladed parts, a different approach has to be taken. These volumes are treated as having a homogeneous density that is determined by specifying the fraction of air that takes up the volume. For this analysis, it is assumed that the blades take up only 10% of the volume in the bladed area. Therefore the mass fraction of air, $x = 0.9$. With this information the density of area III and V are defined as follows:

$$\rho_{(III)} = x \cdot \rho_{air} + (1-x) \cdot \rho_{aluminum} \tag{B.13}$$

$$\rho_{(IV)} = x \cdot \rho_{air} + (1-x) \cdot \rho_{nimonic} \tag{B.14}$$

The turbocharger shaft is now composed of 5 different shapes with each having a different homogeneous density. The contribution of each of these shapes can be determined by modeling the shapes as a series of finitely small disk/annular-ring elements. This method is explained by using the following analytic example, figure B.2 shows a red cone that rotates around the black striped y-axis and its radius y is defined along the x-axis with: $y = x^2$

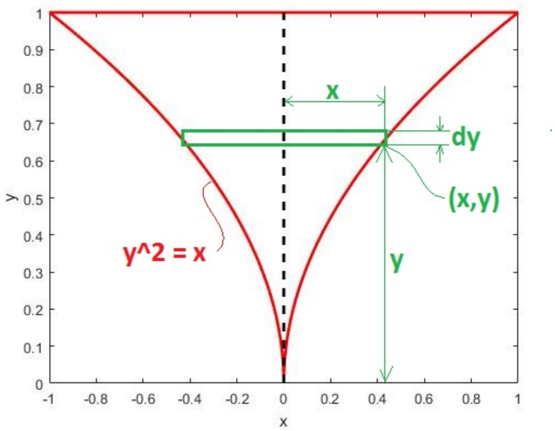

Figure B.2: A cross-section of a cone defined by $y = x^2$.

The green rectangle represents a disk element at an arbitrary point (x,y). This disk element has the following mass:

$$dm = \rho \cdot dV = \rho \cdot \left(\pi \cdot x^2\right) \cdot dy \tag{B.15}$$

Although all the portions of the element are not located at the same distance from the y-axis, it is still possible to determine the moment of inertia dI_y of the elements about the y-axis. The moment of inertia of a homogeneous cylinder about its longitudinal axis is $I = 0.5 \cdot m \cdot R^2$, where m and R are the mass and radius of the cylinder respectively. Since the height of the cylinder is not involved in this formula, the cylinder itself can be thought of as a disk. Thus, for the disk element in figure B.2, the moment of inertia is:

$$dI_y = 0.5 \cdot (dm) \cdot x^2 = 0.5 \cdot \left[\rho \cdot \left(\pi \cdot x^2\right) \cdot dy\right] \cdot x^2 \tag{B.16}$$

Substituting $x = y^2$ and integrating with respect to y, from $y = 0$ to $y = 1$, yields the moment of inertia for the entire solid cone:

$$I_y = \frac{\pi \cdot \rho}{2} \cdot \int_0^1 x^4 \cdot dy = \frac{\pi \cdot \rho}{2} \cdot \int_0^1 y^8 \cdot dy = \left(\frac{\pi \cdot \rho}{2 \cdot 9}\right) \cdot [y^9]_0^1 = \frac{\pi \cdot \rho}{18} \tag{B.17}$$

For the example given above, the radius (x) related to the length (y) through an explicit definition: $x = y^2$. This allowed for x to be substituted in equation B.16 and the integral could be solved analytically. For the real turbocharger parts, their curvatures are not defined by an explicit analytical formula. This makes it impossible to solve the integration analytically. However, it is possible to do the integration numerically with the help of Matlab/Simulink. Simulink is a tool that solves integration problems with ODE solvers, Ordinary Differential Equation solvers. These take place in the time domain but the integration above is performed over the length of the shaft, not over time. It is possible to trick Simulink into integrating over the length of the shaft, by simply treating time as distance and evaluating the simulation from zero until the end of the shaft. This can be done because it is just a name that is given to the variable.

The shape of the turbocharger parts from figure B.1 is digitized through an external tool to load the shapes into Matlab/Simulink. The figure is scaled to the radius of the compressor wheel, which is set to unity. This allows for the cross-section to be scaled up for different sizes. For the calculations of the NA34 turbocharger, the compressor wheel has a diameter of 34 cm; a radius of 17 cm. The digitized shape of the cross-section is shown in figure B.3.

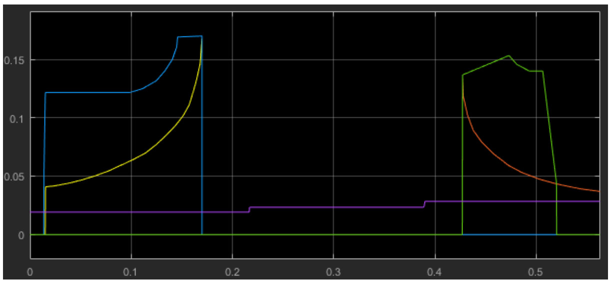

Figure B.3: The cross-sectional area of the turbocharger in Simulink, axis are in [m].

Equation B.16 is used to numerically integrate the inertia over the length of the shaft. The outer parts form an annular ring instead of a disk, the inertia of these parts is calculated by subtracting the inertia of the inner disk(s) from the outer disks. In this sense, the same formula applies but with some minor modification.

The inertia of the five components as well as the total inertia is given in table B.2, both in absolute and relative units.

Table B.2: Inertia of the turbocharger shaft and the contribution of its components

	[kg/m^2]	[%]
I - shaft	0.0239	57.95
II - compressor wheel solid core	0.1504	1.548
III - compressor wheel blades	0.0040	27.44
IV - turbine wheel solid core	0.0712	3.864
V - turbine wheel blades	0.0100	9.200
Total	0.2596	100.0

The inertia found with this calculation is used for all simulations with the Pielstick PA6B V20 STC engine.

C

Steady state analysis at the maximum limit of the operating envelope

During the analysis of the complete ship with the entire drive train, it was witnessed that the engine model was not able to reach the maximum engine torque during acceleration. This sparked the interest into if and how the engine would operate in steady state at the edge of the operating envelope. The results presented below are of the steady state performance of the engine on both the propeller law and the maximum torque rating. The graphs are presented in the same manner as the steady state results from section 5.3.

C.1. Results

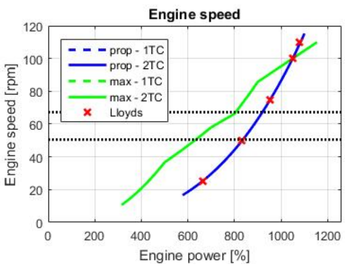

Figure C.1: Steady state simulation results: engine speed.

It can be clearly seen how the engine operating envelope is different for the two operating modes. The maximum power rating line has a higher power for a given engine speed up until 100% engine power. After this point it is limited by the manufacturer, whereas the propeller law increases to loads in excess of 100%. For naval purposes, the operating point at 110% engine power on the propeller curve is temporary allowed.

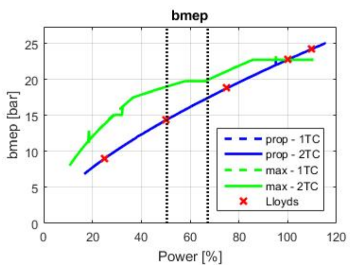

Figure C.2: Steady state simulation results: brake mean effective pressure.

The brake mean effective pressure is related to the engine torque. It is apparent from the graph that the engine torque of the green operation is higher than that of the blue propeller law operation.

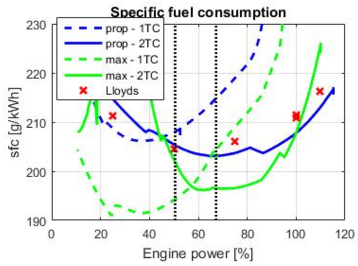

Figure C.3: Steady state simulation results: specific fuel consumption.

The specific fuel consumption is much lower when the engine is operating on the maximum load limit. This is a common trend for Diesel engines, the increase of the thermal loading of the engine increases the thermal efficiency.

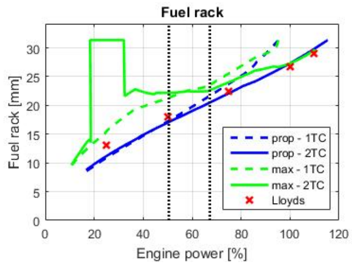

Figure C.4: Steady state simulation results: fuel rack position.

Although the specific fuel consumption was lower, the total fuel consumption is higher because the engine is delivering more power. The strange rectangle that can be seen in the left region is the result of the PID controller of the governor. However, this is only for 2TC operation in the 1TC operating region. In other words this only occurs in the simulation, outside of the physical operating conditions.

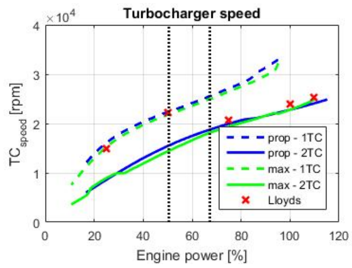

Figure C.5: Steady state simulation results: turbocharger speed.

No significant difference from the propeller law.

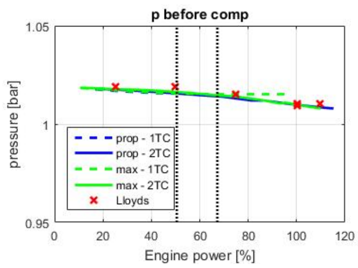

Figure C.6: Steady state simulation results: pressure at compressor entry.

No significant difference from the propeller law.

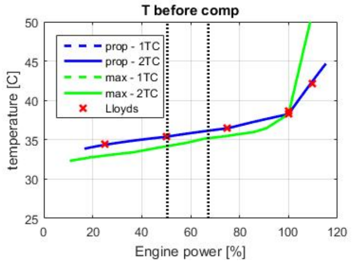

Figure C.7: Steady state simulation results: temperature at compressor entry.

No significant difference in magnitude from the propeller law.

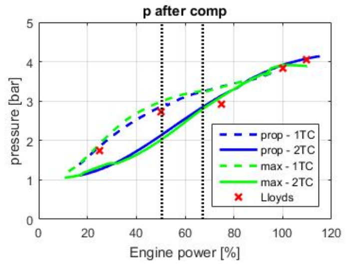

Figure C.8: Steady state simulation results: pressure at compressor exit.

No significant difference from the propeller law.

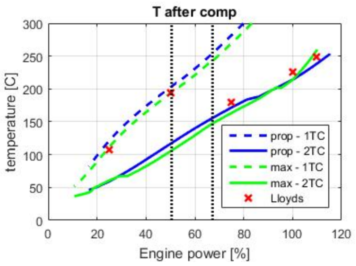

Figure C.9: Steady state simulation results: temperature at compressor exit.

No significant difference from the propeller law.

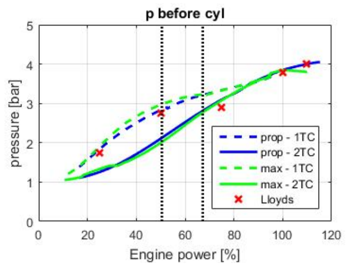

Figure C.10: Steady state simulation results: charge pressure.

No significant difference from the propeller law.

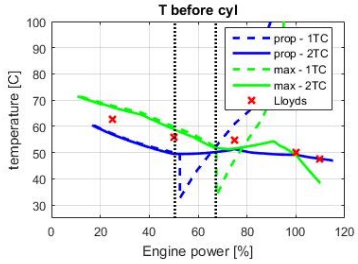

Figure C.11: Steady state simulation results: charge temperature.

No significant difference from the propeller law, the choking effect on the mass flow model of the air cooler occurs at a higher engine load.

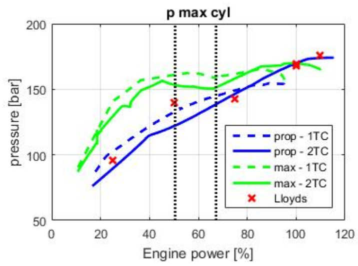

Figure C.12: Steady state simulation results: maximum cylinder pressure.

The maximum cylinder pressure is much higher because the engine loading is higher. This means that more fuel is injected and thus the cylinder pressure is much higher than for the propeller law.

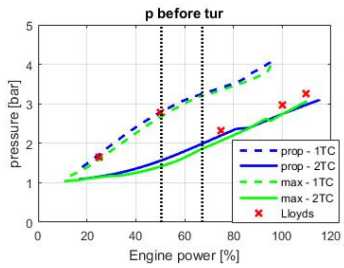

Figure C.13: Steady state simulation results: pressure at turbine entry.

No significant difference from the propeller law.

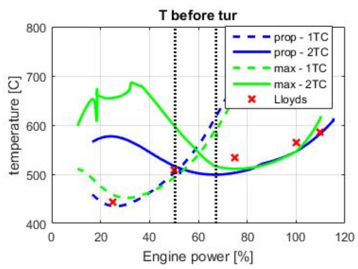

Figure C.14: Steady state simulation results: temperature at turbine entry.

No significant difference from the propeller law.

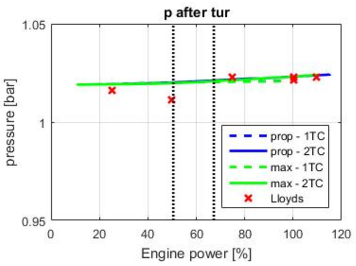

Figure C.15: Steady state simulation results: pressure at turbine exit.

No significant difference from the propeller law.

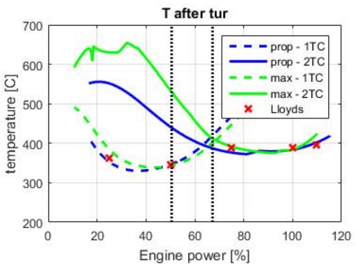

Figure C.16: Steady state simulation results: temperature at turbine exit.

No significant difference from the propeller law.

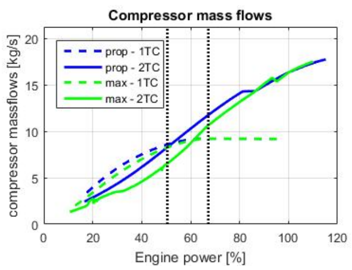

Figure C.17: Steady state simulation results: compressor mass flow.

The mass flow of the compressor on its maximum operating line is somewhat lower than that of the propeller law for the dame given power.

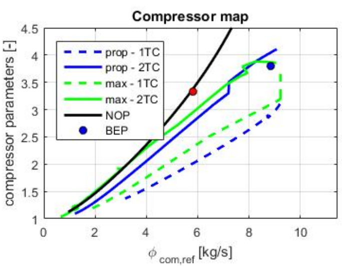

Figure C.18: Steady state simulation results: compressor map.

The compressor map shows that for the same mass flow, the pressure ratio of the engine on the maximum limit is higher than that of the propeller law operating line. It can also be seen that when operating at a higher load, the surge margin becomes smaller and the risk of surge occurring in low load is more likely

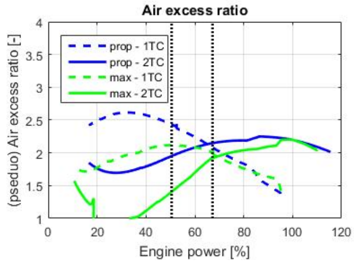

Figure C.19: Steady state simulation results: air excess ratio.

The increased loading is coupled with an increase in fuel injection. This lowers the air excess ratio and increases the thermal loading on the engine.

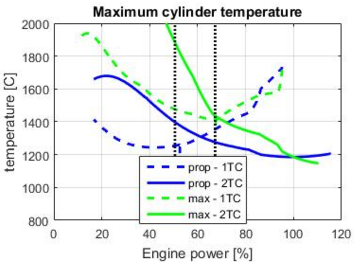

Figure C.20: Steady state simulation results: maximum cylinder temperature.

The maximum cylinder temperature is much higher because the engine loading is higher. This means that more fuel is injected and thus the cylinder temperature is much higher than for the propeller law.

D

A detailed description of the Diesel B-minus model

Diesel Bminus model

Author: M.A. Loonstijn

Date: 22-03-2016

D.1. Motivation

At the start of my thesis I was investigating the possibilities for modeling a turbocharged diesel engine. Two obvious model choices were those developed by the TU Delft; namely the Diesel A and Diesel B models. The Diesel A model was rejected because it is not able to capture the intricate mechanics of the engine-turbocharger interaction needed for the analysis of the research questions. The Diesel B model was also rejected at first due to its complexity and lack of support from documentation and the original authors (later I did receive support and the Diesel B model is used for the rest of my thesis but at the time an alternative seemed desirable).

The approach was to find a model that was less complex then the Diesel B model but provided more information than the Diesel A model. This proposal was of particular interest to Damen Schelde Naval Shipbuilding, the reduced complexity of the model allows for a faster matching to new engines. For this report the focus is on the Pielstick PA6B V20 engine.

D.2. Modeling philosophy

The overall modeling philosophy for the B- model was to reduce complexity of the Diesel B model where possible and remove effects whose contribution where not significant. To reach this goal, several new components are introduced and some existing components are removed from the Diesel B model. The model will be written from scratch in order to gain a full understanding of its implementation.

D.3. Model description

The B- model uses the same mean value principal of the B model. It attempts to model the gas exchange in a turbocharged diesel engine and capture the interaction between the turbocharger and diesel engine. The mean value gas exchange model consists of resistor and volume components that form an electrical analogy circuit. In an electrical circuit the current passing through the resistors is dependent on the potential over the resistor with the relation describe by Ohm's law. This same law can be used for the fluid dynamics in an electrical analogy circuit:

$$I = \frac{V}{R} \tag{D.1}$$

$$\dot{m} = \frac{\Delta p}{R} \tag{D.2}$$

The resistors are sets of equations that describe the mass flow and temperature change over the resistor based on the pressure of the volumes it is connected to. The volumes use the fundamental mass and energy conservation laws to determine the mass, pressure and temperature inside the volume based on the mass and enthalpy entering and leaving the volume. This method provides a physical basis to simulate the gas exchange through a turbocharged diesel engine.

For a full description of the TU Delft Diesel B model, the reader is referred to the work of Schulten [16] and Stapersma [18].

The resistor characteristics are dependent on the type of resistor. In this model there are four resistor components: the compressor, the air cooler, the cylinder and the turbine. All of these components will be described in detail in the following chapters.

An overview of the Diesel B- Simulink model is provided in figure D.1.

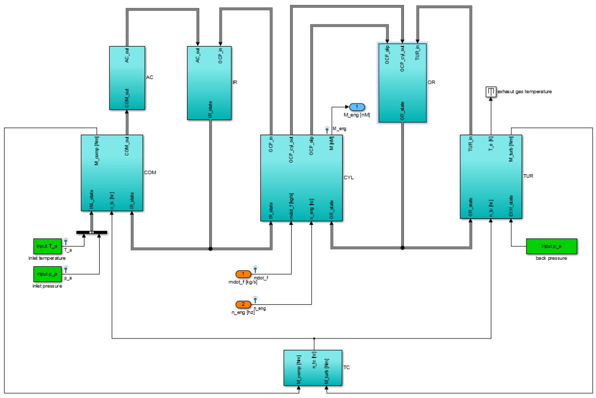

Figure D.1: An overview of the Diesel B- model and its core components.

D.4. Volume elements

The volume elements take mass flow as an input and calculate the state of the volume element. The state consists of the amount of mass in [kg], the concentration of air in [%mass], the pressure in [pa] and the temperature in [K]. This state is the output of the volume element and is used by the resistor elements.

The model only contains two volume elements; the inlet and outlet receiver. By comparison, the Diesel B model has five volumes that each needs to be defined. The simplification in respect to the Diesel B model is that the pressure losses in the inlet, outlet and air cooler are neglected. The compressor inlet and turbine outlet are directly connected to the ambient environment. This also eliminates the air filter and exhaust silencer resistor elements from the diesel B model.

The choice to remove these elements from the diesel B model has been made on the basis of the overall design philosophy of the B- model; to reduce complexity and remove elements with small or insignificant impact on the performance.

D.4.1. Inlet receiver

The inlet receiver connects the air cooler outlet to the cylinder inlet. The mass flow from the air cooler outlet enters the volume and the mass flow from the cylinder leaves the volume. An overview of the Simulink model is shown in figure D.2.

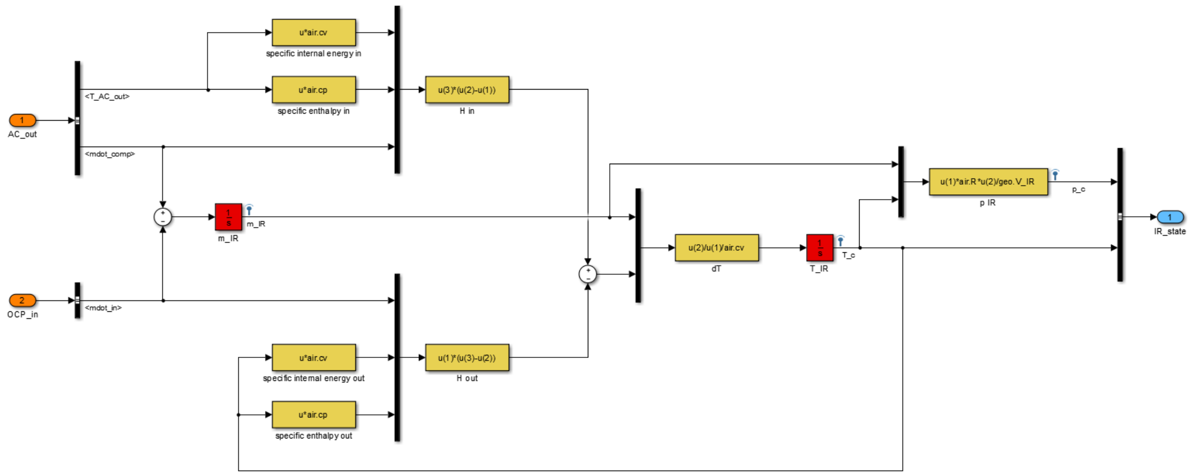

Figure D.2: An overview of the inlet receiver sub-model.

The mass flow entering and leaving are added to find the change of mass over time in the volume. This change of mass is integrated to find the current mass in the inlet receiver according to the fundamental conservation of mass:

$$\dot{m}_{IR} = \dot{m}_{in} - \dot{m}_{out} \tag{D.3}$$

$$m_{IR} = \int \dot{m}_{IR} \cdot dt \tag{D.4}$$

A simplification has been made by assuming that only pure air enters the inlet receiver and that the air can be treated as a perfect gas (constant specific heat, temperature independent). A further simplification is made by ignoring any heat pick-up from interaction with the wall. The fundamental conservation of energy is used to calculate the temperature and pressure in the inlet receiver as follows:

Fundamental 1st law for an open system:

$$\frac{d}{dt} E_{sys} = \dot{Q} - \dot{W}_{sys} + \sum_{i}^{nr\_of\_inlets} \dot{m}_i \cdot \left[h_i + \frac{v_i^2}{2 \cdot g_c} + \frac{g}{g_c} \cdot z_i \right] - \sum_{j}^{nr\_of\_outlets} \dot{m}_j \cdot \left[h_j + \frac{v_j^2}{2 \cdot g_c} + \frac{g}{g_c} \cdot z_j \right] \tag{D.5}$$

The volume performs no work and there is no heat pickup, furthermore height and velocity differences are neglected. The inlet receiver only has a single in and outlet. Taking all this into consideration, the above equation can be simplified to:

$$\frac{d}{dt} E_{sys} = \dot{m}_{in} \cdot h_{in} - \dot{m}_{out} \cdot h_{out} = \dot{H}_{in} - \dot{H}_{out} \tag{D.6}$$

The specific enthalpy for a perfect gas is calculated as follows:

$$h = T \cdot (c_p - c_v) \tag{D.7}$$

The change of internal energy for a finite mass causes a change in temperature:

$$\frac{d}{dt} E_{IR} = m_{IR} \cdot c_v \cdot dT_{IR} \tag{D.8}$$

This is rewritten to find the change in temperature, which can then be integrated to find the current temperature in the volume:

$$dT_{IR} = \frac{\dot{H}_{in} - \dot{H}_{out}}{m_{IR} \cdot c_v} \tag{D.9}$$

$$T_{IR} = \int dT_{IR} \cdot dt \tag{D.10}$$

The current pressure can be calculated by using the ideal gas law and the calculated values for the mass and temperature in the inlet receiver:

$$p_{IR} = \frac{m_{IR} \cdot R_{air} \cdot T_{IR}}{V_{IR}} \tag{D.11}$$

D.4.2. Outlet receiver

The outlet receiver connects the cylinder outlet to the turbine inlet. The mass flow from the cylinder outlet enters the volume and the mass flow from the turbine leaves the volume. The mass flow from the cylinder contains two components: the gas that took part in combustion and the slip flow of fresh air. These two mass flows are mixed in the outlet receiver. An overview of the Simulink model is shown in figure D.3.

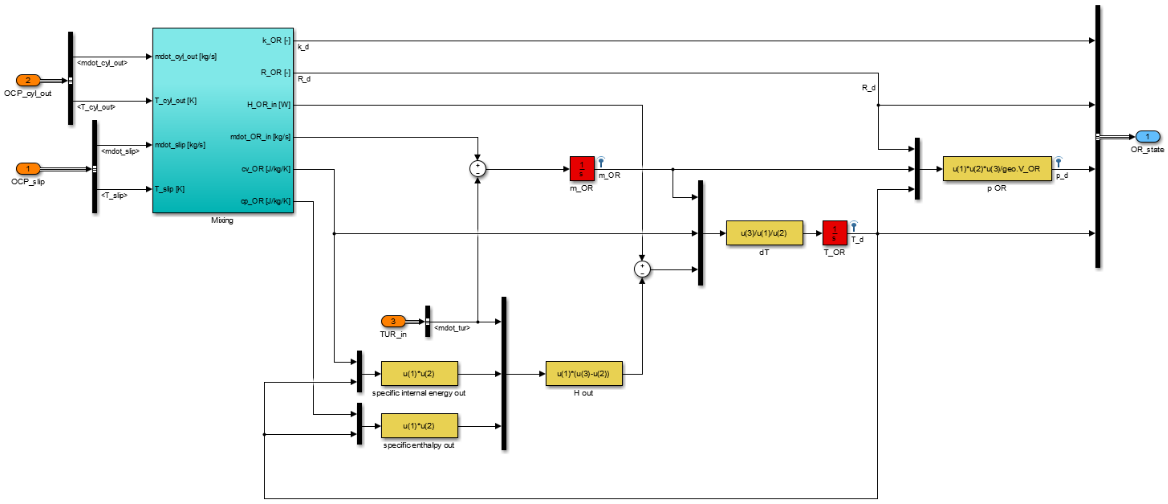

Figure D.3: An overview of the outlet receiver sub-model.

The outlet receiver is similar to the inlet receiver with the exception of the mixing of mass flows entering the volume. An assumption is made that the gas that took part in combustion can be treated as a perfect gas and it is also independent of composition. The gas that took part in combustion is mixed with the fresh air that slips through the engine during scavenging, determining the properties of the mixture entering the outlet receiver:

$$x = \frac{\dot{m_{cyl\_out}}}{\dot{m_{cyl\_out}} + \dot{m}_{slip}} \tag{D.12}$$

$$k_{OR} = x \cdot k_{air} + (1 - x) \cdot k_{cg} \tag{D.13}$$

$$R_{OR} = x \cdot R_{air} + (1 - x) \cdot R_{cg} \tag{D.14}$$

$$cp_{OR} = x \cdot cp_{air} + (1 - x) \cdot cp_{cg} \tag{D.15}$$

$$cv_{OR} = x \cdot cv_{air} + (1 - x) \cdot cv_{cg} \tag{D.16}$$

The enthalpy entering and leaving the outlet receiver as a result of mixing:

$$\dot{H}_{in} = \dot{H}_{cyl\_out} + \dot{H}_{slip} = T_{cyl\_out} \cdot \left(cp_{cg} - cvcg\right) + T_{slip} \cdot \left(cp_{air} - cvair\right) \tag{D.17}$$

$$\dot{H}_{out} = T_{OR} \cdot \left(cp_{or} - cv_{or}\right) \tag{D.18}$$

The mass, temperature and pressure are calculated in the same way as for the inlet receiver:

$$\dot{m}_{OR} = \dot{m}_{cyl\_out} + \dot{m}_{slip} - \dot{m}_{tur\_in} \tag{D.19}$$

$$m_{OR} = \int \dot{m}_{OR} \cdot dt \tag{D.20}$$

$$dT_{OR} = \frac{\dot{H}_{in} - dotH_{out}}{m_{OR} \cdot cv_{OR}} \tag{D.21}$$

$$T_{OR} = \int dT_{OR} \cdot dt \tag{D.22}$$

$$p_{OR} = \frac{m_{OR} \cdot R_{OR} \cdot T_{OR}}{V_{OR}} \tag{D.23}$$

D.5. Resistor elements

The resistor elements are treated individually in detail in the following chapters.

D.5.1. Compressor

The compressor model is comprised of two sub-models, one for the mass flow and one for the efficiency. These two parameters are commonly displayed in a compressor map. The turbocharger on the Pielstick PA6B is a MAN 34NA/S turbocharger. For this turbocharger a compressor map is available from the project guide, this map is shown in figure D.4.

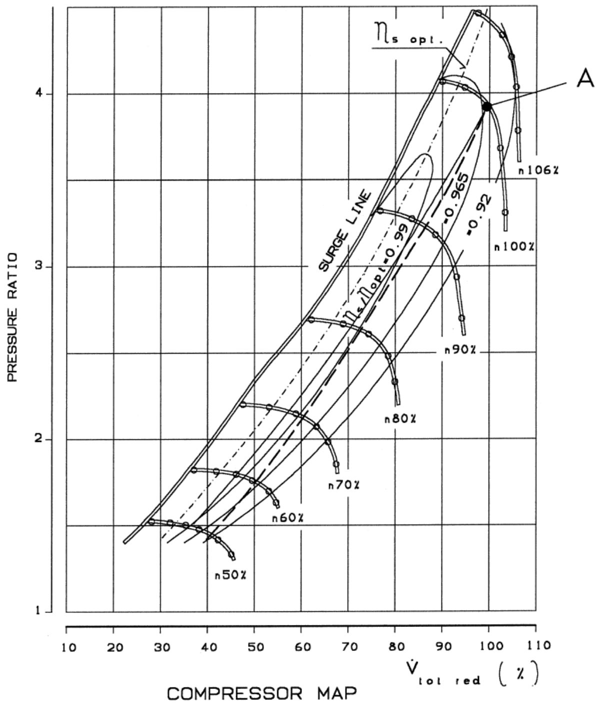

Figure D.4: An overview of the inlet receiver sub-model.

Mass flow model

For the mass flow model a method proposed by Jensen et al. [9] was used. They proposed a mass flow model based on the normalized compressor mass flow rate ϕ_c, the dimensionless head parameter ψ , and the Mach number M as the following:

$$\psi = \frac{A_1 + A_2 \cdot \phi_c}{A_3 - \phi_c} \tag{D.24}$$

$$A_i = a_{i1} + a_{i2} \cdot M, \qquad i = 1,2,3 \tag{D.25}$$

Coefficients a_{ij} are determined through a least square fit on experimental data. The other parameters are defined as follows:

$$\phi_c = \frac{G_c}{0.25\pi d_c^2 \cdot U_c \rho_{in}} \tag{D.26}$$

$$\psi = \frac{cp_{in} \cdot T_{in} \cdot \left(\pi_c^{\frac{\kappa-1}{\kappa}}\right)}{0.5 \cdot U_c^2} \tag{D.27}$$

$$M = \frac{U_c}{\sqrt{\kappa \cdot R \cdot T_{in}}} \tag{D.28}$$

$$\pi_c = \frac{p_{out}}{p_{in}} \tag{D.29}$$

$$U_c = \pi \cdot d_c \cdot n_{tc} \tag{D.30}$$

Where G_c is mass flow in [kg/s], d_c is compressor diameter in [m], ρ_{in} is density at the inlet in [kg/m3], cp_{in} is specific heat at constant pressure at the inlet in [J/kg/K], T_{in} is temperature at inlet in [K], k is specific heat ratio [-], R is specific gas constant in [J/kg/K], p_{in} is pressure at inlet in [pa] , p_{out} is pressure at outlet in [pa], n_{tc} is the speed of the turbocharger in [hz].

By using the Matlab curve fitting tool it is possible to fit coefficients of a custom equation to a given dataset through a least square fit method. The compressor map from the project guide was used as a reference to fit the coefficients mentioned above.

The coefficient fit result is evaluated with the following statistical data, table D.1.

Table D.1: Goodness of fit parameters for Jensen flow model

The sum of squares due to error (SSE)	0.1575
R-square	0.8508
Adjusted R-square	0.8275
The root mean square error (RMSE)	7.016*10-2

The model proposed by Jensen produces the following compressor map, figure.

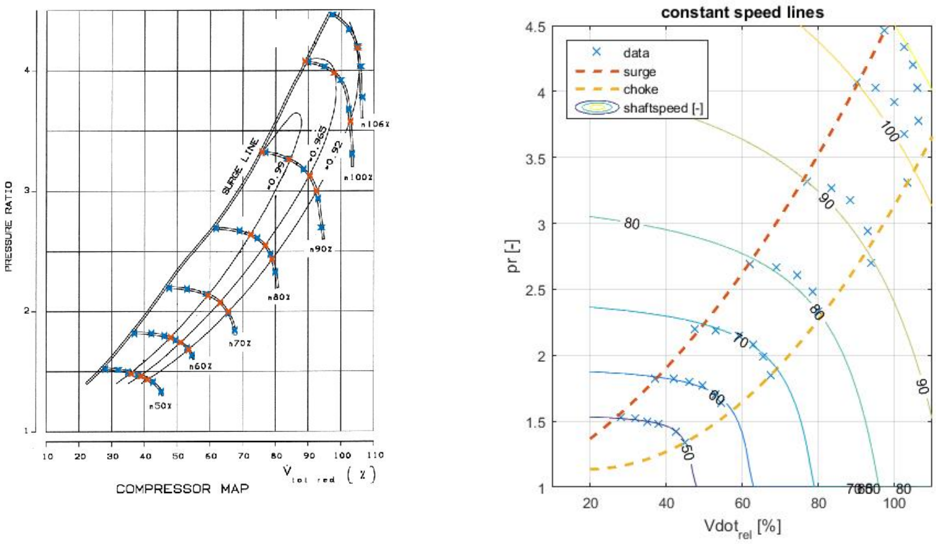

(a) manufacurer's map

(b) simulation results

Figure D.5: Comparison of mass flow between manufacturer's compressor map and simulation results.

The left graph of figure D.5 shows the manufacturer's compressor map where the blue points are used for fitting the coefficients of the mass flow model. The right graph of figure D.5 shows the results of the Jensen mass flow model, where the blue points are the same as those in the left graph of figure D.5. It is clear that the model gives a good approximation in the lower speed ranges but its accuracy degrades in the higher speed ranges.

The model seems to be able to represent the trend in the compressor characteristic. The impact of the deviation at higher speed ranges remains to be investigated when the full model is evaluated.

Efficiency model

For the efficiency model a numerical approach is applied in the form of a polynomial function:

$$z = \sum_{i=1}^{m} \sum_{j=1}^{n} p_{ij} \cdot x^i \cdot y^j \tag{D.31}$$

For this particular model:

$$\text{relative isentropic efficiency} = \sum_{i=1}^{2}\sum_{j=1}^{3} p_{ij} \cdot \phi_c^i \cdot M^j \tag{D.32}$$

Where p_{ij} are the coefficients that are fitted with the Matlab curve fitting toolbox.

The coefficient fit result is evaluated with the following statistical data, table D.2.

Table D.2: Goodness of fit parameters for efficiency model

The sum of squares due to error (SSE)	6.544 10-4
R-square	0.9359
Adjusted R-square	0.8893
The root mean square error (RMSE)	7.713 10-3

The efficiency model produces the following compressor map, figure D.6.

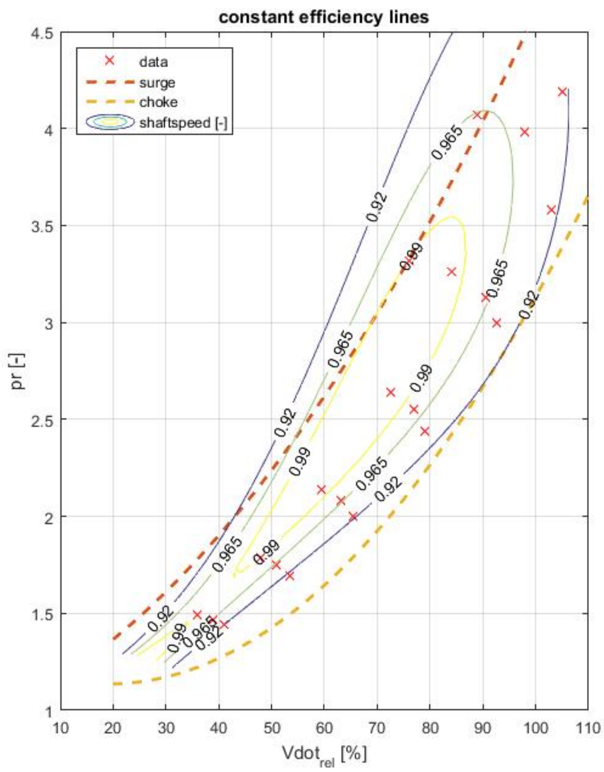

Figure D.6: Constant efficiency lines produced by simulation model.

The red points in figure D.6 are the same as those in the left graph of figure D.5 and are also the points that are used for fitting the polynomial function coefficients.

The compared result of the combined mass flow and efficiency model can be seen in figure D.7. From these figures it becomes evident that the compressor model is able to reproduce the trends of the manufacturers compressor map.

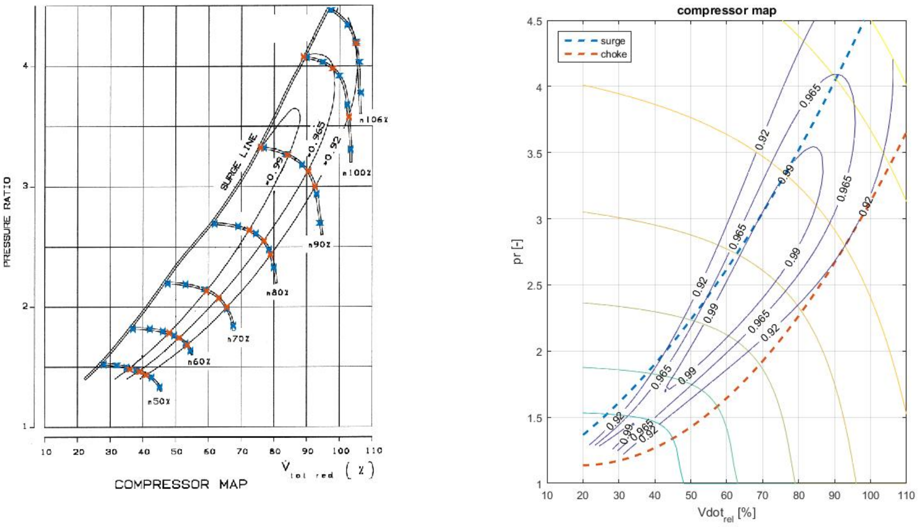

(a) manufacurer's map

(b) simulation results

Figure D.7: Comparison of mass flow between manufacturer's compressor map and simulation results.

The compressor map data is given in relative dimensionless parameters: relative volume flow in [% of nom], relative turbocharger speed [% of nom] and relative isentropic efficiency [% of max]. This map is valid for all the MAN NA/S series of turbochargers and the parameters can be scaled to fit different sized turbochargers. For this report, the model was scaled to a fictional single turbocharger that was matched to the nominal point air swallow characteristic of the Pielstick PA6, table D.3.

Table D.3: Nominal operating point of the air swallow characteristic of the Pielstick PA6.

Nominal mass flow	17.7	[kg/s]
Nominal speed	24 000	[rpm]
Maximum isentropic efficiency	78.0	[%]

This method can also be adapted to fit other compressor if a compressor map or tabulated data is available.

The Simulink model of the compressor is shown in figure D.8.

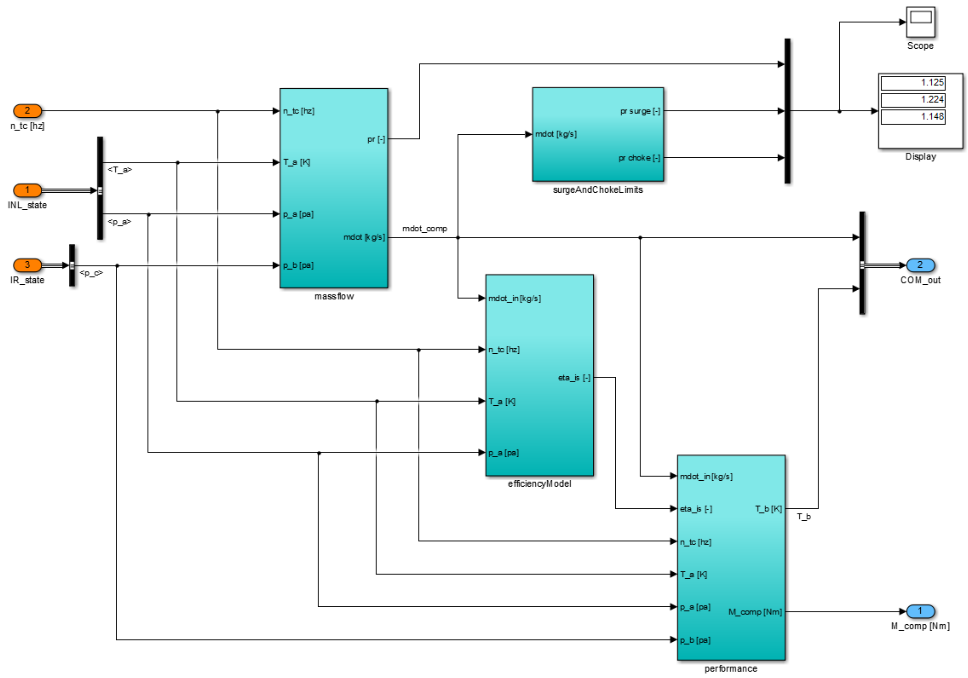

Figure D.8: An overview of the compressor sub-model.

The mass flow and efficiency sub-models hold all the equations discussed above, the performance model calculates the exit temperature, compressor power and compressor torque with the following set of equations:

$$T_{out\_isentropic} = T_{in} \cdot \pi_c^{\kappa-1} \tag{D.33}$$

$$T_{out} = T_{in} + \frac{1}{\eta_{isentropic}} \cdot \left(T_{out\_isentropic} - T_{in}\right) \tag{D.34}$$

$$P_{comp} = \dot{m}_{com} \cdot p_{in} \cdot (T_{out} - T_{in}) \tag{D.35}$$

$$M_{com} = \frac{P_{com}}{n_{tc} \cdot 2 \cdot \pi} \tag{D.36}$$

D.5.2. Air Cooler

The air cooler model is a simpler model then the air cooler model applied in the Diesel B model. It does not take into account a pressure loss, only a temperature change. Therefore the air cooler does not act like the other resistor elements in the sense that it does not calculate a mass flow as a result of a pressure difference, it only calculates the temperature change. The air cooler model calculates the air temperature change as a result of the heat exchange between the hot compressed air and the cold cooling water. There are various ways to approach a solution when analyzing the thermal performance of a heat exchanger, the two methods of interest are the Log mean Temperature Difference (LMTD) and the effectiveness-Number of Transfer Units (NTU) methods. Both share common parameters and concepts and will arrive at the same solution to a heat exchanger thermal capacity. Both methods and their application in the model will be explained in more detail.

The LMTD Method

The LMTD method is the most commonly known method to analyze heat transfer in heat exchangers, it is the logarithmic average of the temperature difference between the hot and cold fluid. It is applicable to both counter and co-current flow arrangements. The definition of the LMTD is:

$$\mathrm{LMTD} = \frac{\Delta T_A - \Delta T_B}{\ln\left(\frac{\Delta T_A}{\Delta T_B}\right)} \tag{D.37}$$

Where delta TA is the temperature difference of one fluid and delta TB is the temperature difference of the other fluid. The LMTD can be used to calculate the heat capacity of a heat exchanger as follows:

$$Q = U \cdot A_{HE} \cdot \mathrm{LMTD} \tag{D.38}$$

Where Q is the heat transfer duty in [W], U is the heat transfer coefficient in [W/K/m2] and AHE is the available area for heat transfer in [m2] . To calculate the heat transfer duty it is necessary to know the geometry, the heat transfer coefficient and the temperatures at the entry and exit for both fluids.

The exit temperature of the hot stream (air) is the parameter of interest, making the LMTD method inapplicable for continuous simulation. However, it is used to calculate the geometry of the heat exchanger by using the fact that the parameters in the nominal operating point are known or estimated. If the temperature change and the mass flow of the air are known in nominal operation, it is possible to calculate the amount of heat rejected by the air:

$$Q = \dot{m}_{air} \cdot c_{p\_air} \cdot \Delta T_{air} \tag{D.39}$$

The heat rejected by the air is absorbed by the water:

$$Q = \dot{m}_{water} \cdot c_{p\_water} \cdot \Delta T_{water} \tag{D.40}$$

This allows for the calculation of the mass flow or temperature change in the water. If one of these parameters is known the other can be calculated. With the heat transfer duty and all four temperatures known it is now possible to calculate the geometry and heat transfer coefficient:

$$U \cdot A_{HE} \cdot \mathrm{LMTD} = \dot{m}_{air} \cdot c_{p\_air} \cdot \Delta T_{air} \tag{D.41}$$

$$UA = U \cdot A_{HE} = \frac{\dot{m}_{air} \cdot c_{p\_air} \cdot \Delta T_{air}}{\mathrm{LMTD}} \tag{D.42}$$

The heat transfer area and coefficient are lumped together into one parameter: UA. Both of these values are constant values and are always used in conjunction. When designing a heat exchanger they offer information about the actual size of the heat exchanger. When analyzing the thermodynamic performance of the heat exchanger it is not necessary to know the individual contribution of the geometry and heat transfer coefficient to UA.

The effectiveness-NTU Method

The Effectiveness-NTU method takes a different approach to solving heat exchange analysis by using three dimensionless parameters: heat capacity rate ratio (R), effectiveness (eta), and Number of Transfer Units (NTU). The relationship between these three parameters depends on the type of heat exchanger and the internal flow pattern.

The first dimensionless parameter is the heat capacity rate ratio, the ratio of the minimum to the maximum value of heat capacity rate (C) for the hot and cold fluids. The heat capacity rate of a fluid is a measure of its ability to release or absorb heat. The heat capacity rate is calculated for both fluids as the product of the mass flow rate times the specific heat capacity of the fluid.

$$C = \dot{m} \cdot c_p \tag{D.43}$$

Where C is the heat capacity rate in [W/K], mdot is the mass flow in [kg/s] and cp is the specific heat at constant pressure in [J/kg/K]. The heat capacity rate ratio is calculated by dividing the smaller heat capacity rate by the larger one, this ensures that R is defined between 0 and 1:

$$R = \frac{C_{min}}{C_{max}} \tag{D.44}$$

The second parameter, effectiveness, is defined as the ratio of the actual heat transfer rate to the maximum possible heat transfer rate for the given flow and temperature conditions:

$$\xi = \frac{Q}{Q_{max}} \tag{D.45}$$

The maximum possible heat transfer rate is achieved if the fluid with the minimum value of C experiences the maximum dT across the heat exchanger:

$$Q_{max} = C_{min} \cdot \Delta T_{max} \tag{D.46}$$

$$\Delta T_{max} = T_{hot\_in} - T_{cold\_in} \tag{D.47}$$

The last dimensionless parameter, the Number of Transfer Units, is the ratio of the heat exchanger's ability to transfer heat (UA) to the fluid's minimum ability to absorb heat (Cmin):

$$\text{NTU} = \frac{UA}{C_{min}} \tag{D.48}$$

Notice that the value of UA is the same as calculated with the LMTD method. The relationship between the three parameter groups of the NTU method is tabulated for different types of heat exchangers. For the air cooler model an unmixed cross-flow arrangement is considered, the effectiveness/NTU relation for this type of heat exchanger is given in figure D.9:

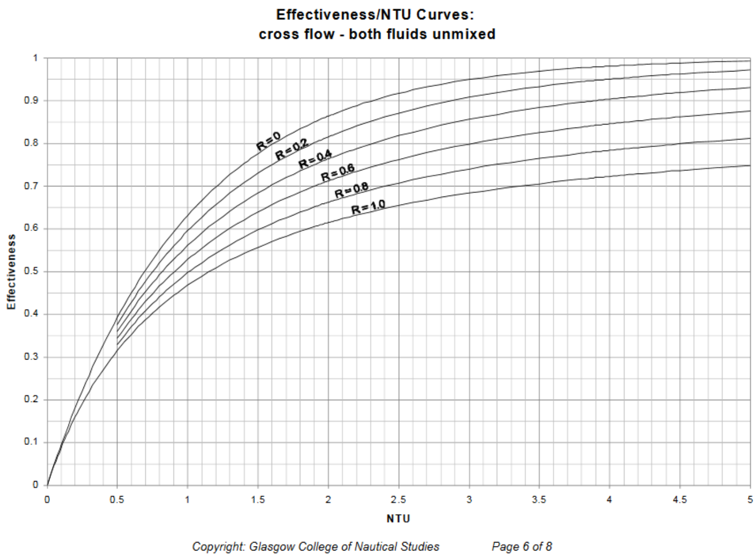

Figure D.9: Effectiveness – NTU curves for a cross flow heat exchanger.

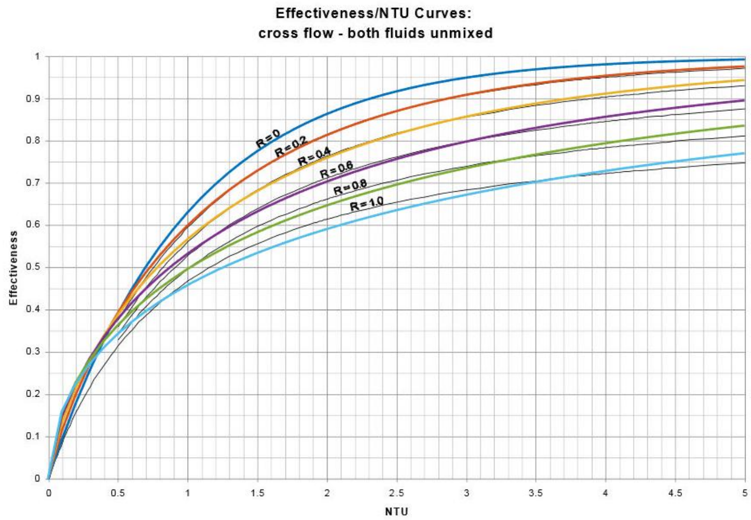

Figure D.10: Comparison of proposed equation to the graphical data.

The curves in figure D.9 have been fitted to an asymptotic function:

$$\xi = 1 - \exp\left(A_1 \cdot \mathrm{NTU}^{A_2}\right) \tag{D.49}$$

$$A_i = a_{i1} + a_{i2} \cdot R + a_{i3} \cdot R^2, \qquad i = 1, 2... \tag{D.50}$$

The coefficients are fitted with Matlab's curve fitting tool and provide the following result, figure D.10:

An asymptotic logarithmic function was chosen to reflect the logarithmic characteristic of the driving force in a heat exchanger, the LMTD. The quality of the fit degrades for higher heat capacity ratios. For typical air cooler arrangements the value of R is in the range of 0.01 to 0.3 and operates at a Number of Transfer Units higher than 1.5. For this region the proposed equation provides a very good fit to the original graph.

The Simulink model uses these NTU-curves to find the effectiveness corresponding to the current R and NTU. The amount of heat rejected by the air can be calculated with the effectiveness and the entry temperature of both the air and cooling water.

The Simulink model of the heat exchanger is shown in figure D.11:

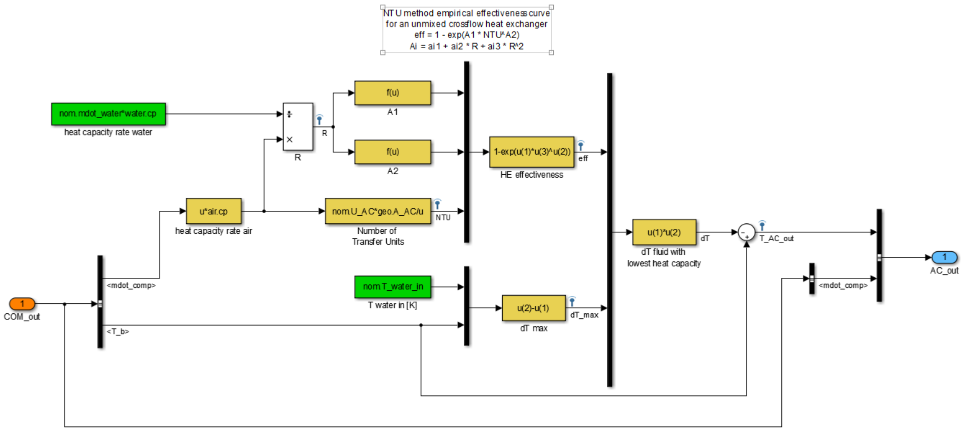

Figure D.11: An overview of the air cooler sub-model.

The model uses the equations mentioned above. Both the temperature and mass flow of the cooling water are taken as constant and are calculated in the nominal operating point.

D.5.3. Turbine

The turbine mass flow characteristic is modeled according to the simplified turbine characteristic proposed by Stapersma [18]. In this method the flow through the turbine is replaced with the well-known mass flow formula for isentropic flow through a nozzle:

$$\dot{m}_{tur} = A_{eff} \cdot \frac{p_{OR}}{\sqrt{R_{OR} \cdot T_{OR}}} \cdot \psi(\pi_{tur}) \tag{D.51}$$

Where the head parameter ψ is defined by the pressure ratio over the turbine and the specific heat ratio of the fluid up to the choking limit. Above the choking limit, the head parameter ψ is defined only by the specific heat ratio of the fluid:

$$\psi = \sqrt{\frac{2\kappa}{\kappa - 1}} \cdot - \sqrt{\left(\frac{1}{\pi_{tur}}\right)^{\frac{2}{\kappa}} \left(\frac{1}{\pi_{tur}}\right)^{\frac{\kappa+1}{\kappa}}}, \qquad \pi_{tur} \pi crit \tag{D.52}$$

$$\psi = \sqrt{\kappa \left(\frac{2}{\kappa + 1}\right)^{\frac{k+1}{k-1}}}, \qquad \pi_{turb} \leq \pi_{crit} \tag{D.53}$$

The effective area is calculated on the basis of the nominal values of the outlet receiver conditions, turbine pressure ratio and turbine mass flow. This area is used as a constant value for the continues simulation.

The turbine isentropic efficiency is simplified as a constant value; the implications of this on the results are to be determined. No suitable alternative was available to give a simple solution to the turbine efficiency. In the case of a turbocharger turbine the efficiency tends to remain near constant, this was the motivation to choose a constant value for modeling purposes.

An overview of the turbine model in Simulink is shown in figure D.12.

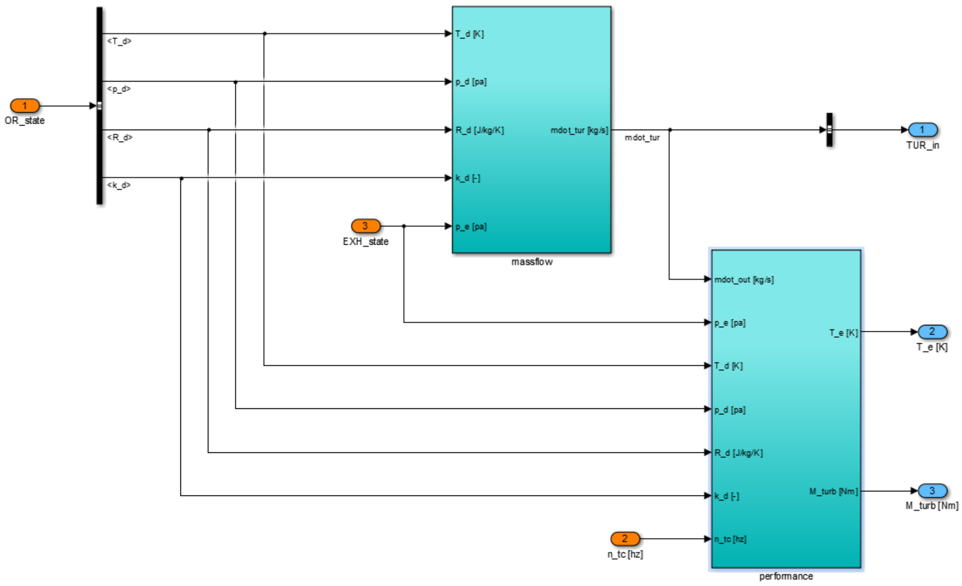

Figure D.12: An overview of the turbine sub-model.

The mass flow sub-model holds the equations discussed above. In the performance sub-model, the following equations are evaluated:

$$T_{out\_isentropic} = T_{or} \cdot \pi_{tur}^{\kappa-1} \tag{D.54}$$

$$T_{out} = T_{OR} - \eta_{isentropic} \cdot \left(T_{OR} - T_{out\_isentropic}\right) \tag{D.55}$$

$$P_{tur} = \dot{m}_{tur} \cdot cp_{in} \cdot (T_{OR} - T_{out}) \tag{D.56}$$

$$M_{tur} = \frac{P_{tur}}{n_{tc} \cdot 2 \cdot \pi} \tag{D.57}$$

D.5.4. Cylinder

The cylinder model can be divided into two different processes: the open and the closed cylinder process. The open cylinder process takes place when at least one intake or exhaust valve is open. In the open cylinder process mass gets transferred from the inlet receiver into the cylinder (Air swallow) and from the cylinder to the outlet receiver (foul gas disposal). Stapersma [18] has treated the analysis of these processes in detail; the methods proposed for this model are based on this work with a few simplifications to reduce the complexity of the model:

- The effective scavenge area is constant and defined at nominal condition
- The scavenge efficiency is constant
- The slip factor is constant
- The scavenge out temperature is equal to the scavenge trapped temperature

Open cylinder process – air swallow

The mass getting swallowed by the engine can be divided into several fractions. These fractions are displayed graphically in figure **??**:

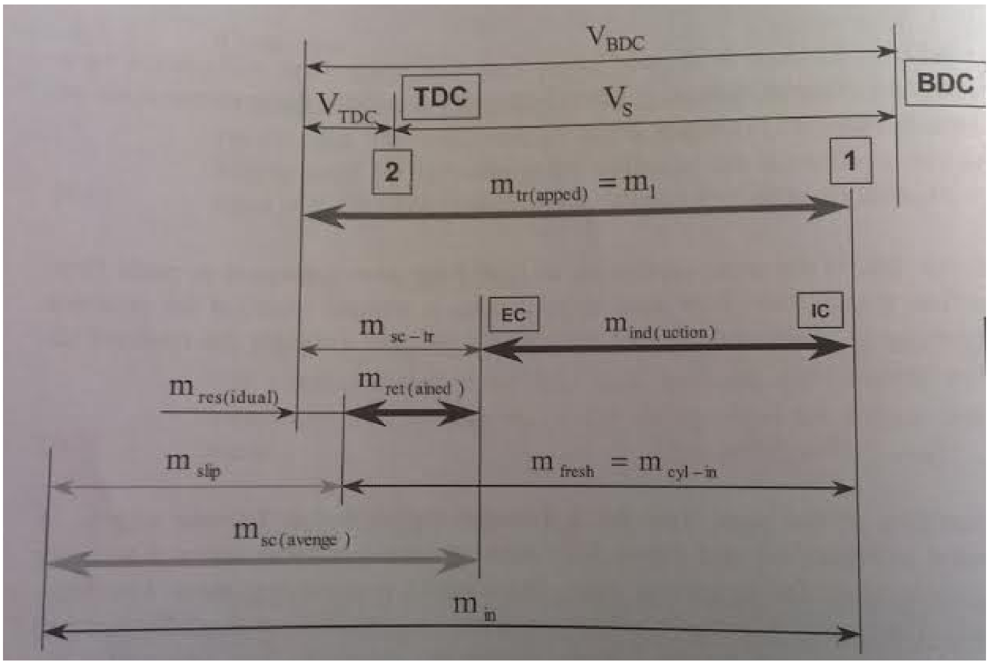

Figure D.13: Breakdown of the fractions of the air swallow capacity of a 4-stroke engine (source: Stapersma [18]).

The parameter of interest is the total mass flow into the cylinder in [kg/s]. Figure **??** shows that the total mass flow in can be divided into two contributions: the mass from induction and the mass from the scavenge process. The mass flow from these processes can be calculated with the state conditions of the inlet and outlet receiver, the geometry of the engine and the valve timing.

The valve timing is of particular interest because it determines the fraction of the total engine cycle available for each of the gas exchange processes. The four valve timing events are (in order of occurrence in the engine cycle):

- Exhaust valve opens (EO)
- Inlet valve opens (IO)
- Exhaust valve closes (EC)
- Inlet valve closes (IC)

At the particular time that one of these events occurs, the cylinder volume can be calculated with the following geometrical equation:

$$V = V_{TDC} + A_b \cdot \left(\frac{L_s}{2} + L_{conrod} - x\right) \tag{D.58}$$

$$x = \frac{L_s}{2} \cdot cos(\alpha) + L_{conrod} \cdot cos(\beta) \tag{D.59}$$

$$\beta = sin^{-1}\left(\frac{L_s}{2 \cdot L_{conrod}} \cdot sin(\alpha)\right) \tag{D.60}$$

Where V is the volume when the event occurs in [m3], VTDC is the volume at top dead centre in [m3], Ab is the bore area in [m2], Ls is the stroke length in [m], Lconrod is the length of the connecting rod in [m] and α is the crank angle when the event occurs in [rad]. The volumes denoted by EO, IO, EC and IC are the volumes at the given valve event occurrences and are calculated with the formula given above.

According to Stapersma [18] 6.2.3, the induction mass can be calculated for a turbocharged diesel engine with the following equation:

$$m_{ind} = \frac{p_{ind} \cdot V_{ind}}{R_{ind} \cdot T_{ind}} = \frac{p_{IR} \cdot (V_{IC} - V_{EC})}{R_{IR} \cdot T_{ind}} \tag{D.61}$$

The induction temperature Tind is slightly higher than TIR due to heat pick up during passage through the hot inlet port. This heat pick up effect is modeled with a simple heat exchanger model with a constant effectiveness and a constant wall temperature:

$$T_{ind} = T_{IR} + \epsilon \cdot (T_{wall} - T_{IR}) \tag{D.62}$$

Stapersma [18] 6.2.1 gives typical values for the effectiveness and wall temperature as follows:

$$\epsilon = 0.02 \;\text{ to }\; 0.10 \tag{D.63}$$

$$T_{wall} = 80\text{C} \;\text{ to }\; 200\text{C} \tag{D.64}$$

The induction mass flow can be calculated by multiplying the induction mass by the engine firing frequency:

$$\dot{m}_{ind} = m_{ind} \cdot f = m_{ind} \cdot \frac{i_{cyl} \cdot n_{eng}}{k_{eng}} \tag{D.65}$$

Where icyl is the number of cylinders, neng is the engine speed in [hz] and keng is the engine type (keng = 1 for 2-stroke, keng = 2 for 4-stroke.

The scavenge mass flow is the result of a difference in pressure over the inlet and outlet receivers and the overlap in the opening of the inlet and exhaust valves. During scavenging the flow going through the valve ports can be modeled as a flow through a pipe with flow restrictors. Stapersma [18] 6.3.1 proposed the following formula for calculating the scavenge mass flow:

$$\dot{m}_{sc} = i_{cyl} \cdot A_{eff} \cdot \frac{p_{IR}}{\sqrt{R_{IR} \cdot T_{IR}}} \cdot \psi \tag{D.66}$$

$$\psi = \sqrt{2} \cdot \sqrt{1 - \frac{1}{\pi_{sc}}} \tag{D.67}$$

$$\pi_{sc} = \frac{p_{IR}}{p_{or}} \tag{D.68}$$

Where Asc_eff is the effective scavenge area in [m2]. This area is calculated with the conditions at the nominal operating point and the area remains constant for the continuous simulation (first simplification).

The total air swallow capacity of the engine can now be described with the induction mass and scavenge mass:

$$\dot{m}_{in} = \dot{m}_{ind} + \dot{m}_{sc} \tag{D.69}$$

$$\dot{m}_{in} = \frac{p_{IR} \cdot (V_{IC} - V_{EC})}{R_{IR} \cdot T_{ind}} \cdot \frac{i_{cyl} \cdot n_{eng}}{k_{eng}} + i_{cyl} \cdot \frac{p_{IR}}{\sqrt{R_{IR} \cdot T_{IR}}} \cdot \sqrt{2} \cdot \sqrt{1 - \frac{p_{OR}}{p_{IR}}} \tag{D.70}$$

This is the total mass flow into the engine; however it is not the mass flow that gets trapped in the cylinder to take place in the closed cylinder process. For the closed cylinder process it is necessary to find the trapped pressure p1 and the trapped temperature T1. In figure 13 it can be seen that the mass flow in can be divided into two other fractions:

$$\dot{m}_{in} = \dot{m}_{fresh} + \dot{m}_{slip} \tag{D.71}$$

The second and third simplifications of the air swallow are the constant scavenge efficiency and the constant slip factor. With these assumptions the trapped mass can be calculated as follows:

$$m_{in} = \dot{m}_{in} \cdot \frac{1}{f} = \dot{m}_{in} \cdot \frac{k_{eng}}{icyl \cdot n_{eng}} \tag{D.72}$$

$$m_{in} = (1+s) \cdot m_{fresh} \tag{D.73}$$

$$\eta_{sc} = \frac{m_{fres}}{m_1} \tag{D.74}$$

Rewriting the above equations to form an explicit definition for m1:

$$m_1 = \frac{m_{fresh}}{\eta_{sc}} = \frac{m_{in}}{(1+s)} \cdot \frac{1}{\eta_{sc}} = \dot{m}_{in} \cdot \frac{k_{eng}}{i_{cyl} \cdot n_{eng}} \cdot \frac{1}{(1+s)} \cdot \frac{1}{\eta_{sc}} \tag{D.75}$$

The trapped temperature T1 can be calculated with the ideal gas law. The trapped temperature is equal to the inlet receiver pressure; pressure loss across the valve ports is neglected. The trapped volume is equal to the cylinder volume at the moment the inlet valve closes:

$$p_1 \cdot V_1 = m_1 \cdot R_1 \cdot T_1 \tag{D.76}$$

$$T_1 = \frac{p_1 \cdot V_1}{m_1 \cdot R_1} = \frac{p_{IR} \cdot V_{EC}}{m.R_{air}} \tag{D.77}$$

Closed cylinder process – foul gas disposal

As with the air swallow characteristic of an engine, the mass getting disposed by the engine can be divided into several fractions. These fractions are displayed graphically in figure **??**.

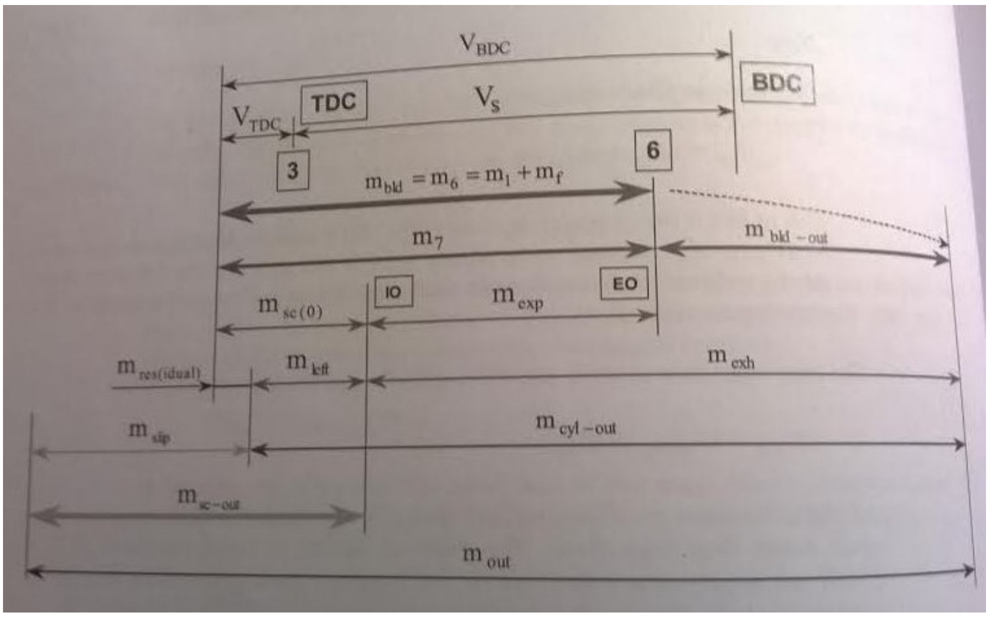

Figure D.14: Breakdown of the fractions of the foul gas disposal capacity of a 4-stroke engine (source: Stapersma [18]).

The total mass flow out of the engine is equal to the total mass flowing into the engine with the addition of the fuel that is injected during the close cylinder process:

$$\dot{m}_{out} + \dot{m}_{in} + \dot{m}_{fuel} \tag{D.78}$$

This mass flow can be divided into two fractions, the mass that took part in the combustion and the mass that slips through the engine during scavenging:

$$\dot{m}_{out} = \dot{m}_{cyl\_out} + \dot{m}_{slip} \tag{D.79}$$

The slip mass was calculated in the air swallow model:

$$\dot{m}_{slip} = s \cdot \dot{m}_{fresh} = \dot{m}_{in} \frac{s}{s+1} \tag{D.80}$$

Thus the mass flow of gas that took part in combustion is:

$$\dot{m}_{cyl\_out} = \dot{m}_{out} - \dot{m}_{slip} = \dot{m}_{in} \cdot \left(1 - \frac{s}{1+s}\right) + \dot{m}_{fuel} \tag{D.81}$$

For the outlet receiver mixing sub-model it is necessary to know the temperatures of these two mass flow fractions. The temperature of the mass flow that took part in combustion is the blow down temperature which is calculated as follows:

$$T_{bld} = \tau_{bld} \cdot T_5 \tag{D.82}$$

$$\tau_{bld} = \pi_{bld}^{\pi_{bld}-1} \tag{D.83}$$

$$\pi_{bld} = \frac{p_{OR}}{p5} \tag{D.84}$$

Where T5 is the temperature at the end of the closed cylinder process in [K], p5 is the pressure at the end of the closed cylinder process in [bar] and nbld is the polytropic exponent for the blow down expansion.

The temperature of the slip flow is more complex to calculate, in this model a simplification has been applied where the temperature of the scavenge flow out of the engine is approximated to be equal to the temperature of the scavenge flow at the moment when the exhaust valve closes. This condition is defined by Stapersma [18] as the trapped scavenge temperature Tsc_tr and is calculated as follows:

$$T_{sc\_tr} = \frac{1}{\left(\frac{V_{IC}}{V_{EC}} \cdot \frac{1}{T_1}\right)} - \frac{V_{IC} - V_{EC}}{V_{EC}} \cdot \frac{1}{T_{ind}} \tag{D.85}$$

$$T_{sc\_out} \approx T_{sc\_tr} \tag{D.86}$$

The temperature of the slip mass is defined as the temperature of the scavenge out flow with an additional heat pick up from the exhaust port. This heat pick up is treated in the same way as the heat pick up of the induction air flow:

$$T_{slip} = T_{sc\_out} + \epsilon \cdot \left(T_{wall} - T_{sc_out}\right) \tag{D.87}$$

Closed cylinder process

The closed cylinder process treats the thermodynamic heat release from the fuel and the consequential work performed by the engine. The closed cylinder process is modeled as a 5 point Seiliger cyle. It is practically a copy of the TU Delft Diesel A engine model with the exclusion of the turbocharger of the Diesel A model. An overview of the close cylinder process in Simulink is given in figure **??**.

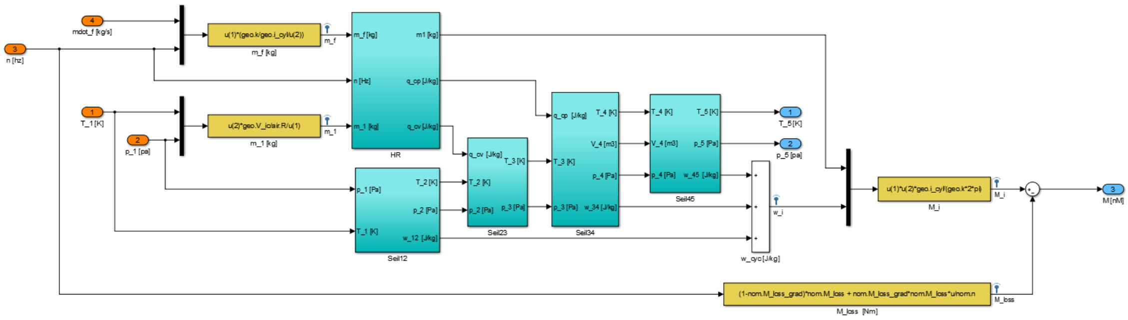

Figure D.15: Overview of the closed cylinder process sub-model.

The difference is that in the B- model, the initial state of the pressure, temperature and mass are calculated with the open cylinder process. The Diesel A model uses a constant initial temperature T1 and the initial pressure p1 is derived from a simple 1st order interpretation of the buchi power balance. The trapped mass is derived from the calculated pressure, constant temperature and cylinder geometry with the use of the ideal gas law.

For a full explanation of the Seiliger cycle and the Diesel A model, the user is referred to Stapersma [18] chapter 3 – Performance prediction with the Seiliger process.

D.6. Results

The B- model has been evaluated by manually controlling the fuel rack from 110% of its nominal value to 20% of its nominal value. The results of the simulation have been plotted against the relative engine power in %, with the exception of the first graph which shows the power-speed curve, a traditional indicator of engine performance. The results are presented in the following graphs:

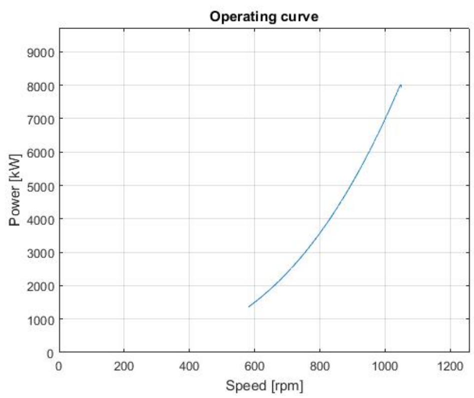

Figure D.16: Simulation result: engine speed-power diagram.

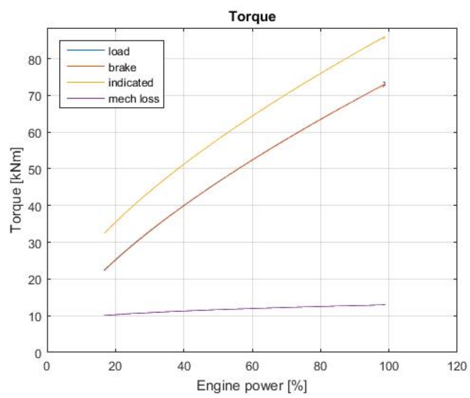

Figure D.17: Simulation result: engine torque.

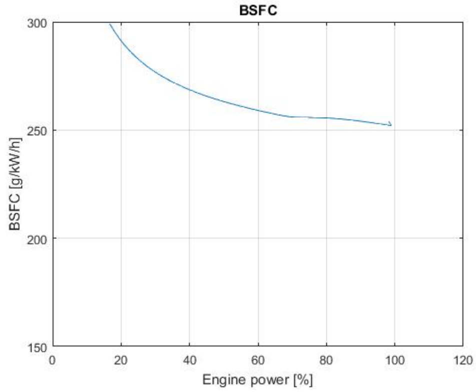

Figure D.18: Simulation result: specific fuel consumption.

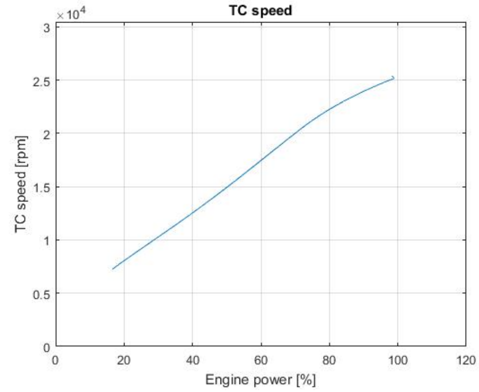

Figure D.19: Simulation result: turbocharger speed.

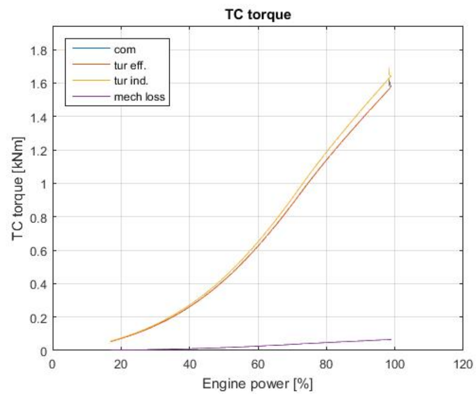

Figure D.20: Simulation result: turbocharger torque.

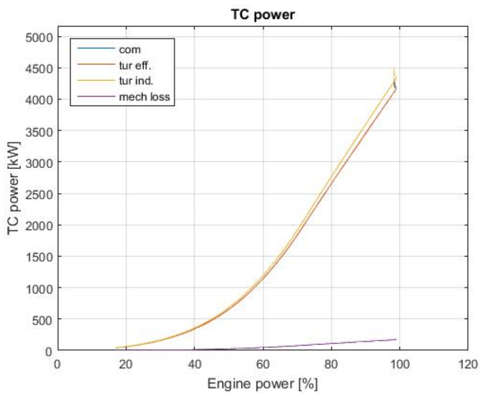

Figure D.21: Simulation result: turbocharger power.

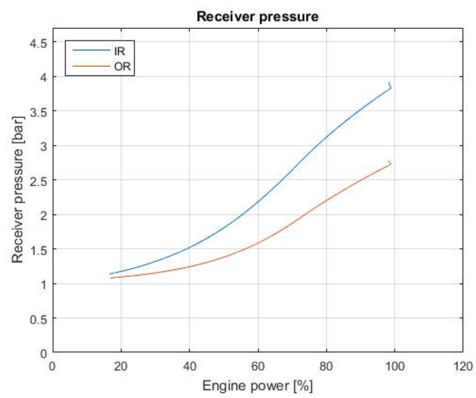

Figure D.22: Simulation result: receiver pressure.

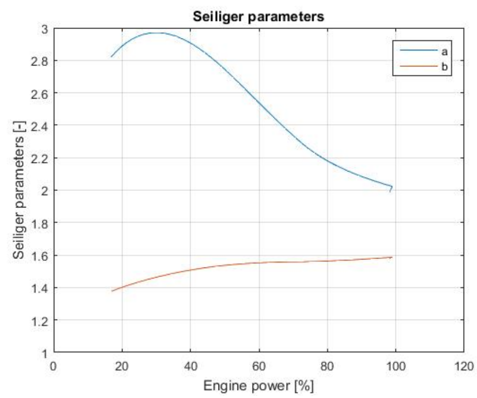

Figure D.23: Simulation result: Seiliger combustion parameters.

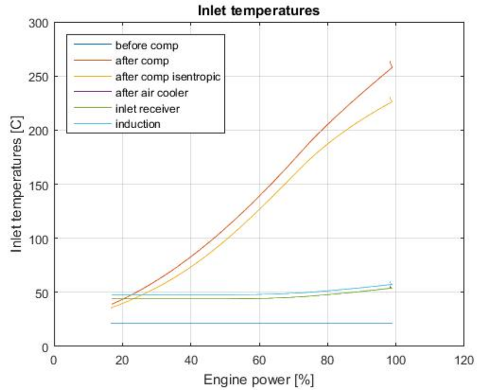

Figure D.24: Simulation result: inlet temperatures.

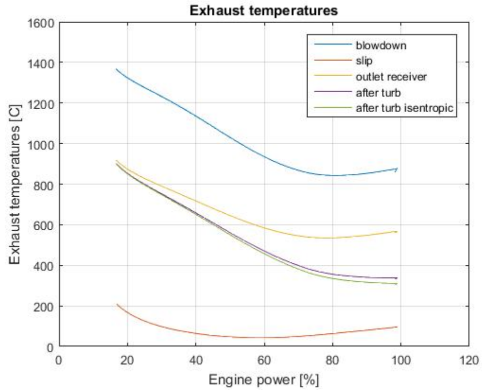

Figure D.25: Simulation result: exhaust temperatures.

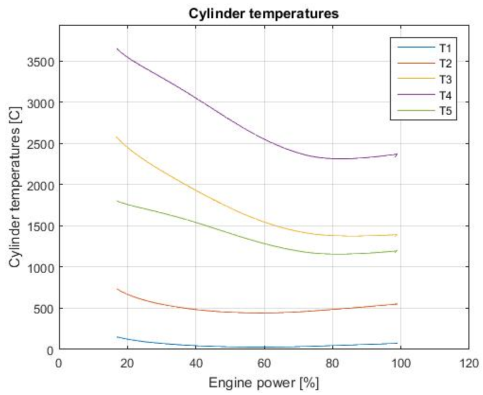

Figure D.26: Simulation result: Seiliger temperatures.

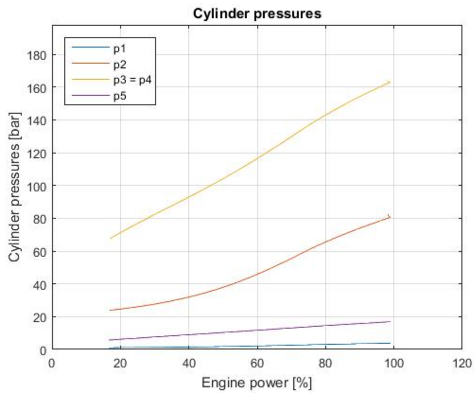

Figure D.27: Simulation result: Seiliger pressures.

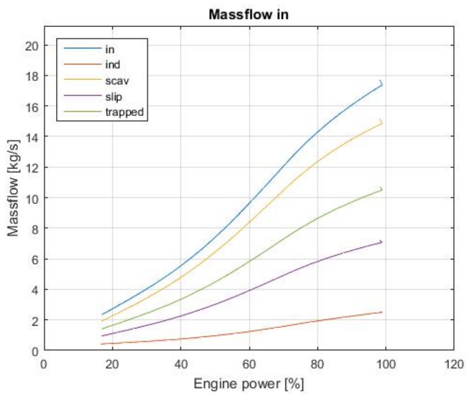

Figure D.28: Simulation result: mass flow into the engine.

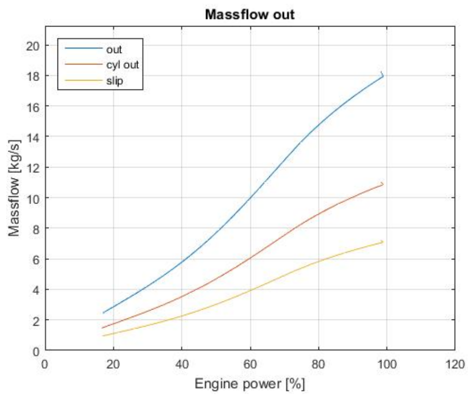

Figure D.29: Simulation result: mass flow out of the engine.

D.7. Conclusion

The results show trends that are expected of a diesel engine and bear similarity to the results of the TU Delft Diesel B model. However at low load the performance deviates a lot from the expected trend.

The outcome of the model has not been verified. The first impression shows that there is a serious error in some of the assumptions made for the construction of the model.

At the time when this model was first proposed it was proposed as an alternative to the TU Delft Diesel B model due to the fact that there was little information and support on the use of the Diesel B model. Later I got in contact with Professor Stapersma and it turned out that the lack of support was due to miss-communication during the holidays. Eventually I got an up to date version of the Diesel B model and the documentation to calibrate the model.

Because the construction of a new Diesel model was not included in the scope of my Msc. Thesis, I decided to abandon any further investigation into this model and focus my attention on the Diesel B model. It still served a purpose as a good modeling exercise and gave me insight into the methods employed in the Diesel B model. This document is made to secure the transfer of knowledge on the construction and methodology of this model.

I am confident that this method can be investigated and corrected in order to have a modeling technique that fits in between the complexity of the Diesel A and Diesel B models. I would suggest investigating the assumptions made to calculate the slip mass temperature. Another cause for concern is the high cylinder temperatures caused by the 5 point Seiliger cycle. It seems that at low load the lack of an isothermal combustion phase (stage 5-6) leads to large deviations in the exit temperatures. These errors in temperature have a large influence on the Buechi balance of the turbocharger, which creates even more uncertainty in the final results.

E

Derivations of the equations used for the basic volume and resistor elements

These derivations are taken from the appendix in Schulten [16].

E.1. Resistance element

The resistance element calculates the mass flow $\dot{m}$ as a function of the pressure ratio over the element, using the momentum equation:

$$\dot{m} = A_{eff} \cdot \frac{p_i}{\sqrt{R \cdot T_i}} \cdot \psi \tag{E.1}$$

In this equation A_{eff} is the effective resistance area and p_i and T_i the conditions of the volume preceding the resistanec element. the ψ function is a function of the pressure ratio $\pi = {}^{p_i}/_{p_o}$ and can be calculated in two different ways:

If the flow is compressible:

$$\psi = \sqrt{\frac{2 \cdot \kappa}{\kappa - 1}} \cdot \sqrt{\left(\frac{1}{\pi}\right)^{\frac{2}{\kappa}} - \left(\frac{1}{\pi}\right)^{\frac{2}{\kappa}}} \tag{E.2}$$

If the flow is choked:

$$\psi = \sqrt{\kappa \cdot \left(\frac{2}{\kappa + 1}\right)^{\frac{\kappa+1}{\kappa-1}}} \tag{E.3}$$

Choking occurs when the local velocity of sound is reached or, expressed in pressures, when the pressure ratio is larger than the critical ratio π_{crit}.

E.2. Volume element

A volume element basically acts as an integrator, using the in- and outflow to calculate the state of the volume. This can be done using the concepts of conservation of mass and the first law of thermodynamics. Conservation of mass states that the mass accumulation within a volume is equal to the net inflow:

$$\frac{dm}{dt} = \left(\frac{d_e m}{dt}\right)_{out} - \left(\frac{d_e m}{dt}\right)_{in} \tag{E.4}$$

Neglecting kinetics and potential energy, the first law of thermodynamic states:

$$\frac{d(m \cdot u)}{dt} = u_e \cdot \frac{d_e m}{dt} + \frac{dQ}{dt} - \frac{dW}{dt} \tag{E.5}$$

In these equations, the subscript $_e$ denotes in- or outflow. For example, u_e is the internal energy of an inflow while u is the instantaneous internal energy of the volume.

Work is separated into three forms: volumetric work, flow work and isochoric work, but only flow work applies:

$$\frac{dW}{dt} = -p_e \cdot v_e \cdot \frac{d_e m}{dt} \tag{E.6}$$

Introducing the enthalpy h:

$$u_e \cdot \frac{d_e m}{dt} + p_e \cdot v_e \cdot \frac{d_e m}{dt} = (u_e + p_e \cdot v_e) \cdot \frac{d_e m}{dt} = h_e \cdot \frac{d_e m}{dt} \tag{E.7}$$

Inserting in the energy balance:

$$\frac{d(m \cdot u)}{dt} = h_e \cdot \frac{d_e m}{dt} + \frac{dQ}{dt} \tag{E.8}$$

Applying the chain rule:

$$u \cdot \frac{dm}{dt} + m \cdot \frac{du}{dt} = h_e \cdot \frac{d_e m}{dt} + \frac{dQ}{dt} \tag{E.9}$$

Inserting in the mass balance, equation E.4:

$$m \cdot \frac{du}{dt} = h_e \cdot \left(\frac{d_e m}{dt}\right)_{in} - h_e \cdot \left(\frac{d_e m}{dt}\right)_{out} - \left[u \cdot \left(\frac{d_e m}{dt}\right)_{in} - u \cdot \left(\frac{d_e m}{dt}\right)_{out}\right] + \frac{dQ}{dt} \tag{E.10}$$

Rearranging:

$$m \cdot \frac{du}{dt} = (h_e - u) \cdot \left(\frac{d_e m}{dt}\right)_{in} - (h_e - u) \cdot \left(\frac{d_e m}{dt}\right)_{out} + \frac{dQ}{dt} \tag{E.11}$$

Assuming an ideal gas:

Rearranging:

$$\frac{du}{dt} = c_v \cdot \frac{dT}{dt} \tag{E.12}$$

Substituting:

$$m \cdot c_v \cdot \frac{dT}{dt} = (h_e - u) \cdot \left(\frac{d_e m}{dt}\right)_{in} - (h_e - u) \cdot \left(\frac{d_e m}{dt}\right)_{out} + \frac{dQ}{dt} \tag{E.13}$$

The specific enthalpy h_e is calculated through:

$$h_e = c_{p,e} \cdot T_e + h(T_{ref}) \tag{E.14}$$

The internal energy u is calculated through:

$$u = c_v \cdot T \tag{E.15}$$

Inserting in the energy equation:

$$m \cdot c_v \cdot \frac{dT}{dt} = (c_{p,in} \cdot T_{in} - c_v \cdot T) \cdot \left(\frac{d_e m}{dt}\right)_{in} - (c_{p,out} \cdot T_{out} - c_v \cdot T) \cdot \left(\frac{d_e m}{dt}\right)_{out} + \frac{dQ}{dt} \tag{E.16}$$

Now substitute:

$$\left(\frac{d_e m}{dt}\right)_{in} = \dot{m}_{in} \tag{E.17}$$

and

$$\left(\frac{d_e m}{dt}\right)_{out} = \dot{m}_{out} \tag{E.18}$$

and

$$\frac{dQ}{dt} = \phi_q \tag{E.19}$$

The energy balance then becomes, after rearranging:

$$\frac{dT}{dt} = \frac{(c_{p,in} \cdot T_{in} - c_v \cdot T) \cdot \dot{m}_{in} - (c_{p,out} \cdot T_{out} - c_v \cdot T) \cdot \dot{m}_{out} + \phi_q}{m \cdot c_v} \tag{E.20}$$

Separating variables and integrating results in the volume temperature T.

The heatloss ϕ_q is calculated:

$$\phi_q = -\alpha \cdot A \cdot (T - T_{wall}) \tag{E.21}$$

Once the temperature T is known, the pressure p can be calculated:

$$p = \frac{m \cdot R \cdot T}{V} \tag{E.22}$$

The specific heat c_p, c_v and the heat transfer coefficient α are temperature and medium dependent and have to be calculated.

F

A detailed description of the Design of Experiments calibration method

Design of Experiments method – theory and application

M.A. Loonstijn – 13/05/2016

F.1. Theory and application – general concept

Design of Experiments (DOE) is a systematic method to determine the relationship between factors affecting a process and the output of that process. The DOE method can be used to show cause-and-effect relationships in a complicated system.

With the DOE methodology, an experiment aims at predicting the outcome by introducing different input conditions, this prediction variable is often referred to as the predictor. The change in the predictor is hypothesized to result in a change of the outcome variable. The difference between the predictor and the process outcome gives an indication for the cause-and-effect relationship between the input and the output. A schematic overview is given in figure F.1:

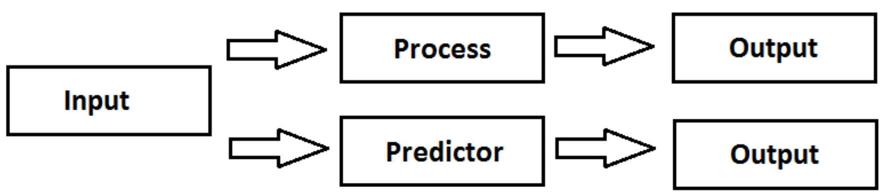

Figure F.1: A schematic overview of the DOE methodology.

The components in figure F.1 are listed and explained for general usage of the DOE method:

- **Input:** any parameter(s) or boundary condition(s) that is/are applied to the experiment. Both the process and predictor receive the same input.
- **Process:** usually a physical process or physical system, where different input parameters can be applied and the outputs are measured with sensor equipment.
- **Predictor:** usually a simulation model of the physical process or physical system.
- **Output:** any parameter(s) that is/are of interest to the experiment, in most cases the process and predictor will supply different values for the same output.

The DOE method provides two sets of output, one by the process and one by the predictor. The difference in these two gives an indication to how accurate the prediction was to the real process. A quantitative analysis of the predictor's accuracy can be performed by comparing the absolute and relative differences of the two outputs.

Two statistical indicators are used to quantify the accuracy for the entire set of input/output combinations. These indicators are: the root mean square error (RMSE) and the normalized root mean square error (NRMSE). These concepts are frequently used for assessing statistical datasets. The RMSE represents the sample standard deviation of the differences between the predicted and observed values. The NRMSE is determined by normalizing the RMSE, this facilitates the comparison of different datasets with different parameter scales. There is no consistent means of normalization in the literature; a common choice is to normalize the RMSE with the mean of the range of the observed data (the maximum value in the observed data set minus the minimum value). This form of the NRMSE is also called the coefficient of variation of the RMSE, CV(RMSE). This is an analogy to the coefficient of variation with the RMSE as the standard deviation of a given dataset.

The RMSE and NRMSE are declared below:

RMSE = root mean square error

$$\text{RMSE} = \sqrt{\frac{\sum_{i=1}^{n} (y_{sim(i)} - y_{obs(i)})^2}{n}} \tag{F.1}$$

NRMSE = normalized root mean square error

$$\text{NRMSE} = \frac{\text{RMSE}}{(y_{obs\_max} - y_{obs\_min})} \tag{F.2}$$

F.2. Theory and application – applied to the Diesel B model

The Diesel B model has a large number of unknown or estimated parameters. In most cases these parameters influence a large number of output variables. There is some documented correlation between the input and output, appendix G and Stapersma [19], but it is a very demanding task to manually fit all these parameters. Therefore, the DOE methodology is applied to systematically find the values that provide the best fitted result for the output or the simulation model. A schematic overview is shown in figure F.2:

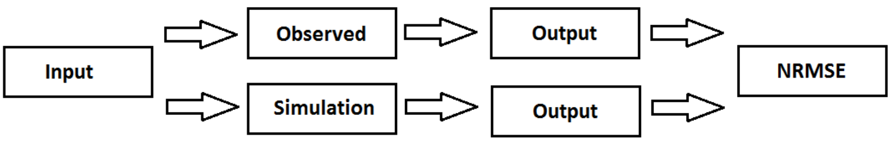

Figure F.2: A schematic overview of the DOE method applied to the diesel B model.

In figure F.2, the input represents a combined set of unknown parameters. This parameter set is used to simulate the engine model at steady state for each of the operating points in the observed data set, in this particular case there are six data points in the observed data set. The output of these six simulations is compared to the observed output of the same six operating points. The two outputs are compared with the NRMSE. The NRMSE of all variables are added to create the sum total of the NRMSE. The input data set that results in the lowest sum total of the NRMSE is taken as the best fitted solution.

This application of the DOE method allows the user to evaluate a large combination of unique sets for the unknown parameters of the Diesel B engine. By convoluting the outcome into a single indicator (sum total NRMSE), it is possible to quickly quantify the "goodness of fit". Another added benefit is the possibility to investigate combined parameter sets instead of only varying a single parameter each time. For the Diesel B engine model, the following "functional" sets of estimated parameters have been defined:

- Compressor map scale
  - COM.nu_nom_r: relative velocity of NOP to BEP
  - COM.fi_nom_r: relative flow of NOP to BEP
- Compressor map shape
  - COM.PSI_0: steepness of constant speed curves
  - COM.Ma_0: curvature of constant speed curves
  - COM.x: width of efficiency ellipses
  - COM.y: length of efficiency ellipses
  - COM.e: power of ellipse law
  - COM.s: spread of constant speed curves
  - COM.f: surgeline relative to top of speed curves
- Turbine map scale
  - TUR.nu_nom_r: relative velocity of NOP to BEP
  - TUR.fi_nom_r: relative flow of NOP to BEP
- Turbine map shape
  - TUR.PSI_0: steepness of constant speed curves
  - TUR.Ma_0: curvature of constant speed curves
  - TUR.x: width of efficiency ellipses
  - TUR.y: length of efficiency ellipses
  - TUR.e: power of ellipse law
  - TUR.s: spread of constant speed curves
- Engine air demand
  - CYL.IC: closing angle of inlet valve
  - CYL.IO: opening angle of inlet valve
  - CYL.EC: closing angle of exhaust valve
  - CYL.EO: opening angle of exhaust valve
  - CYL.muphi: discharge coefficients of the valve ports
  - CYL.delta_EO: virtual opening angle of exhaust valve
- Combustion shape
  - CYL.x_a_c: constant factor in contribution of isochoric combustion
  - CYL.x_a_n: speed dependent factor in contribution of isochoric combustion
  - CYL.x_b_c: constant dependent factor in contribution of isobaric combustion
  - CYL.x_b_n: speed dependent factor in contribution of isobaric combustion

The parameters of these sets have been evaluated as a group. A group is selected and for each parameter a range is defined, this set is henceforth called a "DOE batch". For each DOE batch, a range of values has been selected for each of the parameters in a group. All of the possible combinations in this range are evaluated with the DOE method. An example of the presentation of the results for one DOE batch are given in figures F.3 and F.4:

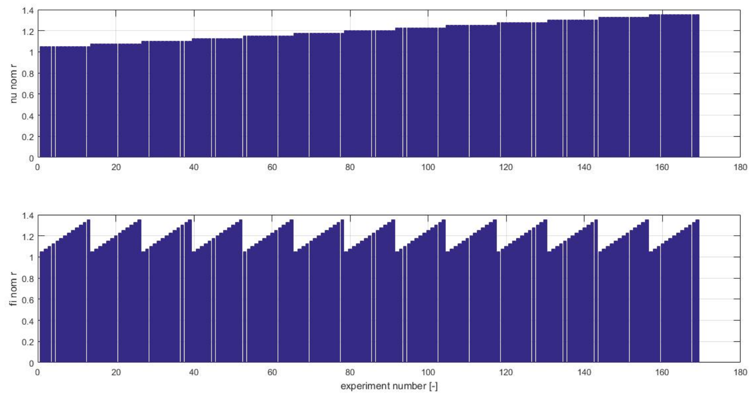

Figure F.3: Input parameters of the DOE batch, nu_nom_r (1.05:0.025:1.35) and fi_nom_r (1.05:0.025:1.35), each experiment has a unique combination of these two parameters.

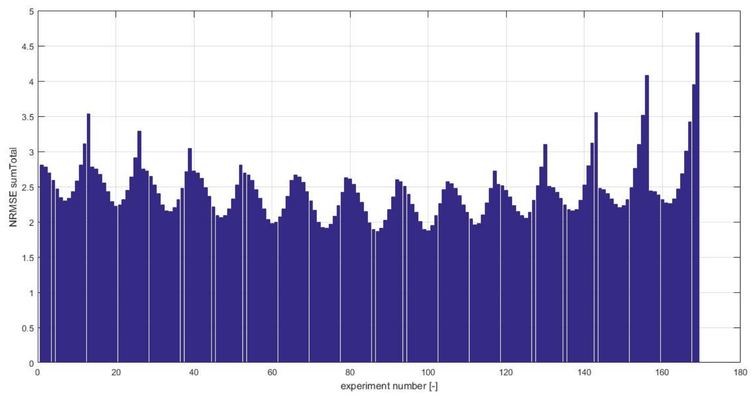

Figure F.4: Sum total of the NRMSE for all experiments in a single DOE batch, 169 experiments in batch.

In figure F.3 the variation of the input variables is displayed. For this DOE batch, the two parameters that govern the relative position of the NOP to the BEP are varied; they make up the "compressor map scale" group from the list above. These parameters both hold 13 different values in their ranges. The engine model is simulated for each unique combination of these parameters. The simulation is run six times, once for each of the six datapoints in the Lloyds data set. Each set of these six experiments is henceforth called an "experiment". The variation of the two parameters results in a total of: 13 x 13 = 169 experiments.

Figure F.4 shows the convoluted analysis of the DOE batch, the sum total of the NRMSE for all selected values in one experiment. For this example, the sum of the NRMSE is taken from: specific fuel consumption, turbocharger speed, charge pressure, charge temperature, maximum cylinder pressure, turbine entry and exit pressure as well as turbine entry and exit temperature. It can be seen that the sumtotal NRMSE of these parameters shows multiple local minima. If the solution converges to a global minimum sum total NRMSE, a best fit has been found for that particular parameter group. In figure 4, the global minimum is found in experiment number 87. The input parameter values of the best fitted solution are selected as the new default value for these parameters and the next group of parameters is evaluated with the DOE method.

This is an iterative process that has to be done for each of the parameter groups defined in the list above. After all of the parameter groups have been analyzed, the process is repeated to see if the earlier groups converge to a different solution when the later groups have new values. If the DOE batch iterates to the same value, a final solution has been found; the global minimum of the relative error.

This re-iteration of the DOE batch is needed because it is not possible to do a full parameter sweep for all parameters in the same batch. The DOE method uses a nested loop for each parameter. This means that each parameter increases the total number of parameters exponentially. For example:

Batch 1

- Parameter 1: range = (0 : 2 : 10), 6 variables in range.
- Parameter 2: range = (10 : 0.1 : 11), 11 variables in range.
- Parameter 3: range = (0.01 : 0.01 : 0.1), 10 variables in range.

Total number of experiments in DOE batch: 6 x 11 x 10 = 660 experiments.

Each experiment consists of 6 Simulink simulations: 660 x 6 = 3960 Simulink experiments.

Each Simulink experiment runs for 5 sec on average: 3960 x 5 =19800 sec = 5.5 hours.

Batch 2

- Parameter 1: range = (0 : 2 : 12), 7 variables in range. ← increased by 1
- Parameter 2: range = (10 : 0.1 : 11), 11 variables in range.
- Parameter 3: range = (0.01 : 0.01 : 0.1), 10 variables in range.

Total number of experiments in DOE batch: 7 x 11 x 10 = 770 experiments.

Each experiment consists of 6 Simulink simulations: 770 x 6 = 4620 Simulink experiments.

Each Simulink experiment runs for 5 sec on average: 4620 x 5 =23100 sec = 6.4 hours.

The example above shows that an increase of the parameter range results in an exponential increase of the number of simulations and the needed computational time. In batch 2, parameter 1 is increased in range from 6 to 7. This small increase of the parameter range results in a large increase of the required computational time; almost an hour longer needed to compute.

The best way to cope with this problem is to do multiple simulations with smaller ranges and refining the spread of the range based on the results of the prior DOE batch. This decreases the computational time significantly because there are less "un-used" solutions present in the batch; however this does require the user to make educated guesses for starting points and possible ranges.

The DOE method can potentially be used to automate the calibration of the Diesel B model. An optimization scheme can be defined by making an algorithm that can make "smart" guesses for parameter selection. Selection criteria on the error of specific output variables can determine whether to increase or decrease a given input parameter and by how much. This can replace the "dumb" method of nested loops that evaluate every possible combination and instead find the fastest way to converge to the global minimum.

Unfortunately such an optimization scheme costs a significant effort to construct. This is outside of the scope of this Msc. thesis and is only mentioned here to illustrate its potential. I would recommend that this could be a subject for any future B.Sc. or M.Sc. work by students of the TU Delft.

G

Qualitative sensitivity analysis of the Diesel B Simple STC model unknown parameters

The Diesel B model has a number of unknown parameters that have to be found. A qualitative sensitivity analysis of the individual parameters is performed to get a better understanding of the influence of these parameters. This analysis is used to find a proper starting point for the iteration process explained in appendix F. A single parameter is selected as the "sweep parameter" and the model is evaluated for a selected range, the "sweep range". If a parameter is not selected as the "sweep parameter", it is given its default value. The influence of these parameters has also been recorded with a graphic method in the form of animations. These are supplied in the digital archive, the animations show the transition of the output based on the input parameter sweep.

This appendix provides a qualitative observation on the influence of the individual parameters, the description is based on the direction of the parameter sweep specified in its format:

<PARAMETER NAME> (<SWEEP RANGE>) [<DEFAULT VALUE>]

G.1. Compressor parameters

COM.N_nom (23000 : 100 : 24500) [23900]

- Raises N_tc, no other effects.

COM.pi_nom (3.500 : 0.025 : 4.200) [3.972]

- Lowers SFC.
- Lowers N_tc for 1 TC at high power, raises N_tc for 2 TC at low power.
- Raises COM pressure and temperate almost linear for both TC operations.
- Raises TUR pressure.
- Lowers TUR temperatures.
- Raises mass flow for 2TC, no significant change for 1 TC.
- Map shape shifts up vertically, no significant change to engine lines.
- Raises Lambda for both modes.

COM.phi_nom_ref(8.000 : 0.100 : 10.000) [8.85]

- Raises SFC for 2TC, lowers for 1TC.
- Lowers N_tc almost linear for both TC operations.

- Lowers COM pressure and temperature.
- Lowers TUR pressure.
- Raises TUR temperature.
- Raises mass flow for 1 TC, lowers for 2 TC.
- Shifts operating lines horizontally.
- Lowers air excess ratio for 2 TC, no significant change for 1 TC.

COM.eta_nom (0.700 : 0.010 : 0.800) [0.785]

- Lowers SFC.
- Lowers N_tc in low range for 2TC, raises N_tc in high range for 1TC.
- Lowers COM_out pressure and temperature.
- Lowers TUR pressure.
- Changes TUR temperature shape, averages around the same.
- Changes mass flow shape, choking at lower power.
- Lowers map operating lines, 1TC lowers faster than 2TC.
- Lowers lambda in lower power ranges.

COM.fi_nom_r(0.800 : 0.025 : 1.250) [1.0]

- Raises SFC.
- Lowers N_tc in low power range.
- lowers COM pressure.
- Makes COM temperature line steeper.
- Lowers TUR pressure.
- Lowers TUR temperature.
- Lowers mass flow.
- Direct influence on BEP, changes map shape and moves surge line.
- Lowers lamba, changes shape slightly.

COM.nu_nom_r(1.000 : 0.025 : 1.250) [1.2]

- Lowers SFC outside of operating regions.
- No significant change to N_tc.
- COM pressure and temperature change shape, outside of operating region mostly.
- Lowers TUR pressure and temperature in low power ranges.
- Changes mass flow shape, choking at lower power.
- Direct influence on BEP, changes map shape and moves surge line.
- Lambda shape change as a result of mass flow.

COM.PSI_0(0.400 : 0.025 : 0.800) [0.8]

- SFC mostly changes outside of operating range.
- Raises N_tc for 2 TC, lowers N_tc for 1 TC.
- Lowers COM pressure for 1 TC, no significance change on temperature.
- Lowers TUR pressure for 1 TC, raises TUR temperature for 1 TC.

- No significant change in mass flow.
- Shifts surge line to the right.
- Lowers lambda for 1 TC.

COM.ma_0(0.300 : 0.025 : 0.500) [0.4]

- SFC curve only affected outside of operating region for TC setting.
- Lowers N_tc for 1TC in high range, slightly raises N_tc for 2TC in high range.
- COM and TUR temp and pressure hardly affected.
- Lowers mass flow.
- Moves BEP in the positive horizontal direction, surge line stays relative to BEP.
- Changes lambda shape outside of operating ranges.

COM.y(0.200 : 0.025 : 0.400) [0.3]

- Small change in SFC outside of operating range.
- No change in N_tc.
- No change in COM pressures and temperatures.
- No change in TUR pressure.
- Raises TUR temperature for 2TC in low power range (outside operating range).
- Small change in mass flow shape.
- No significant change in map, slight shift up and to the right.
- No change of lambda in the operating range.

COM.s(0.600 : 0.025 : 0.950) [0.8]

- Raise SFC outside of operating regions.
- No significance impact on N_tc.
- Lowers COM pressure for 1 TC, no significance change on temperature.
- Lowers TUR pressure for 1 TC, raises TUR temperature for 1 TC.
- Lowers choked mass flow of 1TC.
- BEP moves horizontally to the left, surge line becomes less steep.
- Lowers lambda for low power region.

G.2. Turbine parameters

TUR.eta_nom(0.750 : 0.010 : 0.900) [0.895]

- No significance change on SFC.
- Changes N_tc slightly outside of operating range.
- Lowers COM pressure and temperature.
- Lowers TUR pressure and temperature.
- Shifts mass flow lines to the left.
- Lowers operating lines in map.
- No significant change outside of operating range.

TUR.fi_nom_r(0.800 : 0.025 : 1.250) [1.0]

- No change of SFC outside of operating range.
- Lowers N_tc in lower power range.
- Lowers COM pressure and temperature in lower power range.
- Lowers TUR pressure and raise temperature.
- Increase steepness of mass flow lines.
- Increase steepness of operating lines in map.
- Lower lambda in low power range.

TUR.nu_nom_r(1.000 : 0.025 : 1.250) [1.0]

- Increase SFC in lower power range.
- Lower N_tc in lower power range.
- Lowers COM pressure and temperature in lower power range.
- Lowers TUR pressure and raise temperature in lower power range.
- No significant change in mass flow.
- No significant change in map.
- Lowers lambda in lower power range.

TUR.PSI_0(-1.500 : 0.050 : -0.300) [-1.5]

- No significant change across all parameters.

TUR.Ma_0(0.400 : 0.050 : 1.200) [0.8]

- Increase SFC in lower power range.
- Lower N_tc in lower power range.
- Lowers COM pressure and temperature in lower power range.
- Lowers TUR pressure and raise temperature in lower power range.
- Lowers mass flow in lower power range.
- Lowers operating lines in map in lower power range.
- Lowers lambda in lower power range.

TUR.y(0.200 : 0.025 : 0.400) [0.3]

- No significant change across all parameters.

TUR.s(0.000 : 0.025 : 0.400) [0.0]

- Increase SFC in lower power range.
- Lower N_tc in lower power range.
- Lowers COM pressure and temperature in lower power range.
- Lowers TUR pressure and raise temperature in lower power range.
- Increase steepness of mass flow lines.
- Increase steepness of operating lines in map.
- Lower lambda in low power range.

G.3. Cylinder parameters

CYL.delta_EO(-20.000 : 2.500 : 20.000) [10.0]

- Significantly lowers SFC.
- Lowers N_tc for all operation modes.
- Lowers COM pressure and temperature.
- Lowers TUR pressure and temperature.
- Shifts mass flow lines to the left.
- Raises operating lines in map, map itself remains unaffected.
- Lowers lambda.

CYL.muphi(0.150 : 0.050 : 1.000) [0.4]

- Significant shape change effect on SFC curves.
- Raises N_tc.
- Lowers COM pressure, raises COM temperature.
- Raises TUR pressure, lowers TUR temperature
- Significantly raises mass flow
- Significant changes in mass flow map
- Significant changes in lamba shape, raises to a local maximum

CYL.X_a_c(0.000 : 0.050 : 0.600) [0.45]

- Lowers SFC significantly.
- Lowers N_tc.
- Lowers COM pressure and temperature.
- Lowers TUR pressure and temperature.
- Shifts mass flow lines to the right.
- Shifts operating lines in map slightly up, map unaffected.
- Lowers lambda.

CYL.X_a_n(-0.400 : 0.050 : 0.400) [0.0]

- Small effect on SFC curves.
- Significant changes in maximum pressure.
- No other significant effects

CYL.X_b_c(0.350 : 0.050 : 0.850) [0.74]

- Lowers SFC significantly.
- Lowers N_tc.
- Lowers COM pressure and temperature.
- Lowers TUR pressure and temperature.
- Stretches mass flow lines to the right.
- Lowers operating lines in map slightly, map itself is unaffected.
- Stretches lambda lines to the right.

CYL.X_b_n(-0.600 : 0.100 : 0.600) [-0.4]

- Raises SFC, changes its shape
- Raises N_tc.
- Raises COM pressure and temperature.
- Raises TUR pressure and temperature.
- Raises mass flow slightly.
- No significant change to map.
- Raises lambda slightly.

H

Data sets of logged measurements

Measurement data of the engine is needed in order to match the engine parameters of the diesel B model. Some parameters from the Diesel B model cannot be taken directly from the project guide; instead they need to be estimated. Comparison of the simulation results to the measured data sets is needed in order to evaluate these estimations.

There are three sets of data available for the Pielstick PA6 engine:

- A bench test of the SIGMA class corvette for the Indonesian navy performed by Lloyds.
- A bench test of a frigate of the Moroccan navy performed by MAN.
- Sea trials on board the SIGMA class corvette for the Indonesian, Diponegoro.

Of these three sets the bench test by Lloyds holds the most information. It consists of the measurement of six operating points: 25%, 50%, 75%, 100%, 100% and 110% of the nominal engine power. This data set also contains the most complete picture of the turbocharger performance, all the necessary pressure and temperature data is available in this set. The MAN data set contains the same sensor data as the Lloyds set but is restricted to the working points at 100% and 110% of nominal power. Unfortunately this means that there is no data available for when the engine is running on a single turbocharger.

The last data set is an extensive set of sea trials conducted over the course of a day. The set contains several scenarios: acceleration, load step up, load step down. This set does not contain any data on specific working points because it is a continuous measurement. However, there are certain ranges in this data set where the ship is sailing under near constant conditions. It is possible to get quasi steady state operating points by averaging the sensor data over several minutes under these conditions. Unfortunately the sea trial data set contains less measured parameters, key parameters like turbine and compressor pressures are missing from the data set. This makes the data set unsuitable for matching of the engine under steady state performance.

The Lloyds data set will be the focus of attention for matching and verification. The other two data sets will be used for graphic comparison in plots but nor for statistical evaluation of the simulation model results. The data sets are taken from different engines (all PA6 engines) which all show small deviations due to secondary effects that are not taken into account for simulation purposes. Some examples of these effects are fouling of engine parts, different wear conditions and mechanical hysteresis.

However the raw data set from Lloyds contains some errors that will be discussed in detail. The full Lloyds data set is presented in table H.1:

Table H.1: Lloyds bench test results

TABLE REMOVED - CONTAINS CONFIDENTIAL INFORMATION

With the parameters in this data set it is possible to make some simple calculations to get an indication of the engine and turbochargers thermodynamic performance. These calculations can help to evaluate the measurement itself and see whether the calculated parameters are consistent with expected values.

To perform these calculations, some parameters must be estimated, the estimated parameters and their values are as listed in table H.2:

Table H.2: Estimated parameters for calculation on data sets

TABLE REMOVED - CONTAINS CONFIDENTIAL INFORMATION

The equations used for the calculations are explained in detail below. For the compressor the isentropic efficiency and specific work are calculated as follows with equations H.1 until H.6:

$$\pi_c = \frac{p_{c\_out}}{p_{c\_in}} \tag{H.1}$$

$$\tau_c = \frac{T_{c\_out}}{T_{c\_in}} \tag{H.2}$$

$$\tau_{c\_is} = \frac{T_{c\_is\_out}}{T_{c\_is\_in}} = \pi_c^{\frac{\kappa-1}{\kappa}} \tag{H.3}$$

$$T_{c\_is\_out} = T_{c\_in} \cdot \tau_{c\_is} \tag{H.4}$$

$$\eta_{c\_is} = \frac{T_{c\_is\_out} - T_{c\_in}}{T_{c\_is\_out} - T_{c\_in}} \tag{H.5}$$

$$w_c = c_p \cdot \left(T_{c\_out} - T_{c\_in}\right) \tag{H.6}$$

For the turbine a similar calculation is performed to find the isentropic efficiency and the specific work, equations H.7 until H.12:

$$\pi_t = \frac{p_{t\_out}}{p_{t\_in}} \tag{H.7}$$

$$\tau_t = \frac{T_{t\_out}}{T_{t\_in}} \tag{H.8}$$

$$\tau_{t\_is} = \frac{T_{t\_is\_out}}{T_{t\_is\_in}} = \pi_t^{\frac{\kappa-1}{\kappa}} \tag{H.9}$$

$$T_{t\_is\_out} = T_{t\_in} \cdot \tau_{t\_is} \tag{H.10}$$

$$\eta_{t\_is} = \frac{T_{t\_in} - T_{t\_out}}{T_{t\_in} - T_{t\_is\_out}} \tag{H.11}$$

$$w_t = c_p \cdot \left(T_{t\_in} - T_{t\_out}\right) \tag{H.12}$$

The specific work of the compressor and the turbine have to be compared to find the mechanical efficiency of the turbocharger, a correction is done for the difference in mass flow through the compressor and turbine. The mass flow through the turbine is slightly higher due to the addition of the fuel flow in the engine, equations H.13 until H.15:

$$P_c = P_t \cdot \eta_{tc\_mech} \tag{H.13}$$

$$\dot{m}_c \cdot w_c = \dot{m}_t \cdot w_t \cdot \eta_{tc\_mech} \tag{H.14}$$

$$\eta_{tc\_mech} = \frac{\dot{m}_c}{\dot{m}_t} \cdot \frac{w_c}{w_t} = \frac{1}{\Delta_{tc}} \cdot \frac{w_c}{w_t} \tag{H.15}$$

The equations in the above text are used on the six operating points of the Lloyds dataset and are gathered in table H.3:

Table H.3: Results of the calculations on the original dataset

TABLE REMOVED - CONTAINS CONFIDENTIAL INFORMATION

When analyzing the results in table H.3 it becomes apparent that something is out of order. The values for the isentropic efficiency are very inconsistent for both compressors and turbines. At the operating points of 25% and 50% nominal power, the compressors A and B show a calculated efficiency of higher than 1 and lower than 0 respectively. Both these values are not realistic representations. Turbine B shows an efficiency of above 1 for all the data points, also unrealistic.

The original dataset is carefully studied to find the reason for these inconsistencies. The first indication of an error in the measurement is given for turbine A, the measured value is crossed out with a pen in the original documentation. The second indication of an error can be seen at the operating points of 25% and 50% nominal power, turbocharger A shows a speed measurement of -21 rpm. This is presumed to be the measurement of the turbocharger at rest; the engine is running on one turbocharger, turbocharger B.

However the pressure measurement shows a significant pressure difference across the compressor of turbocharger A while the pressure difference across the compressor of turbocharger B is negligible.

The temperature across compressor A and B also shows anomalies; compressor B has a temperature rise that is consistent with the pressure rise in compressor A. When one turbocharger is running, the temperature on the outlet side of compressor A is the same temperature of the air after the air cooler.

The data for the turbine does seem consistent with the operating modes of single and dual turbocharging.

These findings have led me to believe that some of the sensor data has been switched, either during data logging or during documentation of the data. In particular the measurement of pressure for the compressors seems to have been switched out. The original dataset has been re-ordered with the pressure of the compressors A and B switched around. The same equations for efficiency have been evaluated in order to verify this hypothesis. The re-ordered data set is presented in table H.4:

Table H.4: Lloyds bench test results – pressure of compressor A and B switched

TABLE REMOVED - CONTAINS CONFIDENTIAL INFORMATION

The calculations on efficiency of the re-ordered data set are gathered in table H.5:

Table H.5: Results of the calculations on the re-ordered dataset

TABLE REMOVED - CONTAINS CONFIDENTIAL INFORMATION

The results in table H.5 show a more consistent pattern for the isentropic efficiency of the compressors and turbines. In this new situation, turbocharger B is always in operation and turbocharger A is switched in sequentially at higher engine loads. The values highlighted in red are erroneous due to the fact that the engine is in single turbocharger operation and this turbocharger is switched off. The values highlighted in orange are erroneous due to the error in the temperature measurement of turbine A.

The dataset of MAN contains the same variables as the dataset from Lloyds. The same calculations are performed for this dataset on the operating points of 100% and 110% of nominal engine power. The results from these calculations are compared with the results of the same operating points of the Lloyds data set. This final comparison is used to find out if the re-ordered results of the Lloyds data-set are realistic and consistent with the measurements of MAN.

The raw datasets and calculations are presented in table H.6 and table H.7:

Table H.6: Lloyds and MAN bench test result comparison

TABLE REMOVED - CONTAINS CONFIDENTIAL INFORMATION

Table H.7: Results of the calculations on the Lloyds and MAN dataset

TABLE REMOVED - CONTAINS CONFIDENTIAL INFORMATION

From table H.7 it can be concluded that the values for isentropic efficiency and specific work of the compressors and turbine are comparable between the two independent measurement sets. This leads to the conclusion that he re-ordering of the Lloyds data set was correct. As mentioned before, the Lloyds data set will be used to match the engine model to the real engine.

The third data set is that of the sea trials. This data set contains less measured parameters in comparison to the Lloyds and MAN set. The full data set is presented in table H.8 in the same format as the previous tables:

Table H.8: Sea trial test results – average of quasi-steady state performance

TABLE REMOVED - CONTAINS CONFIDENTIAL INFORMATION

Table H.8 shows the data set from the sea trials, it can clearly be seen what parameters are missing. This data set is derived from a larger data set that contains the parameters of table H.8 measured over a large span of time. This data set will be used to match the dynamic parameters (engine inertia, turbocharger inertia, volumes, etc.) of the model to represent the performance of the physical engine. Any deviation in the steady state performance between the sea trials and bench test must be investigated in order to achieve a correct matching of the dynamic parameters.

The analysis of the sea trial data set cannot be done in the same manner as that of the Lloyds and MAN data sets because the compressor and turbine pressures are not given in the data set. Therefor the sea trial data set will be compared against the simulation results together with the data sets of Lloyds and MAN.

Bibliography

[1] Turbocharging in switzerland - a history. Public Library ABB.

[2] Man v28/33d stc for naval vessels. Technical Paper MAN.

[3] A. Boretti. conversion of a heavy duty truck diesel engine with an innovative power turbine connected to the crankshaft through a continuously variable transmission to operate compression ignition dual fuel diesel-lpg, 2011.

[4] E. Buckingham. On physically similar systems: illustrations of the use of dimensional equations. *Physical Review*, 4:345–376, 1914.

[5] J. Carter, N.K. Sharp, and H. Tennant. Turbocharging technologies for heavy duty diesel engines. Cummins Turbo Technologies UK.

[6] C. Fenske. Further development of mtu series 1163 for imo ii. *MTU General White Paper*, 2014.

[7] R.A. Fisher. *, The Design of Experiments*. Macmillan, 1935.

[8] M. Ghazikhani, M. Davarpanah, and S.A. Mousavi Shaegh. An experimental study on the effects of different opening ranges of waste gate on the exhaust soot emission of a turbocharged di diesel engine, 2007.

[9] J.P. Jensen, A.F. Kristensen, S.C. Sorenson, N. Houbak, and E. Hendricks. Mean value modeling of a small turbocharged diesel engine. *SAE 910070*, 1991.

[10] C.J. Leising, G.P. Purohit, S.P. DeGrey, and J.G. Finegold. Waste heat recovery. *SAE 780686*, 1987.

[11] J. K. Miller. *Real World High-Performance Turbocharger Systems*. CarTech inc., North Branch,MN,USA, 1st edition edition, 2008.

[12] A.F. Mills. *Basic Heat and Mass Transfer*. Prentice Hall, University of California, Los Angeles California, USA, 2nd edition edition, 1999.

[13] Y. Ono, K. Shiraishi, and Y. Yamashita. Application of a large hybris turbocharger for marine electric-power generation. *Mitsubishi Heavy industries Technical Review*, 49, March 2012.

[14] Sam. 2014 f1 explained: The power unit. http://www.racecar-engineering.com/articles/f1/2014-f1-the-power-unit-explained/, 2014.

[15] P.J.M. Schulten. *The interaction between diesel engines, ship and propeller during maneuvering*. PhD thesis, TU Delft, May 2002.

[16] P.J.M. Schulten and D. Stapersma. Mean value modelling of the gas exchange of a 4-stroke diesel engine for use in powertrain applications. *SAE*, O3P-102, 2002.

[17] J.R. Serrano, F.J. Arnau, V. Dolz, A. Tiseira, and C. Cervello. A model of a turbocharger radial turbine appropriate to be used in zero- and one-dimensional gas dynamics codes for internal combustion engines modeling, 2007.

[18] D. Stapersma. *Lecture Notes Diesel Engines WB4408A/B*. TU Delft, 8th print edition, 2010.

[19] D. Stapersma. Calibrating and matching the mean value first principle diesel engine model, 2016.